UNIVERSIDAD TÉCNICA FEDERICO SANTA MARÍA
DEPARTAMENTO DE INGENIERÍA MECÁNICA
VALPARAÍSO - CHILE

"SIMULATION OF A GEOTHERMAL RESERVOIR FOR THE PRODUCTION OF ELECTRICITY USING AN ORC PLANT"

JOSÉ IGNACIO FUSTER JUSTINIANO

MEMORIA DE TITULACIÓN PARA OPTAR AL TÍTULO DE INGENIERO CIVIL MECÁNICO

PROFESOR GUÍA: Dr. Ing. ALEX FLORES M.

PROFESOR CORREFERENTE: Dr. Ing. RODRIGO BARRAZA V.

PROFESOR CORREFERENTE: Dr. Ing. PAOLA BOMBARDA

NOVIEMBRE 2019

Acknowledgments

This thesis is dedicated to my mother, my sister, my girlfriend and all my friends, I am incredible grateful for their constant and unconditional support.

I also want to specially thank Paola Bombarda and Dario Alfani, their help, guidance and good disposition were a fundamental part of this work.

Resumen Ejecutivo

Este trabajo se centra en el análisis de la posibilidad de desarrollar una simulación integrada de una planta binaria ORC para la generación de electricidad, utilizando recursos geotérmicos de temperatura media-baja de un reservorio líquido dominante. La simulación se realizó utilizando dos softwares diferentes, uno para el reservorio geotérmico y otro para la planta binaria ORC.

La primera parte de este trabajo contiene una descripción general de las cosas más importantes que se deben tener en cuenta sobre la energía geotérmica, como la naturaleza de la energía geotérmica, las diferentes clasificaciones de los recursos, las aplicaciones más importantes, etc. Después de esta introducción se describen los aspectos más relevantes de la ingeniería de reservorios geotérmicos y el software utilizado para la simulación del reservorio. El software utilizado para la simulación se llama DoubletCalc v1.4.3, fue creado por TNO y tiene acceso público (código abierto). Todas los inputs necesarios para la simulación y los outputs que se pueden obtener se discuten en detalle. Posteriormente, se presenta el modelo del software y se valida utilizando cuatro casos de estudios tomados de la literatura disponible.

Para la simulación de la planta geotérmica se decidió tomar el proyecto geotérmico de la ciudad de Altheim en Austria como caso de referencia, el cual que fue uno de los casos de estudio utilizados para la validación del modelo DoubletCalc v1.4.3. Después de una breve presentación del proyecto geotérmico y los parametros asumidos para la simulación, algunos de los resultados obtenidos de DoubletCalc v1.4.3 se utilizaron para acoplar el modelo del reservorio con el modelo de la planta ORC. Los outputs requeridos para el acoplamiento de los dos modelos son el flujo másico del fluido geotérmico, la presión y la temperatura al nivel de la superficie.

La simulación y optimización de la planta de ORC se realizó utilizando un software comercial llamado Aspen Plus. Se han planteado dos casos diferentes para la planta de ORC, un ciclo simple de vapor saturado y un ciclo recuperativo de vapor saturado. Para el ciclo simple se han considerado dos casos, uno sin límite para la temperatura de salida del fluido geotérmico del intercambiador de calor primario y el otro con un límite de temperatura de 70 [° C]; mientras que para el ciclo recuperativo solo se consideró un caso teniendo en cuenta el límite de temperatura. El ciclo termodinámico se optimizó para siete fluidos de trabajo diferentes, luego se realizó un análisis de rendimiento comparando la potencia neta producida y la eficiencia de la segunda ley de cada fluido para los tres casos. El análisis ha demostrado que el ciclo simple sin límite de temperatura es el que produce la potencia neta máxima. Por otro lado, el ciclo recuprativo tiene una eficiencia y una potencia neta ligeramente mayores que el ciclo simple con límite de temperatura simple.

Finalmente, se eligió el fluido de trabajo más apropiado para un análisis adicional, en el cual se estudiaron las pérdidas de eficiencia de la segunda ley y el acoplamiento de los dos modelos mediante el análisis general de la planta ORC con ciclo simple de vapor saturado sin límite de temperatura. Este último análisis se llevó a cabo variando el valor de la diferencia de presión de la bomba de producción y la permeabilidad del reservorio geotérmico.

Abstract

This thesis investigates the possibility to realize a simulation of an ORC binary plant for the generation of electricity, utilizing low-medium temperature geothermal resources from a liquid-dominated reservoir. The simulation was performed using two different software's, one for the geothermal reservoir and another for the ORC binary plant.

The first part of this work contains a general description of the most important things to have in mind about the geothermal energy, such as the nature of the geothermal energy, the different classifications for the resources, the most important applications and so on. After this introduction, the most relevant aspects about the reservoir engineering and the software used for the simulation of the reservoir are described. The software used for the simulation is called DoubletCalc v1.4.3, it was created by TNO and it has public access (open source). All the inputs need for the simulation and the outputs that can be obtained from it are discussed in detail; after this, the model of the software is presented and validated using four study cases taken from the literature.

For the simulation of the geothermal plant it was decided to take as reference the Altheim geothermal project located in Austria, which was one of the study cases used for the validation of the DoubletCalc v1.4.3 model. After a brief presentation of the geothermal project and the inputs assumed for the simulation, some of the results obtained from DoubletCalc v1.4.3 were used to couple the model of the reservoir with the model of the ORC plant. The outputs needed for the coupling of the two models are the mass flow rate of geothermal fluid, the pressure and the temperature at surface level.

The simulation and optimization of the ORC plant was performed using a commercial software called Aspen Plus. Two different configurations for the ORC plant were assumed, a simple saturated steam cycle and a saturated steam recuperative cycle. For the simple cycle were considered two cases, one without any limit for the outlet temperature of the geothermal fluid from the primary heat exchanger and the other case with a temperature limit equal to 70 [°C]; while for the recuperative cycle was considered just one case taking into account the temperature limit. The thermodynamic cycle was optimized for seven different working fluids, then a performance analysis was done comparing the net power produced and the second law efficiency of each fluid for the three cases. The analysis shown that the simple cycle without temperature limit is the one that produces the highest net power. On the other hand, the recuperative cycle has a slightly higher efficiency and net power produced than the simple cycle with the temperature limit.

Finally, the most appropriate working fluid was chosen for further analysis, in which the second law efficiency losses and the coupling of the two models were studied analyzing the overall performance of the simple saturated ORC plant without temperature limit. This last analysis was carried out varying the value of the down-hole pump pressure difference and the permeability of the reservoir.

Acronyms and Nomenclature

Acronyms

AH	Along Hole
COND	Condenser
COP	Coefficient of Performance
CSV	Comma-separated values
ECO	Economizer
EGS	Enhanced Geothermal System
ESP	Electrical submersible pump
EVA	Evaporator
GEN	Electric Generator
GWP	Global Warming Potential
HX	Heat exchanger
NCG	Non-condensable gases
NIST	National Institute of Standards and Technology
NLOG	Netherlands Oil and Gas
ODP	Ozone Depletion Potential
ORC	Organic Rankine Cycle
P10	Percentile 10
P50	Percentile 50
P90	Percentile 90
PHE	Primary heat exchanger
REC	Recuperator
REFPROP	Reference Fluid Thermodynamic and Transport Properties Database
SDE+	Subsidy for the stimulation of renewable energy production
TNO	Netherlands Organization for Applied Scientific Research
TURB	Turbine
TVD	True vertical depth
VITO	Flemish Institute of Technology
WGC	World Geothermal Congress
WF	Working Fluid

Nomenclature

A	Area [m^2]
C_D	Drawdown coefficient [MPa/(kg·s)]
c_p	Heat capacity [kJ/(kg·K)]
D	Diameter [m]
D_{in}	Inner diameter of the well [m]
D_{out}	Outer diameter of the well [m]
d	Depth [m]
d_i	Depth at the inlet of the well [m]
d_{pump}	Depth of the downhole pump [m]
$d_{top,p}$	Depth of the top of the reservoir at production well level [m]
f	Friction factor [-]
f_{db}	Momentum balance [Pa] or [bar]
g	Acceleration of gravity (9.81 [m/s^2])
$h_{0,geo}$	Enthalpy of the geothermal fluid at reference conditions [kJ/kg]
$h_{in,geo}$	Enthalpy of the geothermal fluid at the inlet of the primary heat exchanger [kJ/kg]
$h_{lim,geo}$	Enthalpy of the geothermal fluid at the outlet of the primary heat exchanger in the case with the temperature limit [kJ/(kg·K)]
I_{ani}	Anisotropy index [-]
J	Well productivity [m^3/(Pa·s)]
$J_{inclined\ well}$	Well productivity with an inclined well [m^3/(Pa·s)]
$J_{vertical\ well}$	Well productivity with a vertical well [m^3/(Pa·s)]
K	Hydraulic conductivity [m/s]
k	Permeability [mD] or [m^2]
k_h	Horizontal permeability [mD] or [m^2]
$k_{t,g}$	Thermal conductivity of the rocks surrounding the well [W/(m·K)]
k_v	Vertical permeability [mD] or [m^2]
L	Distance between production and injection well at reservoir level [m]
L_F	Distance from the inlet of the well up to the flash point [m]
L_R	Aquifer thickness [m]
$L_{R,d}$	Dimensionless aquifer thickness [-]
L_W	Well length [m]
l	Distance along well [m]
MM	Molecular mass [g/mol]
$\dot{m}$	Mass flow rate [kg/s]
$\dot{m}_{cw}$	Mass flow rate of the cooling water at the condenser [kg/s]
$\dot{m}_{geo}$	Mass flow rate of the geothermal fluid [kg/s]
$\dot{m}_{wf}$	Mass flow rate of the working fluid [kg/s]
N	Number of nodes in the doublet system [-]
P	Pressure [Pa] or [bar]
P_{cond}	Condensation pressure [bar]
P_{cr}	Critical pressure [bar]
P_{eva}	Evaporation pressure [bar]

P_{DH}	Down-hole pump pressure difference [bar]
P_F	Pressure at the flash point [Pa] or [bar]
P_{MD}	Maximum discharge pressure [Pa] or [bar]
P_{min}	Minimum pressure at the inlet downhole pump inlet [Pa] or [bar]
P_R	Initial hydrostatic pressure at the reservoir [Pa] or [bar]
P_{RNPSH}	Required net positive suction head [Pa] or [bar]
P_s	Suction pressure of the downhole pump [Pa] or [bar]
P_{sat}	Pressure at saturation conditions [Pa] or [bar]
$P_{stat,p}$	Initial hydrostatic pressure at production well [Pa] or [bar]
$P_{stat,i}$	Initial hydrostatic pressure at injection well [Pa] or [bar]
P_w	Pressure in the well at the top of the reservoir [Pa] or [bar]
$\dot{Q}$	Heat exchanged [W]
$\dot{Q}_{in}$	Thermal power given by the geothermal water [kW]
$\dot{Q}_{in,max}$	Maximum thermal power that can be recovered [kW]
$q_{w,well}$	Heat loss per unit length in the well [W/m]
R_{ntg}	Net to gross ratio [-]
r	Radius [m]
r_R	Reservoir radius [m]
r_W	Well radius [m]
S	Skin factor [-]
S_θ	Skin as result of obliquely drilling in the reservoir [-]
s	Salinity [ppm]
$s_{0,geo}$	Entropy of the geothermal fluid at reference conditions [kJ/(kg·K)]
s_{aq}	Salinity of the aquifer brine [ppm]
$s_{in,cond}$	Entropy of the working fluid at the inlet of the condenser [kJ/(kg·K)]
$s_{in,cw}$	Entropy of the cooling water at the inlet of the condenser [kJ/(kg·K)]
$s_{in,geo}$	Entropy of the geothermal fluid at the inlet of the primary heat exchanger [kJ/(kg·K)]
$s_{in,PHE}$	Entropy of the working fluid at the inlet of the primary heat exchanger [kJ/(kg·K)]
$s_{in,pump}$	Entropy of the working fluid at the inlet of the pump [kJ/(kg·K)]
$s_{in,turb}$	Entropy of the working fluid at the inlet of the turbine [kJ/(kg·K)]
$s_{lim,geo}$	Entropy of the geothermal fluid at the outlet of the primary heat exchanger in the case with the temperature limit [kJ/(kg·K)]
$s_{out,cond}$	Entropy of the working fluid at the outlet of the condenser [kJ/(kg·K)]
$s_{out,cw}$	Entropy of the cooling water at the outlet of the condenser [kJ/(kg·K)]
$s_{out,geo}$	Entropy of the geothermal fluid at the outlet of the primary heat exchanger [kJ/(kg·K)]
$s_{out,PHE}$	Entropy of the working fluid at the outlet of the primary heat exchanger [kJ/(kg·K)]
$s_{out,pump}$	Entropy of the working fluid at the outlet of the pump [kJ/(kg·K)]
$s_{out,turb}$	Entropy of the working fluid at the outlet of the turbine [kJ/(kg·K)]
T	Temperature [°C] or [K]
T_0	Reference temperature [°C] or [K]

T_{amb}	Ambient temperature [°C] or [K]
T_c	Casing temperature [°C] or [K]
$T_{evap,LP}$	Evaporation temperature at low pressure [°C] or [K]
$T_{evap.HP}$	Evaporation temperature at high pressure [°C] or [K]
$T_{geo,in}$	Inlet temperature of the geothermal water in the primary heat exchanger [°C] or [K]
$T_{geo,out}$	Outlet temperature of the geothermal water in the primary heat exchanger [°C] or [K]
T_{gt}	Initial temperature profile [°C] or [K]
$T_{hx,in}$	Temperature at the inlet of the heat exchanger [°C] or [K]
$T_{hx,out}$	Temperature at the outlet of the heat exchanger [°C] or [K]
T_{in}	Temperature at the inlet [°C] or [K]
T_{max}	Maximum temperature [°C] or [K]
T_{min}	Minimum temperature [°C] or [K]
T_{out}	Temperature at the outlet [°C] or [K]
T_R	Temperature at reservoir level [°C] or [K]
T_{sat}	Temperature at saturation conditions [°C] or [K]
T_{sur}	Average yearly temperature at surface level [°C] or [K]
T_{well}	Temperature of the geothermal fluid in the well [°C] or [K]
t	Time since the start of the heat flow [s]
u	Velocity [m/s]
$\dot{V}$	Volumetric flow rate [m^3/s]
$\dot{W}_{aux}$	Power consumed by the auxiliaries of the ORC plant [kW]
$\dot{W}_{gross,DH}$	Gross power that should be provided to the downhole pump [kW]
$\dot{W}_{gross,pump}$	Gross power required by the pump of the ORC plant [kW]
$\dot{W}_{gross,turb}$	Gross power produced by the turbine of the ORC plant [kW]
$\dot{W}_{HX}$	Power obtainable from the heat exchanger [W]
$\dot{W}_{loss}$	Lost power due to irreversibilities [kW]
$\dot{W}_{net,plant}$	Net power of the geothermal plant [kW]
$\dot{W}_{net,DH}$	Net power that should be provided to the downhole pump [kW]
$\dot{W}_{net,ORC}$	Net power of the ORC plant [kW]
$\dot{W}_{net,pump}$	Net power that should be provided to the pump of the ORC plant [kW]
$\dot{W}_{net,turb}$	Net power produced by the turbine of the ORC plant [kW]
$\dot{W}_{pump}$	Power consumed by the feed pump of the ORC plant [kW]
$\dot{W}_{rev}$	Reversible work [kW]
$\dot{W}_{turb}$	Power produced by the turbine [kW]
$\dot{W}_{water\ loop}$	Power consumed by the water loop in the condenser [kW]
z	Vertical distance to the wellhead [m]
$\alpha_{t,g}$	Thermal diffusion coefficient of the aquifer rock [m^2/s]
$\Delta\eta_{II,i}$	Second law efficiency losses of a certain component i [-]
$\Delta\eta_{II,cond}$	Second law efficiency losses of the condenser [-]
$\Delta\eta_{II,PHE}$	Second law efficiency losses of the primary heat exchanger [-]
$\Delta\eta_{II,pump}$	Second law efficiency losses of the pump [-]

$\Delta\eta_{II,pump,el,mec}$	Pump electrical-mechanical second law efficiency losses [-]
$\Delta\eta_{II,reinj}$	Second law efficiency losses of the geothermal fluid at the outlet of the primary heat exchanger [-]
$\Delta\eta_{II,turb}$	Second law efficiency losses of the turbine [-]
$\Delta\eta_{II,turb,el,mec}$	Turbine electrical-mechanical second law efficiency losses of [-]
ΔP	Drawdown pressure difference [Pa] or [bar]
$\Delta P_{cond,wf}$	Pressure drop in the condenser (hot side) [bar]
ΔP_d	Security pressure difference [Pa] or [bar]
ΔP_{fr}	Friction losses [Pa] or [bar]
ΔP_L	Hydrostatic and friction losses in liquid state [Pa] or [bar]
ΔP_{LV}	Two-phase pressure losses [Pa] or [bar]
$\Delta P_{PHE,wf}$	Pressure drop in the primary heat exchanger (cold side) [bar]
ΔP_{pump}	Pressure difference provided by the downhole pump [Pa] or [bar]
ΔP_{rec}	Pressure drop in the recuperator (cold side) [bar]
ΔP_{skin}	Pressure drop due to the skin factor [Pa] or [bar]
$\Delta T_{pp,cond}$	Pinch point temperature difference in the condenser [°C] or [K]
ΔT_{hx}	Temperature difference in the heat exchanger [°C] or [K]
$\Delta T_{pp,PHE}$	Pinch point temperature difference in the primary heat exchanger [°C] or [K]
$\Delta T_{pp,rec}$	Pinch point temperature difference in the recuperator [°C] or [K]
ε	Absolute roughness of the well casing [mm] or [milli-inch]
η_I	First law efficiency [-]
η_{II}	Second law efficiency [-]
η_{DH}	Efficiency of the down-hole pump system [-]
η_{pump}	Efficiency of the ORC feed pump [-]
$\eta_{pump,el,mec}$	Electrical-mechanical efficiency of the ORC feed pump [-]
η_{rec}	Total heat recovery efficiency [-]
$\eta_{th,rec}$	Thermal recovery efficiency [-]
$\eta_{turb,is}$	Isentropic efficiency of the turbine [-]
$\eta_{turb,el,mec}$	Electrical-mechanical efficiency of the turbine [-]
θ	Well deviation from the vertical [°]
λ	Geothermal gradient [°C/m]
μ	Dynamic viscosity [kg/(m·s)] or [Pa·s]
ρ	Density of the geothermal fluid [kg/m^3]
ρ_{fw}	Fresh water density [kg/m^3]
ρ_R	Density at reservoir level [kg/m^3]

Table of Contents

List of Figures

List of Tables

Introduction

In these days the world is witnessing a considerable increase in the use of the renewable energy sources over the conventional fossil fuels. The main reason of this transition is the well-known global warming, the new policies adopted because of this problem and in some but not few cases, economic motivations.

Among the renewable energy resources, the geothermal energy is unfortunately out of the spotlight, even though its high reliability and low emissions. Compared to biomass and fossil fuels, geothermal energy has the advantages to be practically a zero-emissions technology (in the case of closed-loops doublets), it does not need to transport the fuel and more important, it does not need to pay for the fuel. Compared with solar and wind, which are the most widely spread nowadays, geothermal energy does not depend on climatic changes, it has less land occupation, it has a long lifetime and it produces constant base-load energy.

The main two disadvantages that are holding back the development of geothermal energy from achieving its true potential are the technological uncertainty of the production levels of energy and the elevated and uncertain investment cost.

To achieve the maximum use of geothermal energy, an adequate computational simulation of both the geothermal reservoir and the electric generation plant on the surface is required, optimizing its functional performance. It is therefore the purpose of this thesis to analyze how reliable could be the results of the simulation of a geothermal ORC binary plant, using an open source software for the simulation of the reservoir, and a commercial software for the power plant.

I. Background and research methodology

1.1 Problem

The importance of geothermal exploitation by means of binary plants will grow in the future, since the water – dominated resources are very abundant, and the intrinsic advantages of the binary technology will extend the range of application of this technology in the overlapping area with flash plants.

A geothermal binary power plant consists of a closed power cycle; most commonly, a Rankine cycle adopting an organic fluid (ORC) as working fluid is selected. The cycle is typically designed and optimized considering only the surface equipment of the plant. The optimization process involves selecting the most suitable working fluid for the power cycle together with optimum operating parameters, namely the cycle pressures and temperatures.

Usually, the optimization of the plant only takes into account the ORC plant in the surface, this is mainly caused by the fact that the subsurface parameters of a geothermal project are surrounded by a certain level of uncertainty, which, besides the high economic risk that implies for the proper development of the project, makes difficult the incorporation of these variables in the simulation and optimization of the plant. However, it would be desirable to adopt a more comprehensive approach, which includes also the subsurface part of the geothermal power plant: such an approach, though often invoked, is not commonly adopted.

The simulation of both surface and subsurface plants is very demanding and requires a deep expertise, and, at the moment, no general software is available for an overall simulation. Considering that developing an ad hoc software would require an enormous effort, it is reasonable to start the investigation by means of a cascaded use of existing software.

Several software exist for the subsurface calculation; in the framework of this work, an open-source software, DoubletCalc v1.4.3 [1, 2], which is aimed at evaluating the performance of a doublet system in the context of a sedimentary reservoir, was selected as software for subsurface calculation. This software adopts a simplified methodology and includes a probabilistic calculation and seems particularly promising for the application to binary plants. On the other hand, for the surface performance evaluation, a commercial software, most widely adopted, Aspen Plus v10.0, was selected.

1.2 Objectives

1.2.1 General Objective

The general objective of this thesis is to simulate and optimize a geothermal reservoir and the respective ORC plant on the surface. The thesis is based on the use of an open source software called DoubletCalc v1.4.3 to model the dynamics of the reservoir; on the other hand, the ORC binary plant will be simulated and optimized with a commercial code called Aspen Plus. The results of the reservoir model will be adapted to be used as initial and boundary conditions in the modeling of the binary plant considering a reference case from the literature. Finally, the overall geothermal plant will be optimized using the coupling of the two simulation models.

1.2.2 Specific Objectives

In order to achieve the general objective previously presented, the following specific objectives must be completed as the thesis progresses:

- Describe the state of the art of the geothermal energy resource and the most important application for electricity generation.
- Study and describe the principal transport phenomena in a geothermal reservoir.
- Propose the model to be used to approximate the behavior of the geothermal reservoir.
- Simulate the geothermal reservoir and validate the results with some reference cases available in the literature.
- Describe the design and the approach of the model for the ORC binary plant.
- Simulate numerically the binary plant, taking the results of the geothermal reservoir as initial and boundary conditions
- Couple the two models to simulate some reference cases and compare the results.

1.3 Methodology

The simplest plant scheme for geothermal exploitation consists of a couple of wells, a producer well and an injection well, called “a doublet”, and a power plant, located at surface. The doublet allows the circulation of the geothermal fluid from the reservoir to surface and then back to the reservoir, while the power plant is charged with the conversion of the thermal energy carried to the surface by the geothermal fluid into electric power. In order to have an acceptable mass flow rate for the economic exploitation of the reservoir, a downhole pump is generally adopted.

As it was mentioned before, an open-source software is used in this work for the calculation of the performance of a geothermal doublet; this software is coupled to a commercial software, typically employed for power plant design. Particular attention is given to the combined subsurface/surface calculation, and plant performance will be optimized starting from the reservoir conditions. The simulation model will feature a geothermal doublet coupled to an ORC plant for the power generation, a reference case will be taken into account for the analysis (Altheim geothermal project, Austria); several parametric calculations will be conducted, considering different reservoir conditions and a selection of appropriate working fluids for the ORC plant. Results of simulations will be discussed with the aid of Second Law analysis, with the scope of pointing out the key outcome of the integrated design procedure.

1.3.1 Description of the simulation and optimization model

DoubletCalc sketches the geothermal fluid loop starting from a static condition in the reservoir aquifer, evaluating the flow through the reservoir, the production well, the heat exchanger at surface, the reinjection well, and finally again to the static condition. The loop is divided in a number of small segments and flow evalutation proceeds considering mass balance, momentum balance and energy balance for each segment. Steady flow condition is assumed, and non-adiabatic flow is evaluated through the wells; for further details see Mijnlieff et al. 2014 [2].

To perform the simulation, DoubletCalc needs as inputs the key reservoir parameters of the target location (e.g. reservoir depth and thickness, permeability, water salinity, etc.), the main operating features of the downhole pump (pump pressure difference and global efficiency), the details of the casing scheme and the design data of the surface heat exchanger. The data are collected under three different input sets: Aquifer properties, Doublet and pump properties and Well properties.

Finally, yet importantly, the calculations performed by DoubletCalc are based on a stochastic (Monte Carlo) approach, which allows handling the effect of subsurface uncertainties. Consequently, output results consist of as a set of three values: the percentile 90, 50 and 10 of the probabilistic distribution. However, in the frame of this work, the results provided by DoubletCalc are used deterministically, selecting the mean statistical values (percentile 50), as input to the surface plant simulation code.

The heat exchanger at surface represent the junction point between the subsurface and surface calculation: actually, the subsurface software calculates the thermal power extracted, but, being the heat exchanger a component of the surface plant, this thermal power is evaluated also by the surface software.

The simulation model of Aspen Plus v10.0, for the performance evaluation of the surface plant, sketches the plant by the assembling all the plant components; the evaluation proceeds considering mass, energy and momentum balances for each component. Again, steady flow condition is assumed. It is to underline that the selected process simulator (Aspen Plus) allows to properly evaluate both geothermal fluid and working fluid thermodynamic properties, which are very important in order to fulfill a correct simulation of the plant performance. To run the simulation, Aspen needs as inputs some of the results of DoubletCalc calculation, namely the mass flow of geothermal fluid, the pressure and the temperature at power plant inlet; moreover, the main design and operating features of all the plant components need to be specified.

Before the simulation and optimization of the ORC plant, it will be presented the validation of the DoubletCal model. In this part of the work four study cases were selected from the available literature. The parameters found for each study case were used as inputs for a DoubletCalc simulation and the results obtained from each of these simulations were compared with the declared parameters for the corresponding study case.

One of the study cases used for validation of the DoubletCal model was selected as reference case for the simulation and optimization of the ORC plant (Altheim geothermal project, Austria). For this procedure, after the DoubletCalc simulation, the selection of ORC working fluid was carried out. In the frame of this work seven working fluids were selected for the analysis, six of these fluids correspond to fluids used in similar cases found in the literature and one of them is an innovative refrigerant with very good security and environmental properties. In concert with the working fluid and the selected reference case, the thermodynamic cycle configuration must be selected: in the context of this work, the selection of a simple saturated cycle is appropriate.

The optimization of the ORC plant, taking into account every working fluid, was carried out by fixing the pinch point temperature difference in the primary heat exchanger and in the condenser. Then it was used a sensitivity analysis varying the evaporation pressure to find the point in which the ORC plant produces its maximum power (optimum point).

It is worth mentioning that a second law efficiency analysis was conducted for every case and for all the working fluids considered, mainly in order to compare the performance and the most important losses of each scenario. The second law efficiency was calculated with the net power of the ORC plant and the reversible work that could be obtained from the heat source. The reversible work corresponds to the maximum amount of power that can be produced by a system in reversible conditions with respect to a certain reference state

The downhole pump is a key component for the plant operation and the optimization of the overall geothermal plant, since acting on this component allows changing the geothermal flow rate in the doublet. Actually, no reference is made in DoubletCalc to a specific downhole pump, but modifying the pressure difference across the pump it is possible to simulate the operation of the pump in an extended range of conditions for the considered by the doublet. The overall geothermal plant operation was analyzed by changing the pressure difference of the downhole pump with respect to the design value; at the same time, the ORC cycle was optimized for every geothermal flow rate.

As it was said before, the reservoir properties are estimated with an extent of uncertainty. It is therefore useful to conduct a sensitivity analysis, investigating the possible shift of the optimum operating conditions in case the permeability does not match the expected value. Because of this, one of the working fluids (HFO-1234ze(E)) was selected for the optimization of the overall geothermal plant. The analysis was conducted decreasing the reservoir permeability and maintaining all the other parameters constant. It is expected that, if the drawdown pressure drop increases, because of the lower permeability, a higher pressure difference of the downhole pump will be required. Therefore, the optimization of the reference case was performed for four different values of permeability, the first one with the value of the reference case, the second with half of the permeability, the third with a value multiplied by a factor of 0.25 and the last one with a value multiplied by a factor of 0.1.

In the following paragraphs are presented a brief explanation of the main features of the simulation software that were used in this work.

1.3.2 DoubletCalc v1.4.3.

This tool was developed by the Netherlands Organization for Applied Scientific Research (TNO), with the main intention of helping the users to have a general idea, before the drilling process and the initial investments, of the most important outputs that a potential geothermal doublet system could be able to supply. In these days, the use of DoubletCalc has become mandatory for many grant applications related with geothermal projects in the Netherlands.

A certain range of uncertainty is taken into account by DoubletCalc, as can be seen in the inputs and outputs figures that are presented in the next pages. This is because many variables, such as the reservoir thickness, permeability, aquifer net-to-gross ratio and so on, are not known with a full certainty before the drilling process. To handle this inconvenient, the calculations performed by DoubletCalc are based on stochastic (Monte Carlo) simulations, which allow to present the outputs with a probabilistic distribution.

Monte Carlo simulations are used when you cannot predict with total confidence the exact value of a certain group of parameters, but based on previous experiences, historical data or precedent studies, you can define an estimate. In the case of DoubletCalc v1.4.3, the uncertainty factor is related with the aquifer properties; they are treated as independent of each other by the software and must be specified with a minimum, median and maximum value. The probability distribution of these parameters is modelled as a double triangle:

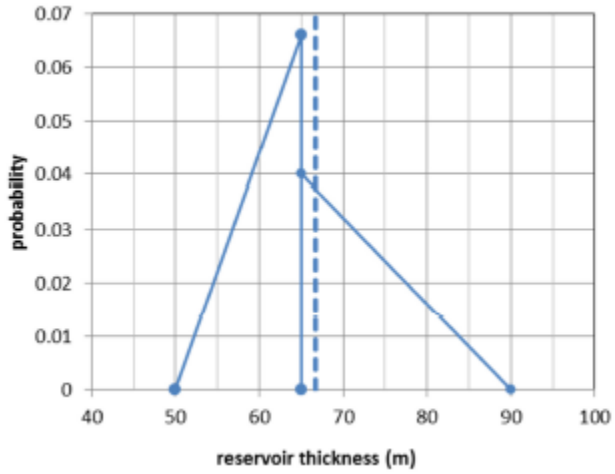

Figure 1: Example of a double triangle probability distribution for the reservoir thickness. Minimum, median and maximum values in this example are 50, 65 and 90. The resulting average is 66.7 (dashed line) [3].

As it was mentioned, DoubletCalc enables the user to calculate the indicative geothermal power extracted, the flow rate, the coefficient of performance (COP) and many more outputs of a potential geothermal doublet system. To perform the simulation, the software needs as inputs the key reservoir parameters of the target location, the properties of the downhole pump and the details of the casing scheme. To have an idea of the inputs required for a simulation and the outputs that can be obtained, the following figures present the inputs and outputs of a simulation example taken from the software manual's [2]:

number of simulation runs (-) 1000 Calculate ! Open Scenario Save Scenario Exit Program

file: ... DoubletCalc\DoubletCalc_143_03022016\pruebas\primera prueba (ejemplo del manual) caso1.xml

Geotechnical input

A) Aquifer properties

Property	min	median	max
aquifer permeability (mD)	199	200	201
aquifer net to gross (-)	0.99	1	1.01
aquifer gross thickness (m)	99	100	101
aquifer top at producer (m TVD)	1800.0	2000	2200.0
aquifer top at injector (m TVD)	1800.0	2000	2200.0
aquifer water salinity (ppm)	69999	70000	70001

Property	value
aquifer kh/kv ratio (-)	1
surface temperature (°C)	10.0
geothermal gradient (°C/m)	0.030
[mid aquifer temperature producer (°C)]	0.0
[inital aquifer pressure at producer (bar)	0.0
[initial aquifer pressure at injector (bar)]	0.0

B) Doublet and pump properties

Property	value
exit temperature heat exchanger (°C)	35
distance wells at aquifer level (m)	1500
pump system efficiency (-)	0.61
production pump depth (m)	500
pump pressure difference (bar)	30

Figure 2: Inputs of a simulation example using DoubletCalc (reservoir and pump parameters) [2].

As is shown in the Figure 2, the part A) of the inputs is referred to the definition of the aquifer properties of the target location. The min and max values that can be seen represent the uncertainty range of these geological parameters, these are defined by the user and can be estimated as +/- 10% of the median value. The parameters required in this block are the permeability of the aquifer, the net-to-gross ratio (explained in the previous section), the aquifer gross thickness, the depths of the top of the aquifer at producer and injector level (measured with respect to the true vertical depth (m TVD)) and the aquifer water salinity (measured in NaCl equivalent).

On the right block of the part A) there are more parameters that must be specified. The aquifer k_h/k_v ratio is related with the anisotropy of the system and describe the ratio between the horizontal permeability (k_h) and the vertical permeability (k_v); the developers of the software suggest assuming this parameter as 1 in case it cannot be found in the literature. The surface temperature and the geothermal gradient vary depending the location of the doublet system; the values shown in the picture represent the average surface temperature and geothermal gradient in the Netherlands. Finally, the last three parameters that are between brackets (optional parameters) can be set equal to zero because they can be ignored by the user.

The part B) of the input screen ask the user to specify the temperature at the exit of the heat exchanger (defined by the configuration and the temperature differences of the heat exchanger), the distance between the production and injection well at aquifer level, the pump system efficiency, the production pump depth (estimated/calculated by the user) and the pump pressure difference.

C) Well properties

calculation length subdivision (m) 50

Producer	
outer diameter producer (inch)	7
skin producer (-)	0
penetration angle producer (deg)	45
skin due to penetration angle p (-)	-0.94

Segment	pipe segment sections p (m AH)	pipe segment depth p (m TVD)	pipe inner diameter p (inch)	pipe roughness p (milli-inch)
1	500	500	5	1.2
2	1000	1000	12.375	1.2
3	1566	1400	8.625	1.2
4	2415	2000	6.625	1.2
5				
6				
7				
8				

Injector	
outer diameter injector (inch)	7
skin injector (-)	0
penetration angle injector (deg)	45
skin due to penetration angle i (-)	-0.94

Segment	pipe segment sections i (m AH)	pipe segment depth i (m TVD)	pipe inner diameter i (inch)	pipe roughness i (milli-inch)
1	50	50	5	1.2
2	1000	1000	12.375	1.2
3	1566	1400	8.625	1.2
4	2415	2000	6.625	1.2
5				
6				
7				
8				

[ ] optional

Figure 3: Inputs of a simulation example using DoubletCalc (casing parameters) [2].

The first thing that can be seen in the picture of the part C) of the input screen is the 'calculation length subdivision (m)', which is the number of sections of equal length in which the well is divided during the simulation; the software does this for reasons of calculation accuracy and the default value of the program, and the one that will be assumed later in this work, is 50 segments.

The first three boxes are needed to define the casing scheme. The outer diameter of the producer/injector at reservoir level determines the surface through which the geothermal fluid enters the well. The skin producer and skin injector, as it was explained before, is the factor related with the resistance around the well in the reservoir section. The penetration angle of the producer/injector is the value (in degrees with respect to the vertical and equal to 45° in the examples of the manual) of the inclination between the production/injection well trajectory and the reservoir; this parameter, together with the reservoir thickness, the anisotropy and the outer diameter of the well determines the length of the production interval. The skin due penetration angle is calculated by the software after specifying the previous parameters.

An inclined well has positive consequences in the flow. An inclined perforation provokes that the length of the intersection of wellbore/reservoir exceeds the thickness of the aquifer, resulting in a larger flow with respect to a vertical well. The software assumes this effect as an 'extra skin' and calculates its value in the box 'skin due penetration angle (-)', depending on the inputs specified by the user. In the examples presented in the manual of DoubletCalc it is suggested to neglect the 'skin producer/injector' box and just considered the skin related with the penetration angle calculated by the software. More information about this parameter can be seen in the Appendix D.

For the last section of the part C) of the inputs the following picture is needed to have a better understanding of the configuration assumed by DoubletCalc v1.4.3:

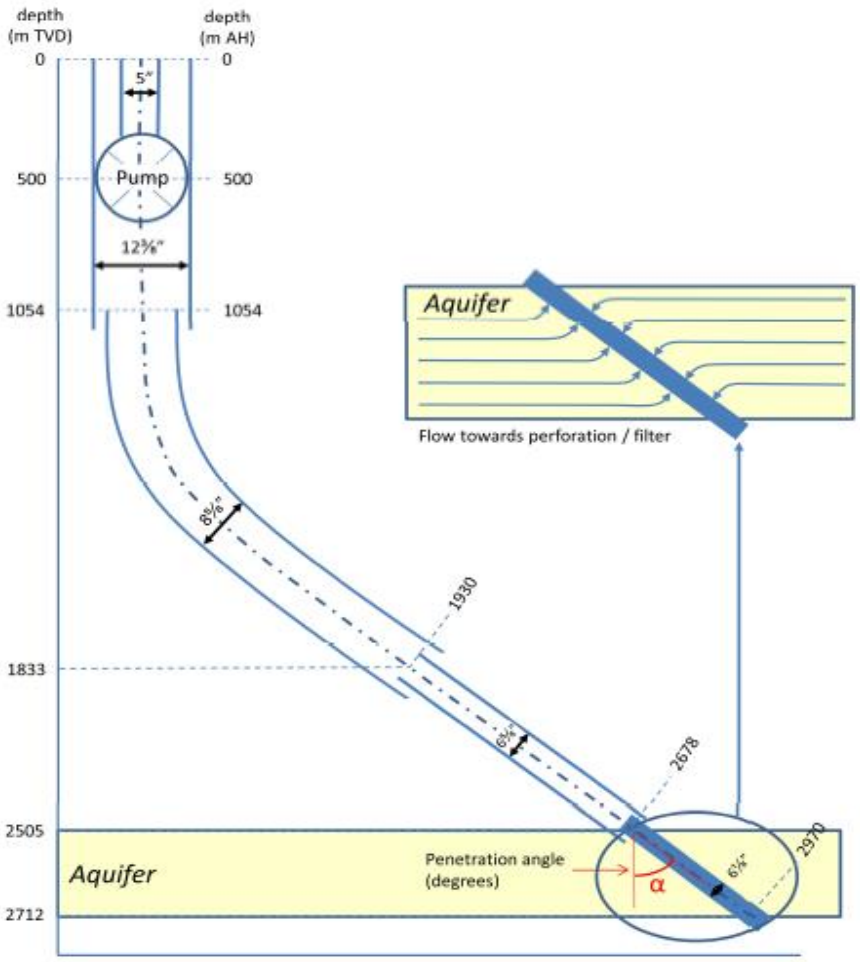

Figure 4: Schematic casing design. The part of the casing located in the reservoir (solid blue) should only be specified under specific circumstances [2].

The software asks the user to divide the well in segments, as can be seen in the picture, for each segment the user must define the pipe length of the segment (relative to the along hole (AH) and true vertical depth (TVD) measures), the pipe inner diameter (in inches) and the pipe roughness (in milli-inch). The software does not ask to specify the last part of the well that is inside the reservoir. The parameters of this part of the input screen help the software to determine the resistance encountered by the geothermal fluid when flows through the pipes in the production and injection wells.

In the two figures previously shown it can be seen that the first segment of the well is specified with a small diameter, then increases after the downhole pump and later starts to decrease until the well reaches the top of the reservoir. Taking as reference the direction of the flow going from the reservoir to the surface, the decrease of the diameter segment after the downhole pump can be explained by the fact that after the pump, to achieve the desire pressure boost, the section of the well must be smaller than the one before the pump, is because of this that, as it can be appreciated in the Figure 4, after the downhole pump the flow enters in a pipe with smaller diameter that the one of the well at the inlet of the pump.

Another consideration that must be mentioned is that the use of an injection pump is not mandatory; in fact, DoubletCalc does not contain any input that allows the user to simulate a theoretical injection pump. In the case that the user wants to consider one, the pressure difference that must be specified for the production pump should be treated as the sum of the pressures of the production and injection pump. The same goes for the efficiency, which is the effective efficiency of both pumps [2]. In the right column of the Figure 3, it can be appreciated that the developers of the software considered in the suggested example the presence of a theoretical injection pump in the first segment of the casing scheme. Due to the fact that the software does not consider an injection pump and that the introduction of a theoretical pump in the injector casing scheme does not affect very much the results, it was not taken into account the presence of an injection pump in the well scheme for the simulations performed on this work.

The next two figures present the output screen of DoubletCacl. The left column shows all the inputs set by the user and considered by the software for the calculation. On the other hand, the right column shows all the results obtained after the simulation, the first two blocks expose the outputs of the stochastic simulation; every output in this section is presented with the probabilistic approach that was discussed before. The third and fourth blocks show the same results of the first two but just for the median value of the simulation, with the addition of the pressure at the heat exchanger at the end of the fourth block. The following two pictures show the output screen with the results of the example suggested in the software manual:

probabilistic plots | fingerprinting | export base case details

file: ... DoubletCalc\DoubletCalc_143_03022016\pruebas\primera prueba (ejemplo del manual) caso1.xml

Geotechnics (Input)

Property	min	median	max
aquifer permeability (mD)	199.0	200.0	201.0
aquifer net to gross (-)	0.99	1.0	1.01
aquifer gross thickness (m)	99.0	100.0	101.0
aquifer top at producer (m TVD)	1800.0	2000.0	2200.0
aquifer top at injector (m TVD)	1800.0	2000.0	2200.0
aquifer water salinity (ppm)	69999.0	70000.0	70001.0

Geotechnics (Output)

Monte Carlo cases (stochastic inputs)	P90	P50	P10
aquifer kH net (Dm)	19.84	20.0	20.15
mass flow (kg/s)	29.82	30.48	31.14
pump volume flow (m³/h)	104.1	106.5	109.0
required pump power (kW)	142.2	145.5	148.9
geothermal power (MW)	3.58	4.01	4.46
COP (kW/kW)	25.1	27.6	30.0

Figure 5: Outputs of a simulation example using DoubletCalc (part 1) [2].

Property	value
number of simulation runs (-)	1000.0
aquifer kh/kv ratio (-)	1.0
surface temperature (°C)	10.0
geothermal gradient (°C/m)	0.03
[mid aquifer temperature producer (°C)]	0.0
inital aquifer pressure at producer (bar)]	0.0
[initial aquifer pressure at injector (bar)]	0.0
exit temperature heat exchanger (°C)	35.0
distance wells at aquifer level (m)	1500.0
pump system efficiency (-)	0.61
production pump depth (m)	500.0
pump pressure difference (bar)	30.0
outer diameter producer (inch)	7.0
skin producer (-)	0.0
skin due to penetration angle p (-)	-0.94
pipe segment sections p (m AH)	500.0,1000.0,1566.0,2415.0
pipe segment depth p (m TVD)	500.0,1000.0,1400.0,2000.0
pipe inner diameter p (inch)	5.0,12.38,8.62,6.62
pipe roughness p (milli-inch)	1.2,1.2,1.2,1.2
outer diameter injector (inch)	7.0
skin injector (-)	0.0
skin due to penetration angle i (-)	-0.94
pipe segment sections i (m AH)	50.0,1000.0,1566.0,2415.0
pipe segment depth i (m TVD)	50.0,1000.0,1400.0,2000.0
pipe inner diameter i (inch)	5.0,12.38,8.62,6.62
pipe roughness i (milli-inch)	1.2,1.2,1.2,1.2

aquifer pressure at producer (bar)	189.72	201.03	212.78
aquifer pressure at injector (bar)	189.91	201.01	212.4
pressure difference at producer (bar)	11.2	11.4	11.62
pressure difference at injector (bar)	17.65	18.01	18.4
aquifer temperature at producer * (°C)	68.19	71.51	74.83
temperature at heat exchanger (°C)	66.04	69.08	72.15

base case (median value inputs)	value
aquifer kH net (Dm)	20.0
mass flow (kg/s)	30.49
pump volume flow (m³/h)	106.6
required pump power (kW)	145.6
geothermal power (MW)	4.01
COP (kW/kW)	27.6

aquifer pressure at producer (bar)	201.02
aquifer pressure at injector (bar)	201.02
pressure difference at producer (bar)	11.41
pressure difference at injector (bar)	18.03
aquifer temperature at producer * (°C)	71.5
temperature at heat exchanger (°C)	69.07
pressure at heat exchanger (bar)	14.62

* @ mid aquifer depth

Figure 6: Outputs of a simulation example using DoubletCalc (part 2) [2].

The reservoir parameters should be estimated considering geothermal maps and previous geological, petrophysical, hydrological and geophysical studies. While the casing and pump specifications are design choices that the user should define.

For each run of the simulation and within the range of the estimates considered for the probabilistic simulation, a random value from each of the triangular distributions is chosen and the calculation is executed based on this random value. The results of the simulation are registered, and the process is repeated again. By the time the simulation has finished, DoubletCalc presents the percentile 90, 50 and 10 of the probabilistic distribution (Figure 5 and Figure 6). However, there are additional options to analyze the results offered by the software, for instance the stochastic plot shown in the Figure 7, which reports the results of the probabilistic distribution of the pump volume flow, the geothermal power or the COP:

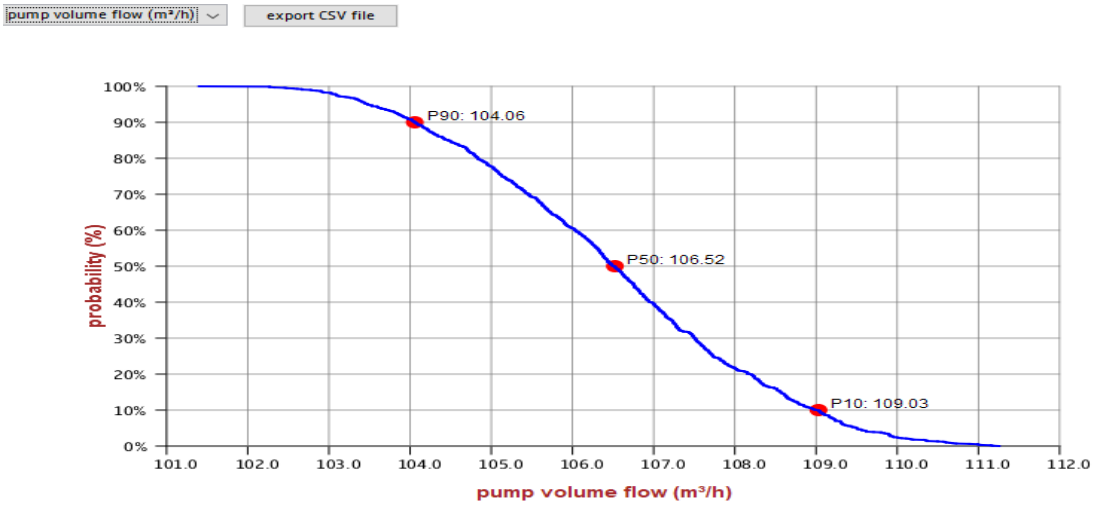

Figure 7: Stochastic Plot for the pump volume flow obtained from the example presented in the manual of DoubletCalc [2].

Based on this example, the value of the highest probability of success is the P90, which establish that there is a 90% of probability that the pump volume flow will be higher than 104.06 [m^3/h]; while in the case of the P10, there is a 10% of probability that the value will be higher than 109.03 [m^3/h].

Another option to analyze the outputs of DoubletCalc v1.4.3 is the 'Fingerprint graph' that can be seen in the Figure 8. This option generates a graph of the variation of the geothermal power (green line), the COP (purple line), the flow rate (red line) and the required pump energy (blue line) with respect to the pump pressure difference. This tool also gives the user the possibility to export the data of the graphs to an CSV file. The calculation of these graphs considers just the median values of the simulation.

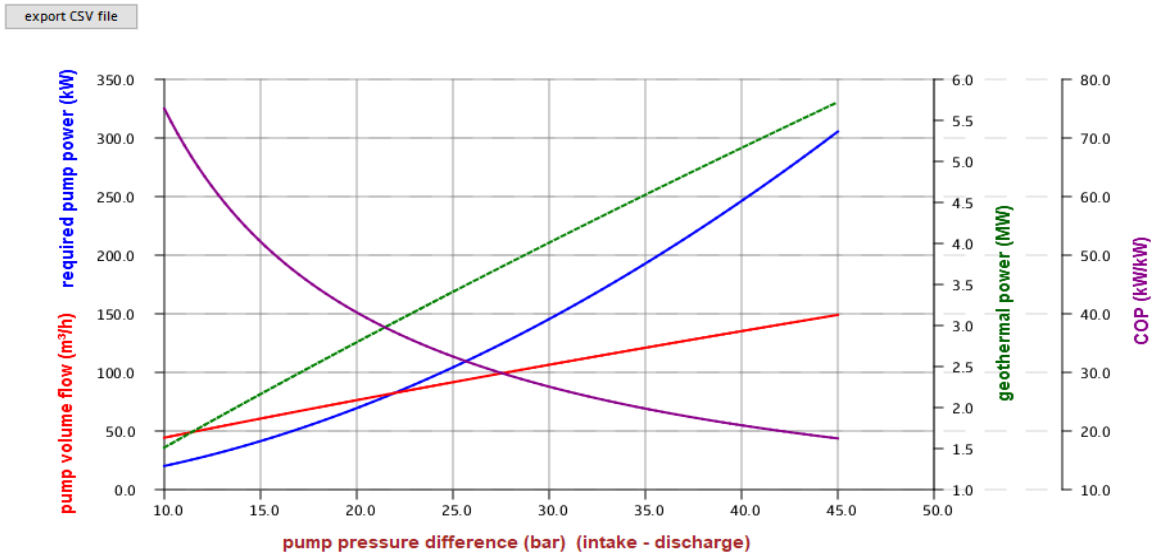

Figure 8: Fingerprint graph of the example presented in the manual of DoubletCalc v1.4.3 [2].

1.3.3 Aspen Plus

As it was discussed, simulation of the ORC plant was done using the commercial software Aspen Plus v10.0, which is an advanced simulation tool widely used in the field of industrial processes. Within the software there are a vast number of thermodynamic models and methods for the calculation of properties; besides, there are also a quite large database of physical and chemical properties of many species that are usually employed for engineering applications, which are taken from the National Institute of Standards and Technology (NIST).

Aspen Plus has a user-friendly graphical interface, which allows the user to perform simulations even with a basic-level knowledge. The first step for every simulation is the selection of the species, which in this case would be the geothermal water (assumed as pure water) and the working fluid. Then, Aspen Plus ask the user to determine the thermodynamic model to be used for the simulation.

After the specification of the species and the thermodynamic model that govern its properties, the user can draw the layout of the system in a dedicated section for that, in this section the required components are inserted and connected between each other. After or during the drawn of the system, the characteristics of each component and flow must be defined (temperatures, pressures, mass flow rates, efficiencies and so on). At this point the user also has the possibility to establish any calculation options, which can be done with the help of Excel or Fortran, which are integrated in the software. Aspen simulates the plant and derives a solution respecting the equations of the momentum, mass and energy balance, it is also possible and very convenient to perform sensitivity analysis of the plant.

II. Theoretical Framework

2.1 Nature of geothermal resources

As the name says, the geothermal energy is the thermal energy stored within the Earth, which can be extracted and then exploited depending on the characteristics of the geothermal resource. This kind of energy is practically present in every place of the planet, and in some cases, it can be seen through geological phenomena on the surface, such as geysers, hot springs, volcanic eruptions, etc. However, not all places have the geothermal characteristics needed to be able to exploit efficiently these resources.

There are a big number of different rock types that conform the composition of the Earth's crust, these rocks contain radioactive isotopes, among which some of the most relevant in this discussion are the Uranium (U-235, U-238), Thorium (Th-232), and Potassium (K-40) [4]**.** The heat that is continuously released by the radioactive decay of these isotopes, in combination with the heat that was "inherited" by the Earth from when was formed, is thought to be the thermal energy stored within the Earth. To have an idea about the immense potential of the geothermal energy, it is worth mentioning the estimation of the total heat flow from the Earth made by Stacey and Loper [5]; This estimation established that the total heat flow from the Earth is 42×10^{12} [W], 8×10^{12} [W] coming from the crust (2% of the total volume of the Earth but with a high content of radioactive isotopes), 32.3×10^{12} [W] from the mantle (82% of the volume) and 7×10^{12} [W] from the core (16% of the volume and does not contain radioactive isotopes). In view of this huge amount of energy available for exploitation, and the fact that it is expected to remain available for millions of years to come, the thermal energy from the Earth's interior can be practically considered as a limitless resource and therefore a renewable source of energy.

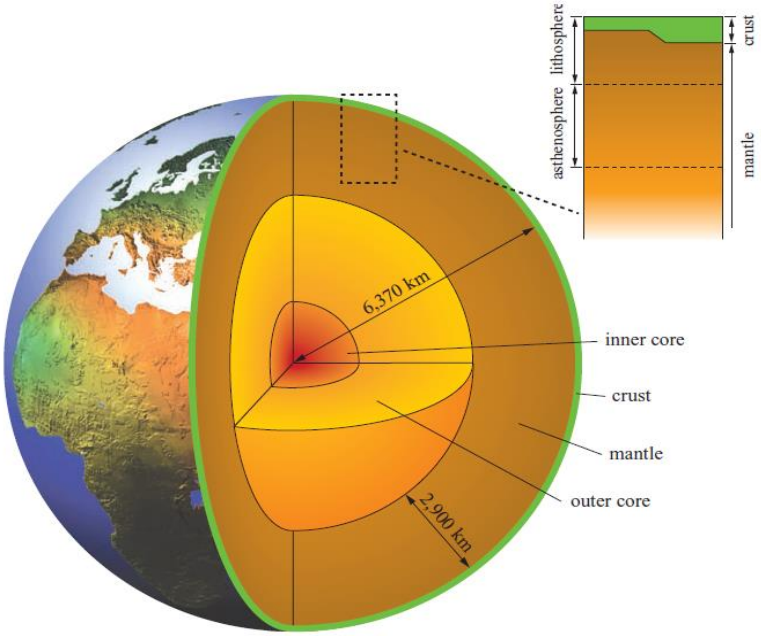

Figure 9: The Earth's crust, mantle and core [6].

The difference between the surface temperature and the temperature of the underground layers of the Earth cause the manifestation of a permanent heat flow transferred by conduction and convection from the core to the crust of the Earth. The rate at which the temperature increases with respect to the depth it is called geothermal gradient, and considering a surface temperature of 10°C, it has an average value of 25 to 30°C/km [7]. The geothermal gradient is a key parameter for the development of geothermal energy projects; the higher the geothermal gradient, the higher the possibility to find suitable places for potential development. However, it is not possible to find high geothermal gradients anywhere in the world, there is a lot of dependence on the composition of the underground layers and because of this it variates considerably depending on the location. Unfortunately, nowadays there is still quite a lot of uncertainties concerning the subsurface of the planet and its behavior, the current technology allows to do explorations of just a few kilometers, which made impossible to fully exploits the geothermal potential of the Earth in these times. In the Table 1 it can be seen the Model of the Earth, its atmosphere and an estimation of temperature and density at certain important layers.

Region	Distance from surface [km]	Approx. temperature [°C]	Density [g/cm^3]
Thermosphere	[300-85]	from 1125 to -90	from 3 x 10^{-14} to 2 x 10^{-8}
Mesosphere	[85-50]	from -90 to 0	from 2 x 10^{-8} to 1 x 10^{-6}
Stratosphere	[50-12]	from 0 to -60	from 1 x 10^{-6} to 3 x 10^{-4}
Troposphere	[12-0]	from -60 to 10	from 3 x 10^{-4} to 2.7 (continental)
Surface	0	10	from 2.7 (continental) to 3 (oceanic)
Crust	[0-35]	from 10 to 1100	from 3 to 3.3
Mantle	[35-2900]	from 1100 to 4100	from 3.3 to 7.95
Liquid (iron) core	[2900-5100]	from 4100 to 5200	from 7.95 to 11.5
Solid inner (iron) core	[5100-6350]	from 5200 to 6600	11.5
Center	6350	6600	11.5

Table 1: Data on the earth and its atmosphere [7].

In light of the previously stated, it can be clearly concluded that there is a direct relationship between the natural movement of tectonic plates and the proper conditions for the exploitation of geothermal resources; in few words, the interaction between tectonic plates produce deep earthquakes, as effect of these the magma from deep layers of the subsurface rise to the surface through active volcanoes, which helps in the same way the heat flow to rise to shallow reservoirs. The most important interaction between tectonic plates, from the perspective of geothermal energy, is the one that takes place along the edges of the Pacific Plate, better known as "The Pacific Ring of Fire" [7]. In the Figure 10 it can be notice that the most attractive locations for future geothermal exploitation are located along The Ring of Fire, also that most of the installed capacity in that date was in countries that are part of the ring, and lastly that there is still an enormous potential for future projects.

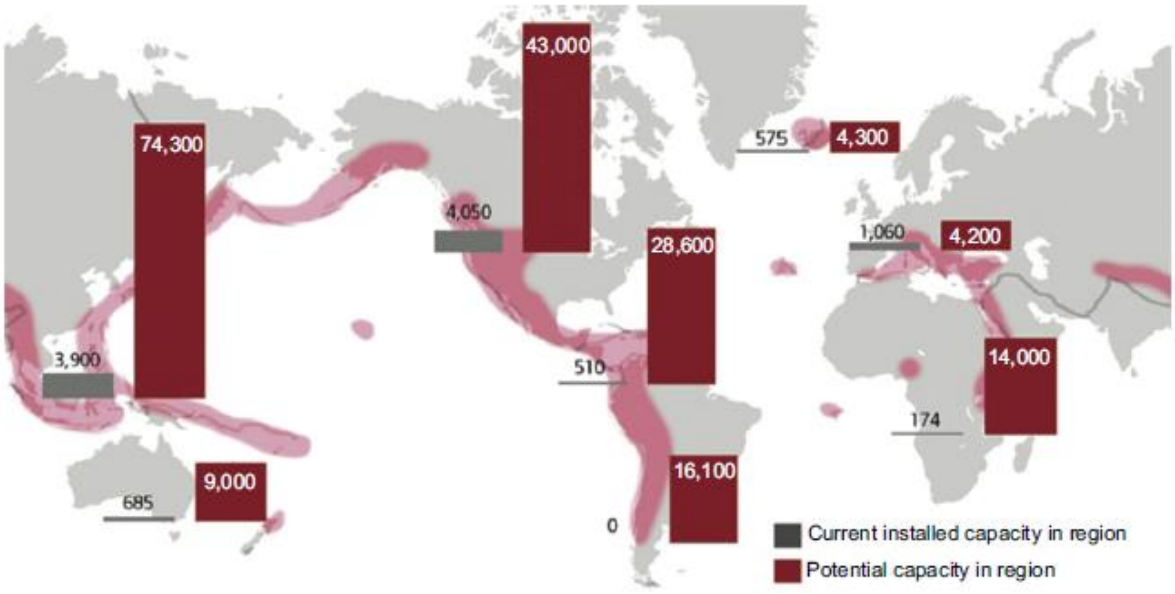

Figure 10: Distribution of geothermal potential along with the ring of fire (2011) [8].

As it was earlier mentioned, the planet Earth is compounded by concentric layers that can be essentially divided in the crust, the mantle and the core. The crust has an average thickness of 5-10 [km] in oceanic zones and 20-65 [km] in continental zones, the mantle about 2900 [km] of thickness and the core has a radius of 3470 [km] approximately. The most external layer of the planet is called lithosphere, it is characterized by a rigid body behavior (in terms of movement) and its thickness goes from a minimum around 80 [km] in oceanic areas to a maximum of 200 [km] in continental areas; from the Table 1, it can be assume that the lithosphere comprises the crust and the upper part of the mantle. After the lithosphere comes the asthenosphere, which is completely made up of the mantle with a thickness of 200-300 [km] and a molten but highly viscous behavior (far less rigid than the lithosphere) [9].

The Figure 11 shows how a subduction zone is formed due to the movement of tectonic plates and why the zones near the plate's boundaries correspond to the zones with the most significant volcanic and earthquake activity.

The constant heat flow transferred by convection and conduction from the deepest parts of the Earth provokes a slow but permanent movement inside the planet. The great temperature difference among layers motivates a corresponding density difference, so the hotter and less dense bodies of rock tend to rise with the plates movements towards the surface, while the colder and denser bodies located in the shallow layers tend to sink, where they will be heated to restart the cycle [6]. In some specific cases, these hot bodies of molten rocks (magma) coming from the asthenosphere, make their path upwards until the surface pushing and breaking the lithosphere, creating in this way a volcano; as a consequence, these kinds of events are accompanied by the

formation of subduction zones. As it can be appreciated in the Figure, a subduction zone is described by the sinking of the lithosphere under its bordering layer until descends to the hot deep zones, where it is heated by the mantle. It is more common to find sort of phenomena in the oceanic zones where the lithosphere is thinner [9].

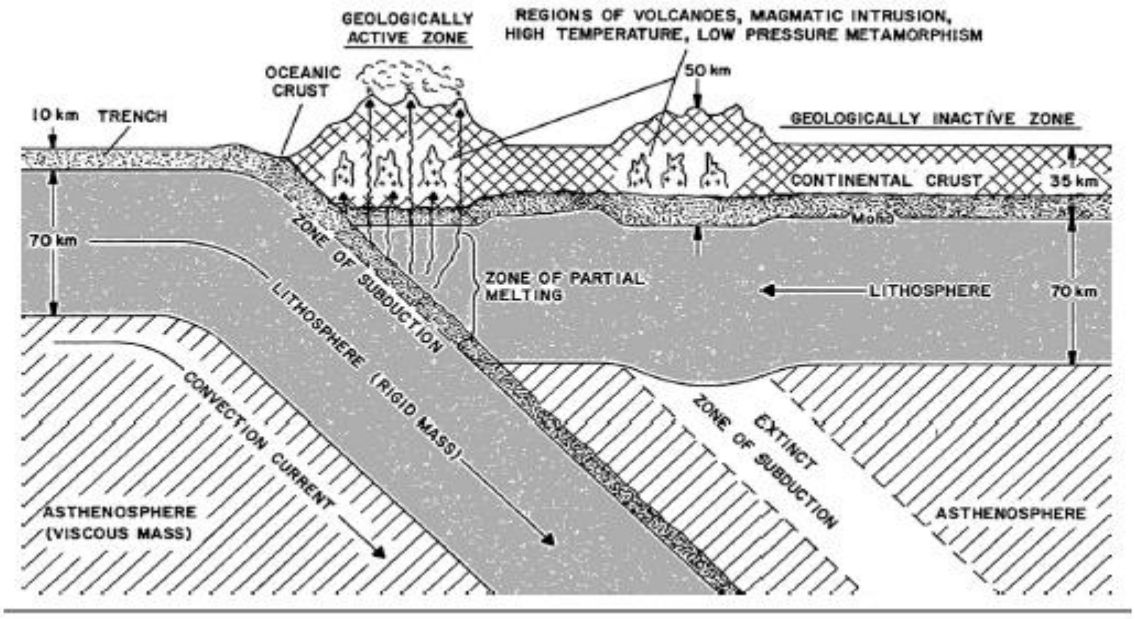

Figure 11: Schematic model of a trench or subduction zone [7].

These magmatic areas that remain in the crust under the volcanoes constitutes a quite valuable heat source for further utilization. Taking this into account, if the surroundings possess the proper conditions, such as high precipitations (or a big water source), rock fractures in the underground (which allow the water circulation), and so on; it could be expected to discover reliable geothermal resources in that region [9]. Because of this information and all what was discussed before, the plate-boundary zones and the volcanic regions are the principal targets for geothermal explorations.

2.2 Geothermal system

As Hochstein said in 1990, a geothermal system is a "convective water in the upper crust of the Earth, which, in a confined space, transfers heat from a heat source to a heat sink, usually the free surface where the heat is absorbed (dispersed or used)" [10]. The Figure 12 describes the elements that comprise a geothermal system, among which there are three main components: a heat source, a fluid and a reservoir. The first one is usually divided in three categories [11]:

- The high-temperature heat source (>180°C): Commonly located near tectonic plate boundaries or at hot spot anomalies.
- The intermediate-temperature heat sources (80-180°C).
- The low-temperature heat sources (<80°C): Normally located in continental regions.

The fluid is responsible for transferring the heat by convection from the heat source to the denser fluid stored in the reservoir and eventually upwards to the surface through the production well. Most of the times, the geothermal fluid is meteoric water (in liquid or vapor phase depending on the situation) and it often contains, after having passed through the natural fractures of the underground rocks until the reservoir, non-condensable gases (NCG) such as CO2, H2S, etc [6]. The composition of the geothermal fluid in terms of the non-condensable gases is one of the most important parameters involved in a geothermal project.

Finally, the reservoir is a volume where the fluid can be stored and recharged, formed by hot permeable rocks (which grant their thermal energy to the circulating fluid), covered by impermeable rocks and connected to recharge sources in the surface through natural or artificial rock fractures.

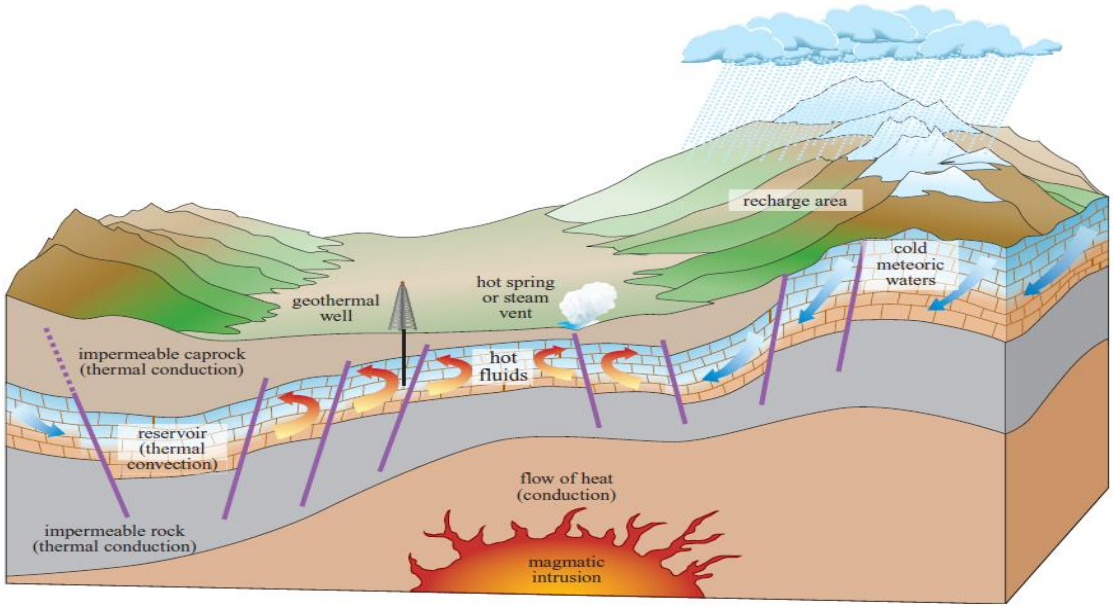

Figure 12: Schematic diagram of a geothermal system [6].

2.3 Types of geothermal systems

Geothermal resources have been classified in many different ways, one of the most common classifications is the one based on the enthalpy content of the fluid stored in the reservoir. As in the previous section with the hot source, the enthalpy content of the geothermal fluid can be divided in three groups: high, medium and low enthalpy (temperature) resources. High enthalpy resources are the ones that can be used to produce electricity with conventional power plants (temperature > 180°C). Medium enthalpy resources have temperatures between 80 and 180°C. Low enthalpy resources are generally used for direct use applications and have temperatures below 80°C, which is the minimum temperature for generating electricity using binary-cycle plants [12].

The other most widely used classification is the one proposed by White in 1973 [13]. It makes the difference between water-dominated or vapor-dominated resources, which is a fundamental distinction at the time of selection the exploitation method. In water-dominated geothermal resources, liquid water is the pressure-controlling phase; depending on the pressure and temperature of the system, they can produce hot pressurized water, water and steam mixtures, wet steam and on rare occasions dry steam. On the other hand, vapor-dominated resources are distinguished by high temperature systems that are able to produce dry or superheated steam; these geothermal resources are quite difficult to find and are the most uncommon.

There are also some classification that are not normally used, such as the one proposed by Nicholson in 1993 [14], which makes the difference between dynamic and static geothermal resources based on the fluid circulation of the reservoir and the heat transfer method. Another categorization that is worth mentioning is the one adopted by ThermoGIS [15]; they sperate the geothermal resources into three groups, depending on the depth of the well, in this way they make the distinction between shallow geothermal resources (300-1500 [m]), deep geothermal resources (1500-4000 [m]) and ultra-deep geothermal resources (4000-8000 [m]).

Aside from the classification of the geothermal resource that one might choose, the geothermal systems differ quite a lot among them in some cases depending on the properties of their environments. They all share the same main components that were discussed in the previous section, but the behavior of those components may be conditioned by the location of the geothermal system. The book of DiPippo [7] describes six different types of geothermal systems that will be explained in the following paragraphs. The most known geothermal system of this group of six is the hydrothermal system; its popularity is mainly due to the fact that it is the one used for the firsts geothermal projects and since then it has been the more commercially developed for electric energy production. It is worth mentioning that the geothermal system that was assumed in the simulations of this thesis was a hydrothermal system.

2.3.1 Hydrothermal System

The Figure 13 shows the model of a hydrothermal system; on the right part of the Figure, it can be clearly seen how the system works, and on the left part how the temperature of the fluid behaves with respect to its depth. A typical hydrothermal system has five essential elements: a big water supply, a recharge mechanism, a reservoir made by permeable rock, an impermeable rock cover and a heat source. If one of them is not available, in most cases the system will not be economically attractive for exploitation.

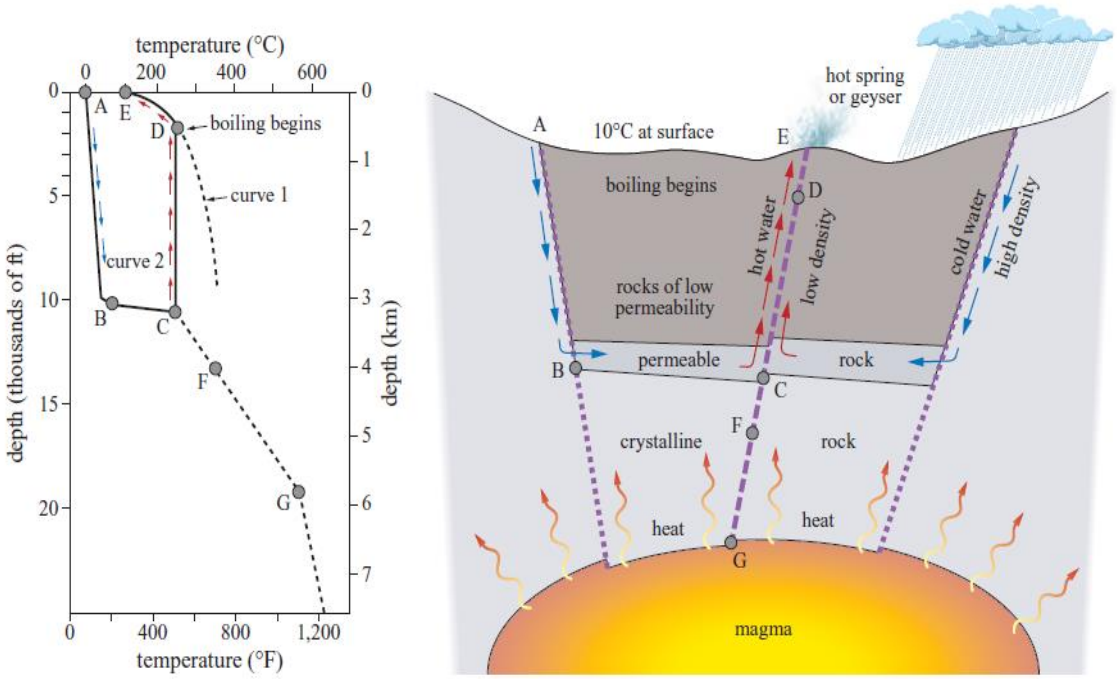

Figure 13: Model of a hydrothermal system. Curve 1 is the boiling-point curve of water; curve 2 shows the fluid temperature profile along a typical circulation path from recharge at point A to discharge at point E [13].

The model of a hydrothermal system can be describes starting by the cold recharge water coming from the rain in the Point A, then it flows through the faults and fractures until arrives to the reservoir in the Point B, there it is heated by the heat source up to the point that becomes less dense. Thanks to the permeable rock its circulation continues and in the Point C, where there is another considerable fault, the fluid tends to ascend on its way to the surface. As it rises, the fluid losses pressure till the Point D, where it reaches the boiling point for its temperature; after this point, the fluid flashes into steam and come out to the surface in the Point E as a hot spring, a fumarole or a steam heated pool.

2.3.2 Hot Dry Rock Systems

As the name says, hot dry rock system are reservoirs characterized by high temperatures from the heat sources, but low permeability and low or non-water content, which imply that they are not suitable for been exploited using the conventional technology. Having said that, it is worth saying that in a geothermal system, the only element that must be compulsory natural, is the heat source. Both the permeability of the underground rocks as the reliable recharge mechanism, can be "replaced" with artificial options. Part of the current status of the hot dry rock systems is related with these topics.

Since the first geothermal explorations, the vast majority of the projects have been focused on zones with enough rock permeability and water or steam dominated systems. Unfortunately, most of the thermal energy within the current economic and technological drilling limits comes from relatively dry resources with low rock permeability [16]. Therefore, these resources would not be ideal candidates for geothermal exploitation.

Given the great number of geothermal prospects with hot dry rock characteristics, a lot of investigations have been made since 1970s to try to take advantage of these resources [16]; the aim is to "enhance" the properties of the geothermal system, from this idea comes the name of "Enhanced Geothermal Systems" (EGS). An EGS, or an artificial hot dry rock system it is shown in the Figure 14; in this system the permeability is improved through directional drillings that intent to intersect fractures that are oriented conveniently and the later injection of high-pressure cold water (blue) to provoke hydraulic fracturing in the rock. Once the formation has achieved certain volume and permeability level, another well is drilled to intercept the artificial reservoir that has been made and to extract the hot water (red) from it. In this way a theoretical closed loop is created, in which cold water is pumped inside the artificial reservoir, heated by the heat source and extracted through the production well. At the surface, the hot water can be exploited either with a binary-cycle plant or with a flash steam plant depending on the situation.

Even though in theory hot dry rock systems (or EGS) sounds like a good idea, with the current technology there are many technical problems with their implementation that make this option not economically feasible. Nevertheless, the technological knowledge obtained thanks to the EGS can be used to improve the performance of a hydrothermal system, to increase the permeability of a formation that is starting to decrease its production, to extend the productivity and longevity of a reservoir, to enlarge the size and the output of an existing system and so on. Thus, on these days, the EGS should be seen as an option for targets on the middle ground between extreme hot dry rock systems and perfectly functioning hydrothermal systems [17].

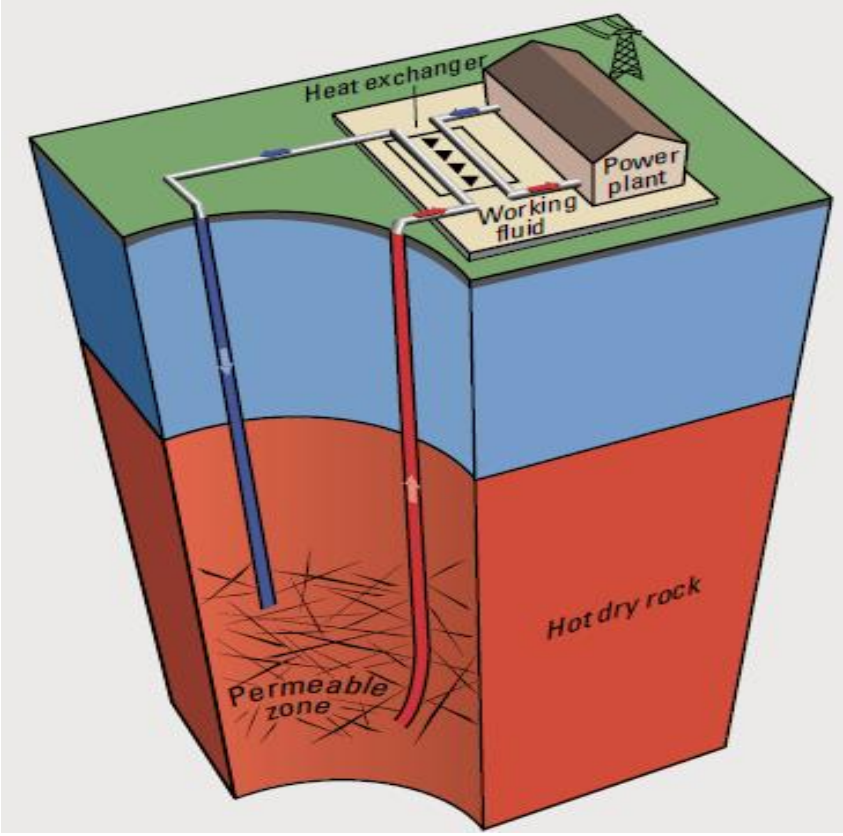

Figure 14: Schematic diagram of an artificial geothermal system (Hot Dry Rock) [17].

2.3.3 Geopressure Systems

Geopressure systems are characterized by their high-pressure level. Normally the geothermal fluid at reservoir level is submitted to a pressure value close to the hydrostatic pressure (which increases with depth proportionally to the weight of water). In geopressured systems, the geothermal fluid must support the structure of the reservoir due to the regularly subsidence of the surroundings and the compaction of the rock layers [7]. This problem causes a considerable increase in the pressure, which could even approximate to lithostatic values (pressure imposed on a layer of soil or rock by the weight of overlying material).

The most attractive attributes of a geopressured system for geothermal applications are their high temperature, their high pressure and the presence of dissolve methane in their reservoirs [6]. With these three properties this kind of systems are able to extract the thermal energy using a heat pump for instance, the mechanical energy of the pressurized water with a hydraulic turbine and lastly to sale the gas or used for combustion.

2.3.4 Magma Energy Systems

Magma energy systems has in theory the same principle of operation that hot dry rock systems, the major difference is the heat source, that in this case is magma instead of a hot rock. The idea is to drill a well till the convective magma and then inject a cold pressurized fluid with the objective of solidify part of the magma near the well. The large thermal stress imposed on the magma produce fractures on its composition; if the fluid injected is able to return to the surface through the cracks previously formed, it would be hot enough to use it to produce electricity.

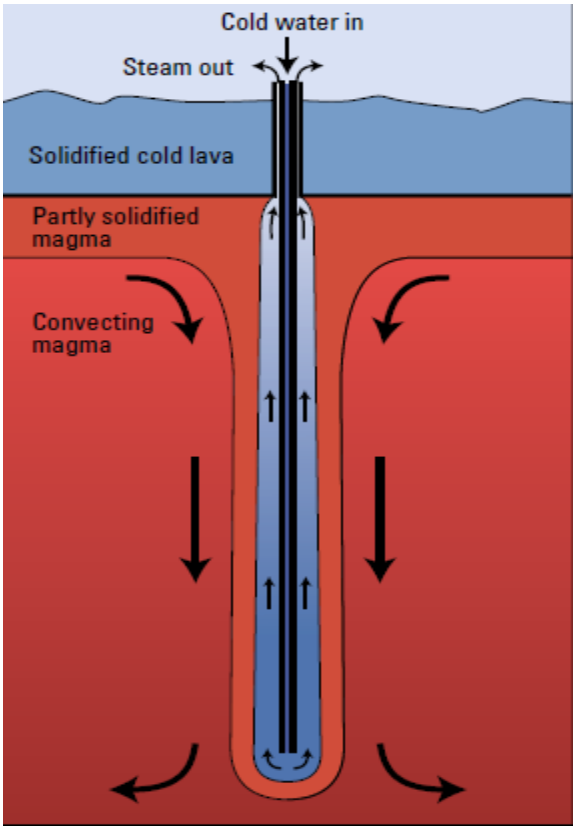

Figure 15: Schematic diagram of the process needed to obtain thermal energy from magma [17].

A magma heat source has the highest thermal energy content that can be expected to find in the planet, its temperature range goes from 650 to 1300°C [17]. Despite this geothermal system has pretty promising expectations, the economic feasibility of this technology is not expected to be achievable in the near future. The most significant constraint at present are the materials needed for the construction of a project like this.

2.3.5 Deep Hydrothermal Systems

As the name says, deep hydrothermal systems are those reservoirs that can be founded at depths around 4 [km] or more [7]. They might be located in zones with an average geothermal gradient, but given their depth, the temperature at reservoir level can be easily equal to 130°C or higher. Usually, this kind of geothermal system does not use techniques like hydraulic fracturing or some similar alternative, principally because the cost that imply the drilling of a well of this sort of depth is already very high. The geothermal fluid that it is produced from these systems is usually within the range of low-temperature resources. In some cases that have exploited a geothermal system with these characteristics, the geothermal fluid it has been used for direct heating applications before being reinjected to the reservoir [18].

2.3.6 Low Temperature Systems

Most of the geothermal resources that have been discovered in the planet are classified as low-temperature resources. As it was said in the former section, some years ago it was thought that for electricity generation, the minimum geothermal fluid temperature should be around 150°C. Nowadays the situation is changing rapidly, the huge engineering progress made by binary-cycle plants in recent years, in combination with the financial incentives that governments are giving to renewable energy projects, are creating a new context in which the low-temperature resources can be feasibly exploited by geothermal applications in many cases. Another good point in favor for these geothermal systems is their low level of scaling comparing with the conventional resources used for electricity production [7]. The main disadvantage of these resources is their low energy conversion efficiency due to the low temperature differences; this fact causes the requirement of large flow rates to generate power and consequently big equipment (high specific cost).

2.4 Reservoir Engineering

Reservoir engineering is needed to efficiently manage the production and injection of a certain fluid from a reservoir; to do this, the behavior of the fluid in this porous and fracture rock formation must be fully understand. Unfortunately, there are many uncertainties surrounding the underground characteristics, mainly because it is a very difficult environment to study and also due to the fact that it is a geologically dynamic system. Taking as reference the book of Ronald DiPippo [7] and an article made by Niyazi Aksoy [19], in the next paragraphs the most relevant relations with respect to the case of this thesis will be briefly described.

2.4.1 Darcy's Law

To begin with the description of the fluid's behavior in the underground environment, the Darcy's law must be introduced [20]. Darcy assumed in his study that a fluid with an absolute viscosity (μ), moves very slow in one direction (horizontally) through a medium with a homogeneous permeability (k) under a pressure gradient dP/dx; from these considerations he stated the equation (2.1) for the fluid velocity, in which the negative sign means that the fluid is moving towards a decreasing pressure.

$$u = -\frac{k}{\mu} \times \frac{dP}{dx} \tag{2.1}$$

To honor the contributions of Henry Darcy to this subject with his studies, the unit of permeability is called the Darcy. To have an idea of the unit, one Darcy corresponds to the slow flow of a single-phase fluid having a viscosity of 1 centipoise [cP] and a volumetric flow rate of 1 [cm^3/s] through an area with a cross-section of 1 [cm^2] under the driving force of a pressure gradient of 1 [atm/cm] [7]. It is worth mentioning that usually, for geothermal applications, the unit used for permeability is the milli-Darcy [mD].

It is worth mentioning that the permeability can be expressed as a function of the hydraulic conductivity (K), the acceleration of gravity and the viscosity (μ) and density (ρ) of the geothermal fluid [21]:

$$k = K \frac{\mu}{\rho g} \tag{2.2}$$

2.4.2 Reservoir – Well Model

In the Figure 16 it is represented the basic model of a reservoir-well system, in which the surface and the reservoir are connected through the production well.

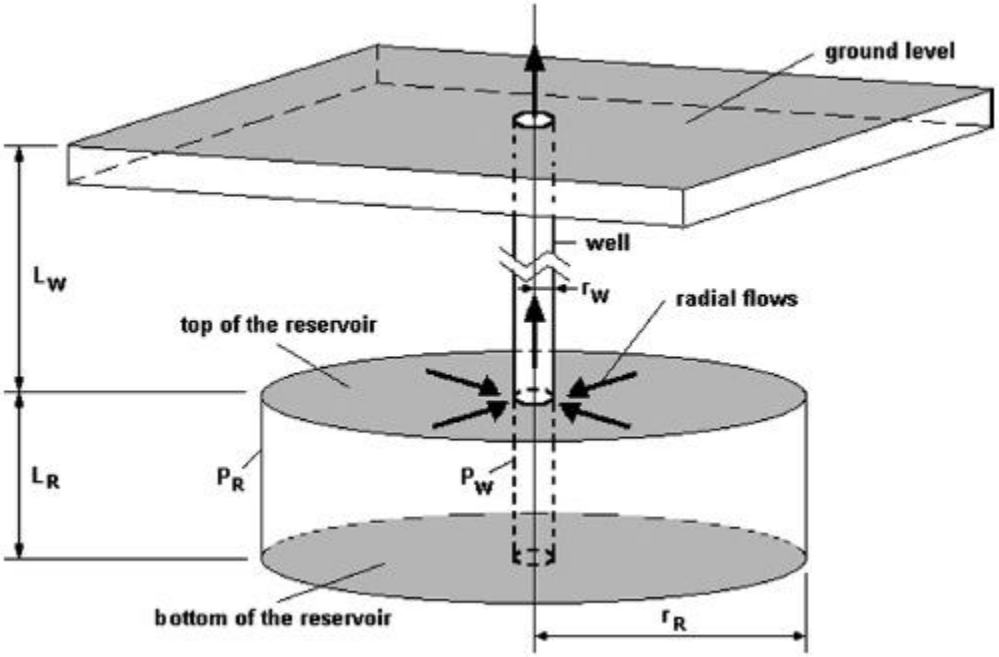

Figure 16: Schematic of simplified reservoir-well system [7].

Under steady state conditions, by continuity, the flow that passes through the well must be equal to the flow that passes through the reservoir. Considering also the Darcy's law, the pressure distribution in the reservoir as a function of the radius is given by:

$$P(r) = \frac{\mu \dot{V}}{2\pi k L_R} \times \ln(r) \tag{2.3}$$

With $\dot{V}$ being the volumetric flow rate that goes into the well, L_r the reservoir thickness and k the permeability.

The highest pressure is located in the undisturbed reservoir level, then it decreases when it enters to the well. The pressure difference between the value at the undisturbed reservoir level and at the entrance of the well is commonly called the drawdown pressure (ΔP), and it is described by the equations used by Verruijt (1970) [3] and Dake (1978) [22]:

$$\Delta P_{w,aq} = P_w - P_R = \dot{V}\frac{\mu}{2\pi k L_R R_{ntg}}\left(\ln\left(\frac{L}{D_{w,out}}\right) + S\right) \quad (2.4)$$

With:

- P_w = Pressure in the well at reservoir level;
- P_R = Hydrostatic pressure at initial conditions in the aquifer;
- $\dot{V} = \frac{\dot{m}}{\rho}$ = Volume flow; positive for flow from well to aquifer;
- μ = Geothermal fluid viscosity;
- k = Permeability of the aquifer;
- L_R = Thickness of the aquifer;
- R_{ntg} = Net-to-gross ratio;
- L = distance between production and injection well at aquifer level;
- $D_{w,out}$ = outer diameter of the well;
- S = skin factor;

This equation accounts for homogeneous aquifers with fluids in stationary conditions that flows to vertical wells. The salinity of the geothermal fluid is assumed to be constant within the whole system.

It is important to have a clear idea of the meaning of all the terms previously presented. In general, all of them should be understood just by reading the name or the symbol, except for the skin factor and net-to-gross ratio, which could be unknown parameters for some readers. The skin factor (S) is related with the resistance around the well in the reservoir section; the properties of the reservoir in the immediate surroundings of the well normally vary from the ones in the undisturbed reservoir level, and the effects of this variation are called 'skin'. The skin is commonly caused by wellbore damage, for instance due to the accumulation of the drilling mud at the inlet of the well [2]; and it represents the difference in pressure drop from the undisturbed condition of the reservoir to the current situation after drilling, completion and so on. The contribution of the skin effect to the pressure drop is given by the following expression:

$$\Delta P_{skin} = \dot{V}\frac{\mu}{2\pi k L_R} S \quad (2.5)$$

The skin is a dimensionless parameter. If the skin has a positive value it means that there is a wellbore damage and a respective extra pressure drop, while a negative value indicates a well simulated without wellbore damage and consequently reduced a pressure drop. On the other hand, the net-to-gross ratio (R_{ntg}) represents the fraction value (between 0 and 1) of the volume of rock that is able to store and/or produce fluids, such as gas, oil, water, geothermal fluid and so on [23].

By the time the fluid has arrived at the inlet of the well and starts to flow upwards to the surface, the pressure starts to decrease. The most significant pressure drops after the entering of the geothermal fluid in the well are:

- Hydrostatic pressure losses in the well, liquid section and two-phase section
- Frictional pressure losses in the two-phase section
- Frictional pressure losses in the liquid section
- Acceleration pressure losses in the two-phase section

These pressure losses, together with the drawdown pressure, can be appreciated in the Figure 17, in which it is also exposed how is the behavior of the pressure depending the value of the mass flow rate that enters the well. In this picture, the heavy line in the left part of the graph is the productivity curve, while the line in the right part is the pressure of the fluid at the inlet of the well. At the bottom, the three pressure values represent the pressure at the reservoir ($P_{R)}$, the saturation pressure (P_{sat}) and the maximum discharge pressure (P_{MD}), which is the one that correspond to the lowest mass flow rate to guarantee stable conditions.

Taking for instance a mass flow rate equal to $\dot{m}_1$, the first pressure loss that experiences after leaving the reservoir level is the drawdown (depicted as $C_D\dot{m}$, with $C_D$being the drawdown coefficient), then the hydrostatic and frictional losses in liquid state (ΔP_L), and finally, after surpassing the flashing (boiling) point, the two-phase pressure losses (ΔP_{LV}). It can be seen that if the mass flow rate increases, the boiling of the fluid begins closer to the inlet of the production well, until the point that the flash occurs before entering the well (like in the case of $\dot{m}_3$).

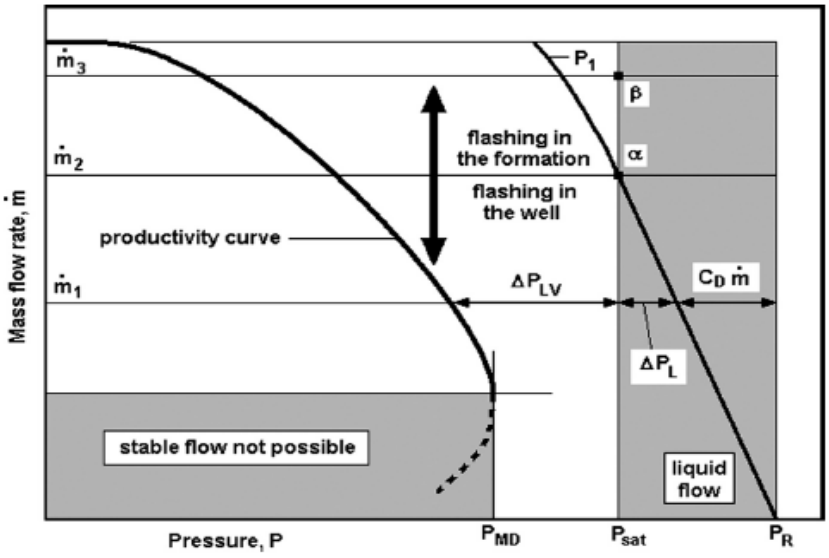

Figure 17: Flow domains from reservoir to wellhead [7].

2.4.3 Liquid-Only Flow

To what concerns to this thesis, the reservoir that will be simulated in the next sections is meant to be liquid dominated and without flashing along the production well. To be sure that the fluid is not going to boil in any point inside the well, it is necessary the implementation of a downhole pump in a certain location to avoid that the pressure drops below the flash-point.

The behavior of a liquid-only flow inside the well can be analyzed using as reference the Figure 18. As it was discussed in the previous chapter, the density difference between a theoretical cold-water column that feeds the reservoir, and the hot geothermal fluid, produce the natural flow of the geothermal fluid through the well when the wellhead valve is opened.

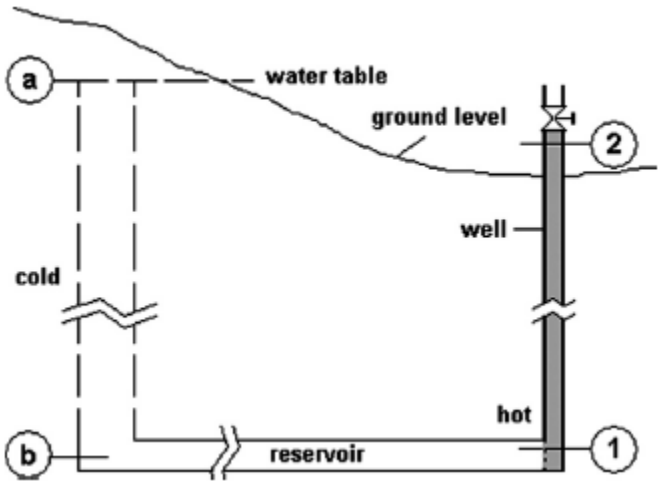

Figure 18: Possible pressurizing mechanism for geothermal well [7].

Applying the momentum equation between the points 1 and 2 in the figure for an incompressible, constant-density fluid flowing under isothermal conditions (low thermal conductivity of the surroundings and high flow velocity) along a wellbore:

$$P_1 + \frac{\rho u_1^2}{2} + \rho g z_1 = P_2 + \frac{\rho u_2^2}{2} + \rho g z_2 + \Delta P_{fr} \qquad (2.6)$$

Where ΔP_{fr} are the friction losses, $\rho g z$ are the hydrostatic losses due to the weight of the fluid (z is vertical distance to the wellhead) and $\rho u^2/2$ are the kinetic pressure changes due to fluid velocity variations, which usually are very low with respect to the other terms. Neglecting the kinetic energy term, and considering two random points within the well (i and j), the pressure difference between these points is given by:

$$P_i - P_j = \rho g(z_j - z_i) + \Delta P_{fr} \tag{2.7}$$

In light of the fact that the density is presumed to be constant, and that the velocity can also be treated as constant, the friction pressure-drop is expressed using the well-known Darcy-Weisbach equation as follows:

$$\Delta P_{fr} = \frac{8 f \rho \dot{V}^2 L_W}{\pi^2 {D_{in}}^5} = \frac{f \rho u^2 L_W}{2 D_{in}} \tag{2.8}$$

Where $L_W = z_1 - z_2$, D_{in} the inner diameter of the well, $\dot{V}$ the volumetric flow and f the friction factor. The friction factor can be found with the equation developed by Beggs and Brill [24]:

$$f = \left[1.14 - 2\log\left(\frac{\varepsilon}{D_{in}} + \frac{21.25}{Re^{0.9}}\right)\right]^{-2} \tag{2.9}$$

This equation can be used when Re > 5000. Being ε the absolute roughness and Re the Reynolds number:

$$Re = \frac{\rho u D_{in}}{\mu} = \frac{\dot{m} D_{in}}{\mu A} = \frac{4\dot{m}}{\mu \pi D_{in}} \tag{2.10}$$

These past equations that have been discussed are the principal relations needed for the behavior description of a liquid geothermal fluid in a production well. Even though it is very difficult to find a location in which a geothermal fluid is able to maintain its liquid state through all the production well and at the same time is suitable por electricity generation application.

In recent years is becoming very popular the utilization of downhole pumps for maintaining the liquid state of the geothermal fluid. The advantages of put in place this technology is not only the fact that low-to-medium geothermal resources can now be exploited to produce electricity (using binary cycles), but also to avoid problems related with the accumulation of non-condensable substances in the casing of the well (scaling). More detailed explanations about how to localize the flash point of the geothermal fluid inside the well is reported in the Appendix B.

2.4.4 Location of the production pump

As it was said in the previous section, the utilization of a production pump is crucial for the maintaining of the liquid state of the geothermal fluid in the production well. Thus, for binary plants in which low-temperature geothermal resources are exploited (like the plant that will be simulated in the upcoming sections of this work), it is quite important to calculate the proper location of the downhole pump.

The calculation of the downhole pump depth can be derived from the articles made by N. Aksoy [19], P. Bombarda and M. Gaia [25]. The Equation (2.11) was taken from these studies, which represents the suction pressure of the pump:

$$P_s = P_w - \left(d_i - d_{pump}\right)\rho g - \Delta P_{fr} \tag{2.11}$$

Where ΔP_{fr} are the friction losses between the inlet of the bottom-hole well and the inlet of the pump, d_i is the depth of the well, P_w is the pressure of the well at reservoir level, g is the gravitational acceleration, ρ is the geothermal fluid density and d_{pump} is the down hole pump's depth.

The maximum flow rate in the well corresponds to the minimum acceptable pressure value for stable conditions. Thus, if the constraint is to maintain liquid flow in every moment, the minimum pressure at the inlet of the pump must be higher than the saturation pressure. Generally, the pump manufacturer adds a security value to the saturation pressure, called the required net positive suction head; this value is specified by the manufacturer on the performance curves of the pump:

$$P_{min} \geq P_{RNPSH} + P_{sat}(T_R) \tag{2.12}$$

Other constraint that must be accounted in this calculation is the one related with the possibility of a pressure reduction in the reservoir after the start of operations. In order to prevent this problem, it is necessary to add to P_{min} an approximation of the possible reservoir pressure-drop (ΔP_d). In this way, it is established that the suction pressure at the inlet of the pump must be equal to:

$$P_s = P_{min} + \Delta P_d \tag{2.13}$$

Finally, joining the Equation (2.11) with the Equation (2.13) and clearing the terms with respect to d_{pump}, the expression for the downhole pump's depth remains as follows:

$$d_{pump} = \frac{\Delta P_{fr} + P_{RNPSH} + P_{sat}(T_R) + \Delta P_d - P_w}{\rho g} + d_i \qquad (2.14)$$

In this last equation, the term related with the friction losses (ΔP_{fr}) also contain the depth of the downhole pump (d_{pump}). Thus, to calculate this equation it is necessary to calculate ΔP_{fr} by applying the Newton-Raphson iteration method or performing an iterative process after the assumption of an initial value for d_{pump}. The reservoir pressure and the approximation of the possible reservoir pressure-drop should be determined depending on the field data.

Finally, the Figure 19 is presented to have a better understanding of the importance and operation of the downhole pump. In this picture it can be seen how the pressure behaves within the production well. After the inlet of the well, the pressure starts to decrease due to friction and hydrostatic losses until the downhole pump, located at the target depth previously calculated; then there is a pressure increase thanks to the pressure difference provided by the pump; later, the pressure starts to decrease again due to the same losses until the geothermal fluid arrives to the surface level.

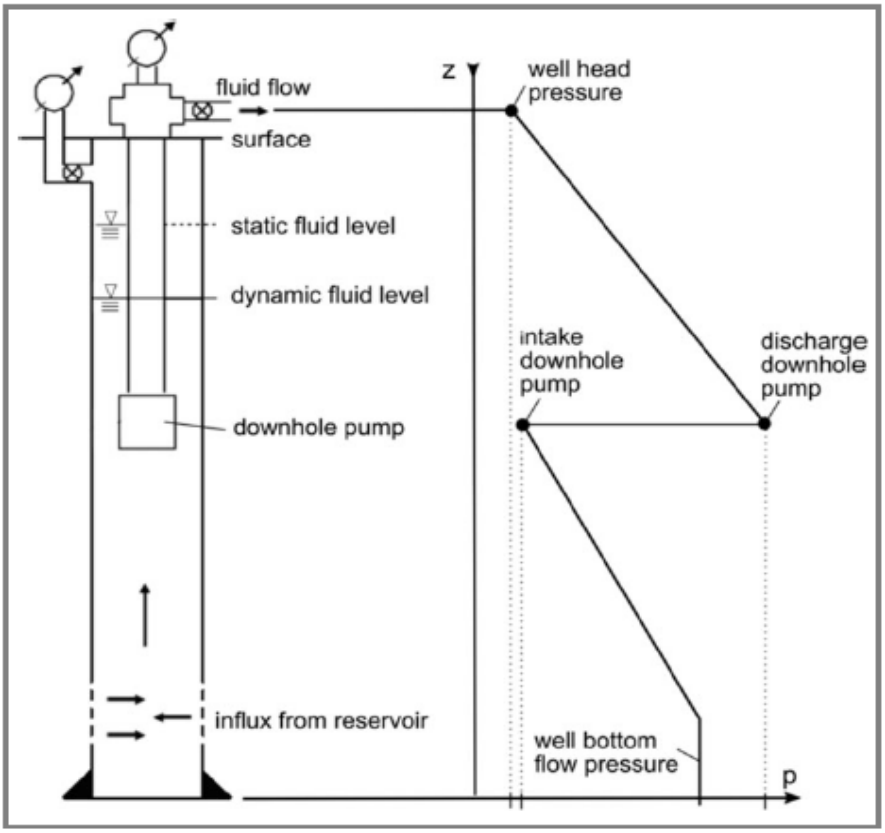

Figure 19: Scheme of a production well showing downhole pump, static fluid level and dynamic fluid level (left) and the pressure curve during fluid production (right) [26].

Back in the days downhole pumps were mainly designed and used for oil and gas applications, because of this, the higher temperatures and larger volumetric flow rates involved in geothermal projects made that the durability and efficiency of the current downhole pumps technology are not yet completely satisfactory.

In these days there are two principal types of downhole pumps, the electrical submersible pumps and the line shaft pumps. Electrical submersible pumps are characterized for being driven by an electrical motor that is located within the production well, this feature imply a wide range of application and allow the user to locate the pump at deeper target depths than the line shaft pumps. However, the fact that the motor is located inside the production well suggest potential overheating problems. Line shaft pumps have a more limited range of application due to the fact that they are driven by a shaft and an electrical motor positioned above the ground.

2.5 DoubletCalc v1.4.3.

To have a better understanding of how DoubletCalc v1.4.3 works, it is useful to have in mind the Figure 20, which represents how is the configuration of the theoretical doublet system assumed by the software. In the picture the layout is expressed as a closed system divided by multiple nodes; besides these nodes, DoubletCalc ask the user to define a number of segments in which the production and injection wells will be divided. These segments, together with the key nodes of the figure, are used for the calculation of the outputs given by the simulation:

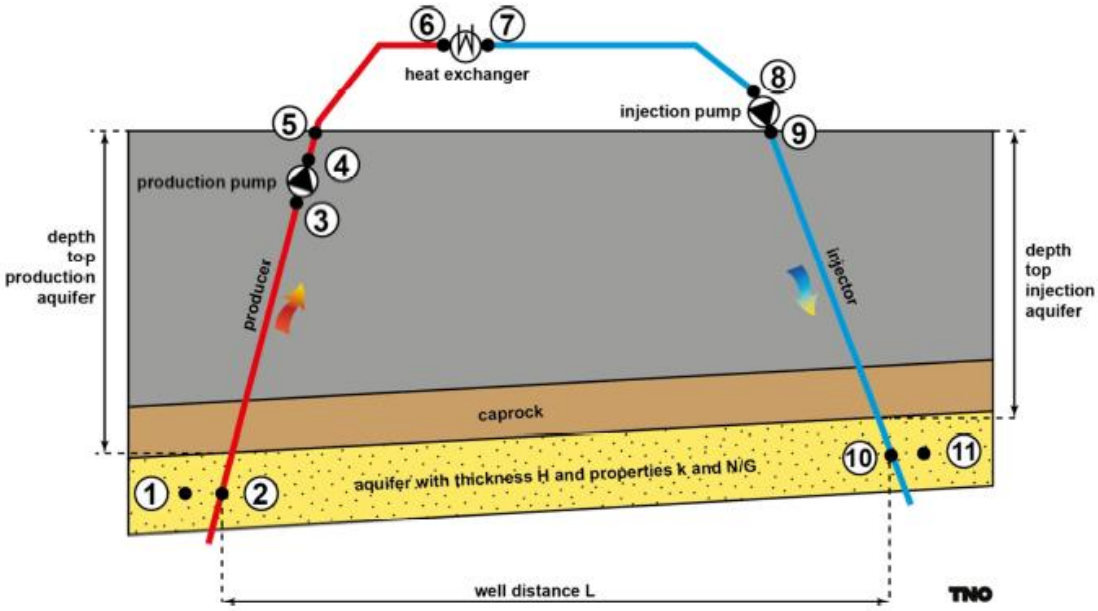

Figure 20: Schematic overview of the geothermal doublet system and its respective the nodes assumed by DoubletCalc [2].

The three principal balances that the software impose for the simulation of the desired doublet system are the mass balance, momentum balance and energy balance. These three constraints will be fully explained in the following sections, taking into account the information reported in the manual of DoubletCalc v1.4.3 [2].

The explanation of the main properties of the geothermal fluid assumed by DoubletCalc can be seen in the Appendix C. These properties are the density, the viscosity and the heat capacity. The viscosity and the heat capacity are functions of the temperature and the salinity, while the density is a function of the temperature, the pressure and the salinity of the geothermal fluid.

The drilling of the reservoir by the production and / or injection well have a direct impact on the flow towards the well depending on the penetration angle that is assumed. As it was mentioned before, the parameter that quantify this impact is the "skin due to penetration angle", and it is calculated automatically by the software using some of the inputs defined by the user. More details about the importance of the penetration angle and how DoubletCalc handles this input are reported in the Appendix D.

2.5.1 Mass Balance

Mass and Volume flow

As it is shown in the Figure 20, a closed doublet system is considered for the simulation. For this reason, the mass balance constraint establishes that the mass flow rate $\dot{m}$ [kg/s] must be constant in all elements of the system, from the inlet of the production well to the injection in the reservoir. Being said that, the equations of the mass flow and the volume flow are respectively as follows:

$$\dot{m} = constant \tag{2.15}$$

$$\dot{V} = \frac{\dot{m}}{\rho} \tag{2.16}$$

2.5.2 Momentum balance

The momentum balance determines the mass flow rate for a certain pump pressure, to calculate this the software considers the following pressure losses within all the elements of the doublet system:

- Pressure loss due to the flow from the aquifer to the production well and from the injection well to the aquifer;
- Pressure loss caused by the 'skin' in the production and injection wells;
- Pressure loss caused by the friction between the fluid and the casing;
- Pressure changes due to gravitational forces and the downhole pump within the producer;

The first thing that DoubletCalc does for the calculation of the pressure balance is to compute the hydrostatic pressures at initial conditions along the production and injection wells. To do this the software uses the following equation for each segment of the well:

$$\frac{dP}{dz} = -g\rho \tag{2.17}$$

This equation is derived from the Equation (2.7) setting the velocity to zero and consequently $\Delta P_{fr} = 0$. The software considers that the hydrostatic pressure at surface-level is 1 [bar], the salinity and temperature are assumed to increase linearly with depth. Then, using the formula proposed by Batzle and Wang [27], the density is calculated with respect to depth.

In the output screen of DoubletCalc there is an option called 'export base case details', this option gives the user the possibility to export the results of the simulation in a CSV file. Among the results given by the software, there are two tables with the hydrostatic aquifer properties at the producer and injector wells. From these tables there are two pressure values that are particularly important, the hydrostatic pressure of the reservoir at the inlet of the production well ($P_{stat,p}$) and at the inlet of the injection well ($P_{stat,i}$). The hydrostatic pressure at the inlet of the production well ($P_{stat,p}$) is the starting point for the calculation of the momentum balance, from this segment the balance is build and the pressure and temperature differences are calculated for the following doublet elements.

To describe the pressure difference between the undisturbed pressure at the reservoir and the one at the inlet of the production and injection wells at reservoir level, DoubletCalc bases its calculation in the Equation (2.4) that was discussed before in the Section 2.4.2.

For the pressure behavior in the casing, as it was mentioned before, just the pipes in the production and injection wells are considered for the momentum balance. Knowing this, three main phenomena must be accounted for the evaluation of the pressure differences when the geothermal fluid flows through the pipes:

- Gravitational forces;
- Friction / viscous forces;
- Acceleration (inertial) forces;

The inertial forces can be neglected since the geothermal fluid can be assumed as an incompressible fluid. Consequently, taking into account just the gravitational and viscous forces, and considering the Darcy Weissbach or Fanning equation [24], DoubletCalc calculates the pressure drop within the pipes using the Equation (2.7), which was presented back in the Section 2.4.3.

The last consideration for the momentum balance is the assumption made for pressure difference provided by the downhole pump to the fluid, this parameter must be specified by the user and it has a constant value:

$$\Delta P_{pump} = constant \tag{2.18}$$

As it was stated before, the presence and the correct location of the downhole pump in the production well is quite essential in the simulation of binary cycle geothermal plant; this tool enables to maintain the liquid state of the fluid through all the production well, avoiding in this way all the problems relate with scaling and phase change inside the well.

The solution method will be explained in the upcoming sections, in the meantime is enough to say that the momentum balance outlines that in all the elements within the doublet system the sum of the pressure differences must be equal to zero:

$$\sum_{K=1}^{N-1} \Delta P_{k+1,k} + \Delta P_{1,N} = 0 \tag{2.19}$$

Where N is the number of nodes in the doublet system and:

$$\Delta P_{k-1,k} = P_{k+1} - P_k \tag{2.20}$$

$$\Delta P_{1,N} = P_{stat,p} - P_{stat,i} \tag{2.21}$$

Then, if the Equation (2.21) is replaced in the Equation (2.19):

$$P_{stat,p} + \sum_{K=1}^{N-1} \Delta P_{k+1,k} - P_{stat,i} = 0 \tag{2.22}$$

These are all the equations considered by the momentum balance. As it was said, the calculation begins at the inlet of the production well, from there, in each simulation performed by DoubletCalc, the Equation (2.7) is solved numerically for the hydrostatic pressure $P_{stat,p}$ and $P_{stat,i}$. In this way, the momentum balance is built segment after segment calculating the pressure difference at a certain pump pressure and mass flow.

Finally, it is useful to summarize, for each node of the doublet system presented in the Figure 20, the conditions contemplated by the momentum balance that were discussed in this section. The conditions, interactions and equations assumed for each node are reported in the Table 2. In this table it can be noticed that the pressure losses related with the surface pipes (larger diameters and smaller lengths than underground casings) and the heat exchanger are ignored in the calculation; also, the cause and the related equation for each pressure loss is stated in the table.

From node		To node		Element	Cause of ΔP	Equation
1	Static aquifer pressure at production well	2	Bottom production well	Aquifer	Viscous forces	2.4
2	Bottom production well	3	Inlet production pump	Tubing/Casing	Viscous forces and gravity	2.7
3	Inlet production pump	4	Outlet production pump	Pump	Pressure increase by pump	2.18
4	Outlet production pump	5	Top production well	Tubing/Casing	Viscous forces and gravity	2.20
5	Top production well	6	Inlet heat exchanger	Casing	Viscous forces and gravity. Ignored	–
6	Inlet heat exchanger	7	Outlet heat exchanger	Heat exchanger	Viscous forces and gravity. Ignored	–
7	Outlet heat exchanger	8	Inlet injection pump	Casing	Viscous forces and gravity. Ignored	–
8	Inlet injection pump	9	Outlet injection pump	Pump	Not modelled separately	–
9	Outlet injection pump	10	Top injection well	Casing	Viscous forces and gravity. Ignored	–
10	Top injection well	11	Bottom injection well	Tubing/Casing	Viscous forces and gravity. Ignored	2.7
11	Bottom injection well	12	Static aquifer pressure at injection well	Aquifer	Viscous forces	2.4

Table 2: Considerations for the momentum balance in the DoubletCalc simulation [2].

2.5.3 Energy Balance

Specifically, the energy balance takes into consideration the temperature difference in the heat exchanger at surface level and the heat exchange between the production/injection well and the surrounding subsurface. The simulation starts at the production well and calculates the energy balance in every segment of the doublet system using the temperature and the pressure at the inlet of each segment and returning the temperature at the outlet. It is worth mentioning that, unlike many models, DoubletCalc does not consider that the well flow is adiabatic.

One of the most important parameters for the calculation of the energy balance is the geothermal gradient. Its value depends on the characteristics of the target location and must be defined by the user taking into consideration previous studies of the subsurface. With this parameter it is possible to derive both the initial temperature T_{gt} at the inlet of the production well and the mean reservoir temperature. The initial temperature at the inlet of the production well is needed for the calculation of the heat loss in the well and the initial reservoir temperature:

$$T_{gt} = T_{gt}(d) = T_{sur} + \lambda d \tag{2.23}$$

With:

- d = Depth (positive downward);
- $T_{sur} = T_{gt}(d = 0)$. Average yearly temperature at surface level;
- λ = geothermal gradient;

To compute the heat loss in the production well DoubletCalc calculates the heat loss per unit length of the geothermal fluid during its ascension to the surface considering the equation proposed by Garcia-Gutierrez (2001) [28]:

$$q_{w,well} = \frac{4\pi k_{t,g}(T_c - T_{gt})}{\ln(\frac{4\alpha_{t,g}t}{\sigma r_w^2})} \tag{2.24}$$

With:

- $q_{w,well}$ = Heat loss per unit length [W/m];
- T_c = Casing temperature, considered to be equal to the temperature of the fluid in the well;
- t = Time since start of heat flow;
- $k_{t,g}$ = thermal conductivity of the rocks surrounding the well;
- r_w = Inner radius of the casing;
- $\sigma = e^{\gamma}$ = 1.781072 (with Euler's constant γ = 0.577216);
- $\alpha_{t,g}$ = Thermal diffusion coefficient of the aquifer rock:

Another way to express the heat loss per unit length of the geothermal fluid to its surroundings is to consider the heat released by the geothermal fluid or formation water:

$$q_{w.well} = \dot{m} c_p \frac{dT_{well}}{dl} \tag{2.25}$$

With:

- T_{well} = Temperature of the geothermal fluid in the well;
- l = Length along the well;
- c_p = Heat capacity of the geothermal fluid;

Rewriting the Equation (2.25) in a different way:

$$\frac{dT_{well}}{dl} = \frac{q_{w,well}}{\dot{m} c_p} \tag{2.26}$$

A common value of a temperature decrease in a production well can be assumed to be equal to 1-3 °C, considering a temperature difference in the heat exchanger of about 25-40 °C, the loss of geothermal power due to this temperature drops would be approximately 3-10% [2] .

Finally, the temperature drop suffers by the fluid after passing through the heat exchanger is given by:

$$\Delta T_{hx} = T_{hx,in} - T_{hx,out} \tag{2.27}$$

With:

- $T_{hx,in}$ = Temperature at the inlet of the heat exchanger. Equal to the temperature at the wellhead;
- $T_{hx,out}$ = Temperature at the outlet of the heat exchanger. Defined by the user in the input screen:

$$T_{hx,out} = constant \tag{2.28}$$

As in the case of the momentum balance, the Table 3 summarize the most relevant equations and interactions between the key nodes of the doublet system needed for the energy balance.

From node		To node		Element	Nature heat exchange	Equation
1	Middle aquifer at production well	2	Bottom production well	Aquifer	None	–
2	Bottom production well	3	Inlet production pump	Tubing/Pipe	With surroundings	2.26
3	Inlet production pump	4	Outlet production pump	Pump	With surroundings. Ignored	–
4	Outlet production pump	5	Top production well	Tubing/Pipe	With surroundings	2.26
5	Top production well	6	Inlet heat exchanger	Pipe	With surroundings. Ignored	–
6	Inlet heat exchanger	7	Outlet heat exchanger	Heat exchanger	Heat exchanged by the heat exchanger	2.27
7	Outlet heat exchanger	8	Inlet injection pump	Pipe	With surroundings. Ignored	–
8	Inlet injection pump	9	Outlet injection pump	Pump	Adiabatic	–
9	Outlet injection pump	10	Top injection well	Pipe	With surroundings. Ignored	–
10	Top injection well	11	Bottom injection well	Tubing/Pipe	With surroundings	2.26
11	Bottom injection well	12	Middle aquifer at injection well	Aquifer	Water warmed by heat exchange with reservoir rock. Ignored	–

Table 3: Considerations for the energy balance in the DoubletCalc simulation [2].

2.5.4 Solution Method

Given the reservoir and design parameters indicated by the user, the momentum balance (defined as f_{db}) reported in the Equation (2.22) is a function of the of pump pressure difference (ΔP_{pump}) and the mass flow rate ($\dot{m}$) of the doublet system:

$$f_{db} = P_{stat,p} + \sum_{K=1}^{N-1} \Delta P_{k+1,k} - P_{stat,i} = f_{db}\left(\Delta P_{pump}, \dot{m}\right) = 0 \qquad (2.29)$$

Using this equation and given a certain pump pressure difference, the mass flow rate of the system is calculated by DoubletCalc employing the widely known secant numerical method. Then, based on the relations and equations for each node described in the Table 2 and Table 3, and considering that the temperature and the pressure at the inlet of the production well are known, after the first node the pressure and energy balance are calculated for each following segment of the doublet system with the equations presented in the previous sections.

At given temperature and pressure values at the inlet of the production well, the equations (2.7) and (2.25) are solved simultaneously for every segment of the well using the secant method, returning the temperature and pressure values at the outlet of the segments. In this way, having these values at the outlet of a certain segment, all the following segments can be calculated using the results of the previous one as inputs.

The final results of the simulation are an estimate of the temperature, pressure and mass/volume flow rate at each node of the doublet system. Also, the geothermal power, the coefficient of performance and the electrical power needed to operate the downhole pump are calculated and presented in the final outputs.

2.5.5 Calculated parameters of the doublet system

As it was discussed before in this chapter, there are three outputs that can be evaluated with a probabilistic plot after the Monte Carlo simulation executed by DoubletCalc:

- Pump volume flow [m^3/h];
- Geothermal power [MW_{th}];
- Coefficient of Performance (COP);

Geothermal power

Knowing that the heat capacity of the geothermal fluid (c_p) depends on the temperature, the pressure and the salinity at the inlet heat exchanger, the power obtainable from the heat exchanger can be calculated as follows:

$$\dot{W}_{hx} = \dot{m} c_p \Delta T_{hx} \tag{2.30}$$

Required pump power

The net power that should be provided to the downhole pump ($\dot{W}_{net,DH}$) is given by:

$$\dot{W}_{net,DH} = \dot{V} \Delta P_{pump} = \frac{\dot{m}}{\rho} \Delta P_{pump} \tag{2.31}$$

While the gross power required is:

$$\dot{W}_{gross,DH} = \frac{\dot{W}_{net,DH}}{\eta_{DH}} \tag{2.32}$$

With η_{DH} being the pump efficiency that must be indicated by the user.

Coefficient of performance (COP)

Once that the previous parameters are obtained, the Coefficient of Performance (COP) can be calculated dividing the geothermal power by the power needed for producing and injecting the geothermal fluid:

$$COP = \frac{\dot{W}_{hx}}{\dot{W}_{gross,DH}} \tag{2.33}$$

2.5.6 Range of Application

As it was already referred at the beginning of this section, DoubletCalc was designed to get pre-drill estimations of the potential productivity of a theoretical geothermal doublet system, before having to realize the first economic investments. Its development was mainly focus for its utilization as a tool for grant applications; in fact, in these days it has become mandatory for some application processes in the Netherlands, such as for the SDE+ (subsidy that stimulates the production of renewable energy) and the Guarantee fund [29].

The main target for exploration and production projects in the Netherlands are clastic aquifers [30]. These aquifers are composed by mudstone, sandstone and conglomerate, from which the first two are the most commonly found. Clastic aquifers are usually represented by decreasing porosity and associated permeability with depth, in which a reduction of the porosity level from about 25% at 1000 m depth to about 10% at 3 km depth could be expected [31]. Because of this reason, as could be expected, DoubletCalc works better and its intended to be used in clastic aquifers with homogeneous reservoir property distributions. Additionally, as it was shown in the previous sections, DoubletCalc needs many inputs parameters to perform an accurate simulation, therefore it is also advisable to select a target location in which exist reliable and statistically representative data for the simulation.

On the other hand, DoubletCalc does not perform very accurate simulations for consolidated carbonates (for instance karstified or fractured reservoirs) [1]. Even if it is possible to simulate these kinds of systems, the user should be aware and take into consideration the limitations of the software in these cases. For instance, the user could drill a well into a fault zone having a high permeability and another one outside the fault zone having low permeability, DoubletCalc cannot properly model that. For cases in which it is desired to simulate a strongly heterogenous reservoir, it is better to use another tool available called DoubletCalc2D. This software was also developed by TNO and it is briefly described in the Appendix A.

III. State of the art

This chapter has the objective to introduce the most important aspects of the geothermal energy, starting from an overview of current status of the geothermal energy in the world, in Europe, in Italy and in Chile. Also, the most important applications of this renewable energy source are presented. The topics that are described in this chapter will help to have a better understanding of the points that were developed in this work.

3.1 Current Status of Geothermal Energy in the world

Geothermal energy has many properties that, in theory, should make it very attractive for public and private investments. It has a high versatility in term of applications (electricity production and many direct-heat uses), it does not depend on climatic variations (unlike solar and wind resources), it is suitable for reliable baseload production (capacity factors around 60 and 90%), the recent technologies have practically zero emissions, and so on. Unfortunately, among the principal renewable energy technologies that are used in these days, geothermal energy is probably one of the most underestimated and one of the less developed. Just around the 2% of the world energy consumption from renewables was from geothermal energy, and just 3% is expected for 2023 [32]. The main reason of this problem is the high pre-development risks that are involved; for instance, exploration and drilling process are one of the most expensive stages in a geothermal project and they do not guarantee positive results.

The two most significant applications for geothermal energy resources are the electricity generation and the space heating. In terms of power, in 2017 the power generated and the cumulative capacity by geothermal energy reached around 84.8 [TWh] and 14 [GW] respectively. By 2023 it is expected to grow a 28% (4 [GW]) [32], with Indonesia, Kenya, Philippines and Turkey providing the biggest contributions. The distribution of the power installed and the energy consumption in 2015 can be seen in the Figure 21, in which single-flash and dry steam plants have the higher values. Binary plants have the fourth place in both diagrams, but it is expected a considerable increase of its share in the near future.

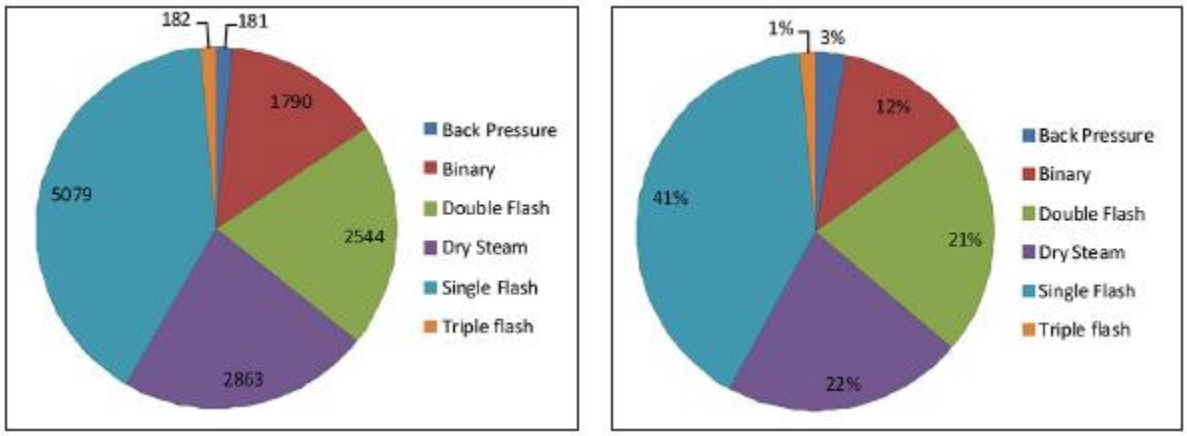

Figure 21: Installed electrical capacity [MW] and produced energy [%] for each type of plant respectively in 2015 [33].

Regarding direct heat applications, there are a limited number of countries that use this resource for direct heat production, having 80% of the consumption between China and Turkey in 2017. In 2023 the installed capacity is expected to grow about a 24% [32]. In the World Geothermal Congress (WGC) of 2015 it was stated that the direct heat utilization was 70,329 [MWt] and the total energy use was 163,287 [GWh], representing a 45 and a 38.7% increase with respect to the WGC2010 respectively [33]. With respect to the distribution, the most widely spread direct use applications are the ground source heat pumps, following by the bathing and swimming and in the third place but growing every year, the space heating.

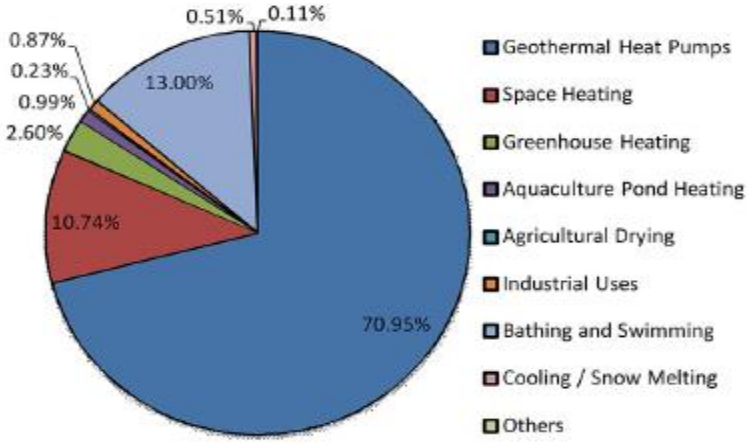

Figure 22: Geothermal direct applications worldwide in 2015 distributed by percentage of total installed capacity [MWth] [33].

Since this work has been developed with the contribution of two different universities, one from Chile and one from Italy, it makes sense to analyze the current status of geothermal energy in in the energy matrix of these two countries; therefore, in the following paragraphs is presented a brief explanation of the current situation of geothermal energy in Italy and Chile.

3.1.1 Italy

The geothermal energy, as we know it in these days, was born in Tuscany (Italy) in 1827, when François Jacques de Larderel invented a way to use the steam thermal energy from a geyser for industrial processes. Since that point the investigation and the number of new projects using this technology started to grow, being Italy one of the most important countries in the development of geothermal energy.

Regardless the vast history between geothermal energy and Italy, the share of this technology in the Italian energy matrix is not quite important; just a 2.2 [%] of all the electricity generated by Italy came from geothermal sources in 2016.

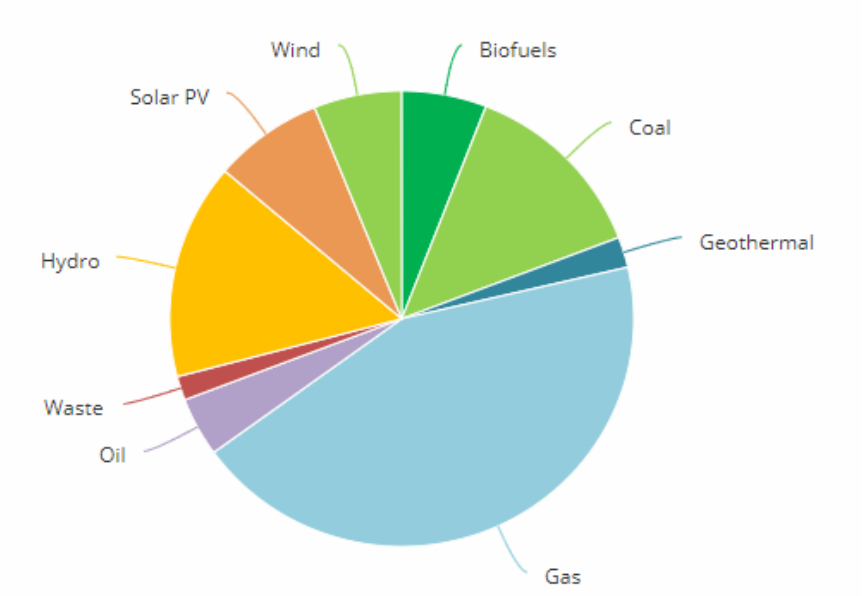

Figure 23: Share of electricity generation by fuel in Italy (2016) [32].

It is worth mentioning that on of the biggest geothermal plants of the world is located in Italy. The Larderello geothermal complex, located in Tuscany, in the same location of the first geothermal plant, has been producing electricity for almost 200 years. The power plant, owned by Enel Green Power, nowadays is composed by 34 plants with a total net capacity of approximately 770 [MW]; this electric energy supplies around two million families, 8.700 customers and 25 hectares of greenhouses [34].

Figure 24: Larderello geothermal complex, Tuscany, Italy.

Regarding the heat generation in Italy, it can be clearly seen in the following picture that the geothermal energy has a less important role than in the electricity generation field, even though in both fields the participation of this technology is much lower than fossil fuels. The share of geothermal energy in heat generation is about 0.4 [%], being the lowest after solar thermal technology.

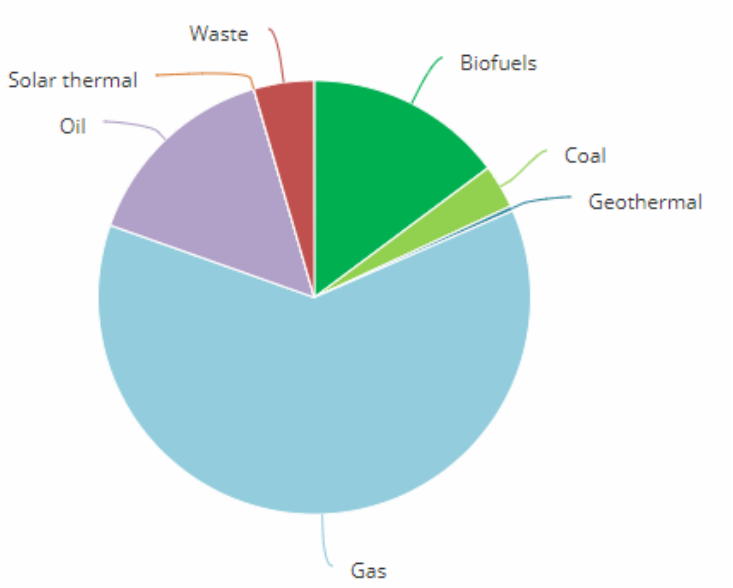

Figure 25: Share of heat generation by fuel in Italy (2016) [32].

3.1.2 Chile

As it can be implied from the Figure 10, Chile has an enormous potential for the development of geothermal projects; practically all its territory is located over The Ring of Fire and it has around 2000 volcanos, from which approximately 500 can be considered geologically active. The volcanic zones of the country can be divided into two main regions within the Cordillera de Los Andes, the northern volcanic zone (ZVN) and the southern-central volcanic zone (ZVCS). A preliminary study of these two zones, made by Alfredo Lahsen in 1988 [35], concluded that the geothermal potential of the area was around 16 [GW], with fluid temperatures higher than 150 [°C] and at less than 3000 [m] depth.

Even though Chile has a tremendous potential for the exploitation of geothermal resources, this technology has practically not been developed, either for electricity generation or for heat supply. The main constraint is related with regulatory and political issues. Unfortunately, nowadays there are not enough incentives for the implementation of this technology, which makes it an unattractive option for the investors due to its high investment cost and economic risk. Between the geothermal zones in the north and south of the country there are almost 300 locations for potential exploration and/or exploitation projects [36].

In these days, from these 300 locations, there are 11 licenses for exploration activities, 10 of these are “expired with exclusive right” and 1 is still “valid”. It is worth mentioning that the term “expired with exclusive right” mean that the exploration license period of validity has already expired; however, the holder has an exclusive right to have the State grant him the exploitation concession over the respective exploration area. This right can be exercised up to two years after the exploration license expires. From the 10 expired licenses with exclusive right, just two of them have asked for an extension, one for a project in the city of Calama (“Linzor” project) and the other in the city of San Pedro de Atacama (“Lascar” project), both in the province El Loa, region of Antofagasta. On the other hand, the only license that is still valid is for the “Peumayén” project, located in the cities of Quilaco-Curacautín in the provinces of BioBio-Malleco, regions of BioBio-Araucanía. On the other side, regarding the exploitation of geothermal resources there 8 licenses, all of them still “valid”. From these 8 licenses, 4 are located in the northern volcanic zone and 4 in the southern-central volcanic zone [37].

Among all of these licenses, the only project that has been implemented is the geothermal power plant “Cerro Pabellón”, located in the city of Ollague, in the region of Antofagasta. This plant started its operations in March of 2017 and is the first geothermal power plant of Chile and South America.

Figure 26: "Cerro Pabellón", geothermal power plant in Ollague, Chile.

The plant is located at 4500 [m] above the see level (highest geothermal plant in the world) and it counts with around 20 wells drilled at depths between 1900 and 2700 [m] [37]. Cerro Pabellón is a binary cycle plant of high enthalpy and counts with the most advanced technologies in order to handle the extreme conditions of its desertic location and altitude. From an environmental point of view, the technology used has almost zero impact on the environment (just land occupation and noise emissions during the construction), since all the geothermal fluids are reinjected into the reservoir and the condensation is done with air, avoiding in this way the utilization of water. The power plant is composed by two units of 24 [MW], making a total installed capacity of 48 [MW] that will be directly injected to the SING (interconnected system of the north) through a transmission line of 220 [kV] that arrives to the substation "El Abra" [38]. The plant is projected to inject around 340 [GWh] per year, which will supply enough energy for approximately 165000 households and reduce 166000 tons of CO2 per year.

The geothermal plant is owned the company Geotérmica del Norte S.A. ("GDN"), a company controlled by Enel Green Power Chile (81,7%) and ENAP (18,3%). The project had an investment cost of around 320 million USD and was developed under the exploitation license of "Apacheta", granted by the State of Chile in 2009. The project also received a fund of 30 million USD thanks to a mechanism called Mitigation of Geothermal Risk (MiRiG), in which the Chilean Ministry of Energy obtained the international cooperation of the Clean Technology Fund (CTF). These funds helped to handle the economic risks of the perforation process of the project, which, as it was said before, is one of the most expensive and uncertain stages of a geothermal project [37].

3.2 Applications of geothermal resources

Before exploiting a geothermal prospect, there must be a certainty that the geothermal resources are appropriate to achieve the desire outputs. To be sure about a potential place for a geothermal project, a previous exploration must be performed; if the results are positive, the drilling process can be carried out.

The geothermal explorations have the objective to determine if a certain location is economically convenient for an eventual exploitation. Because of this, an exploration program must fulfill the following goals to be considered successful:

- Locate systems powered by hot rock resources;
- Approximate the dimensions of the formation (volume, depth, thickness, etc), its permeability and the temperature of the fluid;
- Determine the chemical composition of the geothermal fluid;
- Predict a rough estimation of the electric power that could be produced for at least 20 years;
- Define if the produced geothermal fluid would be dry steam, a two-phase mixture or liquid;

To obtain the required parameters presented before [7], an exploration program has to drill exploration wells and perform geologic, hydrologic, geochemical and geophysical studies. Even though the exploration and the drilling processes are fundamental stages, in this thesis they are not going to be described in detail.

Today, the main disadvantage of the geothermal energy in comparison with other renewable sources are the high initial investment required and the uncertainty related with the exploration and drilling processes. The drilling phase, either for exploration or for deep wells, is quite expensive (one of the most expensive steps in a geothermal project), and unfortunately, the results are practically unknown in advance [16]. As soon as new competitive techniques for geothermal explorations are developed, like databases with reservoir properties, innovative drilling techniques or geothermal resource assessment tools for instance, the investment risk will decrease, and it will be easier for private and public entities to access to these resources.

After the exploration and drilling stages are complete, the geothermal resource can be exploited. The applications of this renewable resources can be separated in two divisions, the direct heat applications and the electricity generation. Although geothermal energy is commonly known for applications like space heating and electricity generation, they are much more options available for the use of geothermal energy; the Figure 27 shows some non-electrical uses in the Lindal diagram.

In this section the principal applications for geothermal energy will be briefly described. The part concerning the direct heat applications will be focused in the heat pumps technology, since is the most currently used in that field. On the other hand, for electricity generation uses there are essentially three options available on the market depending on the characteristics of the geothermal fluid (vapor, two-phase mixture or liquid), these are the dry steam plants, flash steam plants and the most recent binary plants. The main features and operation of each one of them are going to be reported in the following paragraphs.

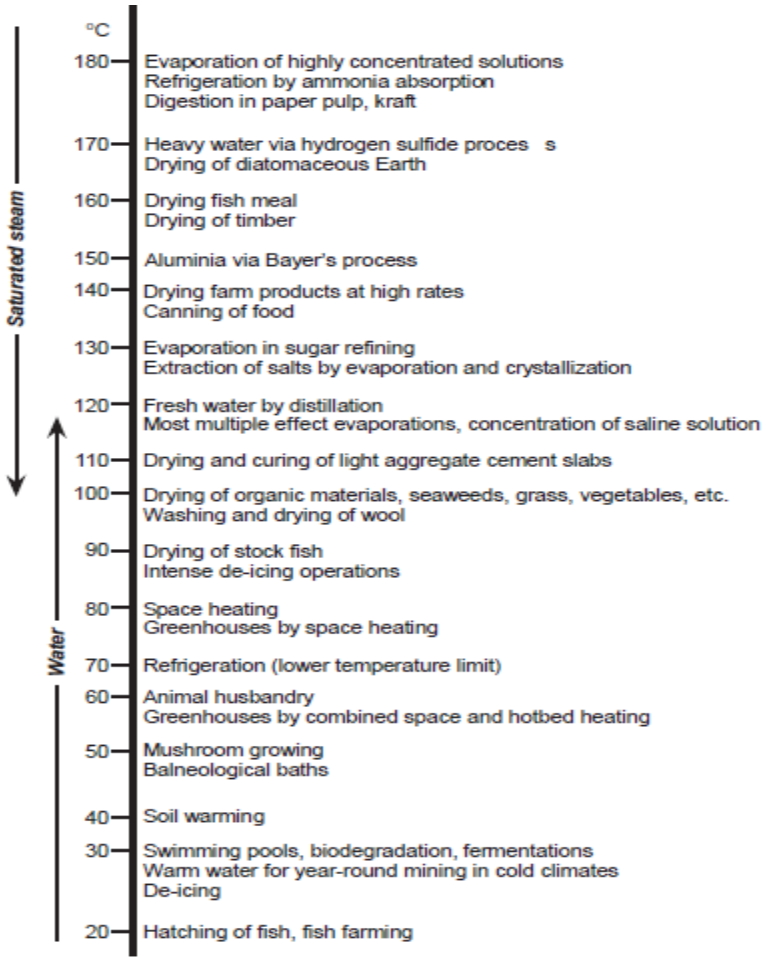

Figure 27: Lindal diagram showing the possible non-electrical uses of geothermal fluids at different temperatures (Lindal, 1973) [9].

3.2.1 Direct Heat Use

Direct heat applications are the oldest and most typically used among the geothermal energy field. It is also a quite versatile energy resource, as it is shown in the Figure 27 where some of the many non-electrical uses are reported. Regardless the great number of utilizations that exist for this resource, the most widespread in recent years and the most promising for further development in the near future is the heat pumps technology, and thanks to its introduction in 1980s, the geothermal space heating (and cooling) and domestic hot water supply have been remarkably growing [9].

The main qualities of heat pumps are to move heat in an opposite direction with respect to which it would move naturally and their capacity to "reverse" their operation mechanism, in that way they can provide space heating in winter and space cooling during summer. To perform this task, the system needs an "extra" energy input (normally electrical energy), the greater the temperature difference between the inside and outside, the higher the required energy input and the lower the efficiency.

Heat pumps exploit geothermal resources in the range of 5-30°C approximately [18], either using closed or open loop configurations. The most environmentally friendly is obviously the closed loop configuration, which is placed horizontally (1-2 [m] depth) or vertically (50-250 [m] depth) into the ground [11], then using an antifreeze-fluid that flows through the pipes, the heat is collected from the ground during winter and rejected to the ground in the summer.

Given the easy accessibility of the geothermal resources needed for the operation of heat pumps and the current status of the technologies used for space conditioning, this direct heat application represents a key element for the introduction and impulse of geothermal energy in the market. Despite the initial investment is higher than the one needed for conventional system, the energy savings during operation hours are around 75 percent more than electrical heating system and about 30-60 percent compared with other space conditioning systems that are in the market. Taking this into account, most of the studies suggest that the initial investment should be amortized after three to four years [17].

3.2.2 Electricity Generation

The exploitation of geothermal energy for electricity generation started at the beginning of the 20th century, before that geothermal resources were used mainly for leisure purposes. Today the technologies available for electricity production are commonly classified depending on the temperature (or enthalpy) range of the geothermal resource [39]:

- 80°C < T < 180°C (medium enthalpy resource): This range is typically associated with binary plants, but they are also suitable in some cases for heat & power cogeneration.
- 180°C < T < 390°C (high enthalpy resource): Dry steam, flash steam and hybrid plants can be used for this temperature range. As in the previous range, this one also has the possibility to use cogeneration plants.
- 390°C < T < 600°C (supercritical unconventional resource): The high temperatures of this range usually imply the utilization of superheated dry steam plants.

Having said that, the three main technologies for geothermal exploitation are the binary plants, flash steam plants and dry steam plants. These power plants, depending on the vapor content of the geothermal resource, produce electricity using one of the following methods:

- The vapor fraction (or dry superheated steam) of the geothermal fluid is expanded in a conventional steam turbine.
- The geothermal fluid transfers its thermal energy to a secondary low-boiling fluid in a heat exchanger, which is vaporized and then expanded in the respective turbine.

The Figure 28 shows the relation between the wellhead pressure, the mass flow rate and the power output of the plant. The selection of the power plant design depends directly on the geothermal fluid conditions at the wellhead, especially on the pressure. Knowing that the pressure is proportional to the exergy of the heat source, which is at the same time proportional to the enthalpy difference of the turbine, if the production pressure decreases, the exergy will decrease as well, and the potential power output of the turbine will be lower. Simultaneously, the power output of the turbine is calculated multiplying the mass flow rate and the enthalpy difference; but as it is shown in the Figure, the mass flow rate and the production pressure are inversely proportional. Consequently, there is an optimum value for the pressure that maximize the power output and determine which is the best option for the power plant selection. The production pressure can be controlled with a downhole pump strategically located in a certain point between the reservoir and the wellhead. In binary plants, the downhole pump is normally located below the boiling point of the geothermal fluid in the well, in this the produced fluid is in liquid phase at the wellhead and the problems related with the non-condensable gases is diminished.

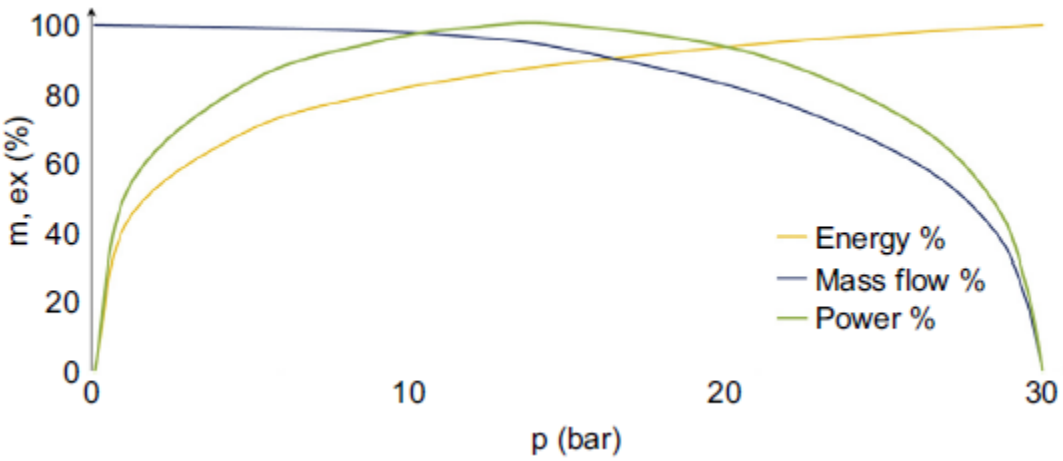

Figure 28: Optimization of well production pressure [40].

In the following paragraphs the most important aspects of each of the three main technologies for electricity generation is going to be described.

Dry Steam Plants

The Figure 29 shows the basic layout of a typical dry steam plant. Essentially, in these plants the geothermal fluid in the form of dry steam (usually superheated) is directly expanded in the steam turbine, then it is condensed using a cooling tower (in the case of the picture) and finally reinjected in the reservoir to avoid any possible environmental impact.

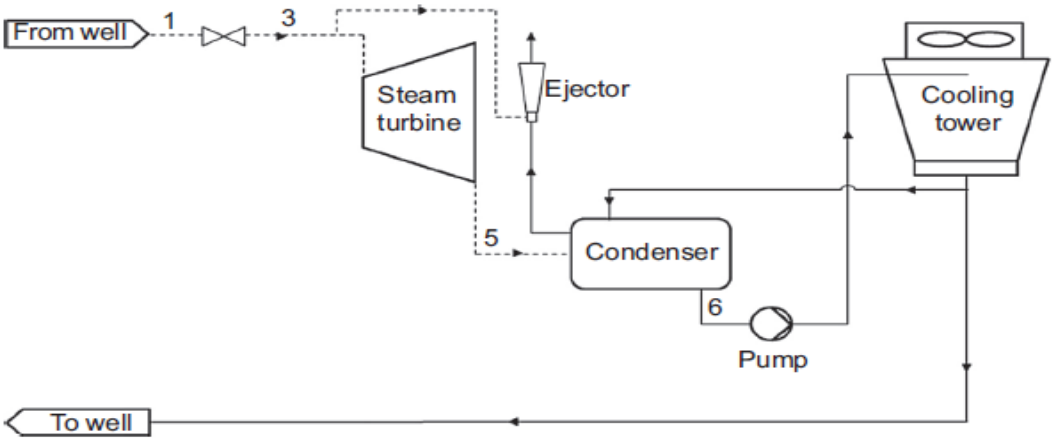

Figure 29: Dry steam plant, typical simplified flow diagram [40].

The two biggest dry steam power plants are Larderello and The Geysers, located in Italy and United States respectively. These two plants, together with other 68 units around the world (reported in December 2014), represent the 12% of all geothermal power plants and approximately the 25% of the total power capacity installed. An average dry steam power plant has a power capacity of about 42 [MW] [7].

In general, it is less complicate to implement a dry steam plant than a flash steam plant. But one of the problems that is more difficult to manage in these kinds of plants than in the others is the recharge rate of the reservoir. The natural recharge rate of dry steam resources is frequently much lower than the production rate, which cause a considerable reduction of the production pressure and a faster resources exhaustion. Approximately just 10-15% of the extracted mass can be reinjected in these plants, while in flash steam and binary plants, the 70-80% and 100% respectively can be reinjected [7].

Flash Steam Plants

These plants exploit liquid-dominated resources, but the pressure losses through the production well make that part of the fluid boils, because of this, the geothermal fluid that arrives to the wellhead has a non-negligible vapor fraction. The main difference between these plants and the dry steam plants is the presence of a flash unit before the steam turbine, in this way the vapor fraction of the geothermal fluid is separated from the liquid fraction before the turbine inlet.

One big advantage of flash steam plants is that they have the possibility to increase their efficiency by implementing more than one separation stage. Nowadays exist single-flash, double-flash and triple-flash configurations. Recent investigations have determined that double-flash plants can produce 15-20% more power than a single-flash plant with the same geothermal fluid conditions, while a triple-flash plants can produce 5-7% more power than a double-flash configuration [7]. The main drawback of these multi-flash arrangements is that the increase in the cycle efficiency due to the heat recovery, leads to a significant increase in the complexity and the cost of the power plant.

In the Figure 30 describes a basic layout of a single-flash, while the Figure 31 shows the layout of a double-flash plant. Fundamentally, the vapor fraction of the geothermal fluid is expanded in the steam turbine after the separation unit, while the liquid fraction is reinjected in the reservoir or, in some cases, used for combined-cycle or cogeneration applications before the reinjection. After the expansion, the fluid goes to the condenser, where, besides the condensation of the fluid, the non-condensable gases must be extracted. The extraction system coupled with the condenser should not be taken lightly in the calculations, their presence complicates the design and operation of the plant, increases the costs and consumes an equivalent of around 15% of the power produced by the turbine [40].

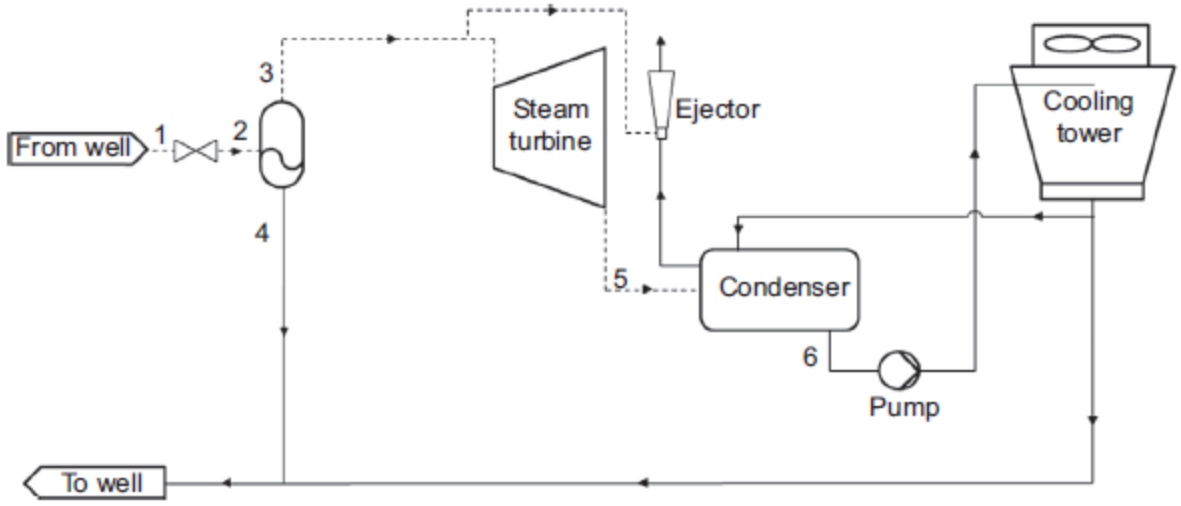

Figure 30: Single-flash cycle, typical simplified flow diagram [40].

In the case of multi-flash designs, the most important difference is that the vapor fraction from the first flash unit feeds a high-pressure turbine, while the liquid fraction, instead of being reinjected, goes to a second flash unit after the pressure reduction experienced in the valve. After being separated again, the resulting vapor fraction is expanded in a low-pressure turbine and the liquid fraction is, either separated again, used in a combined or cogeneration cycle or reinjected.

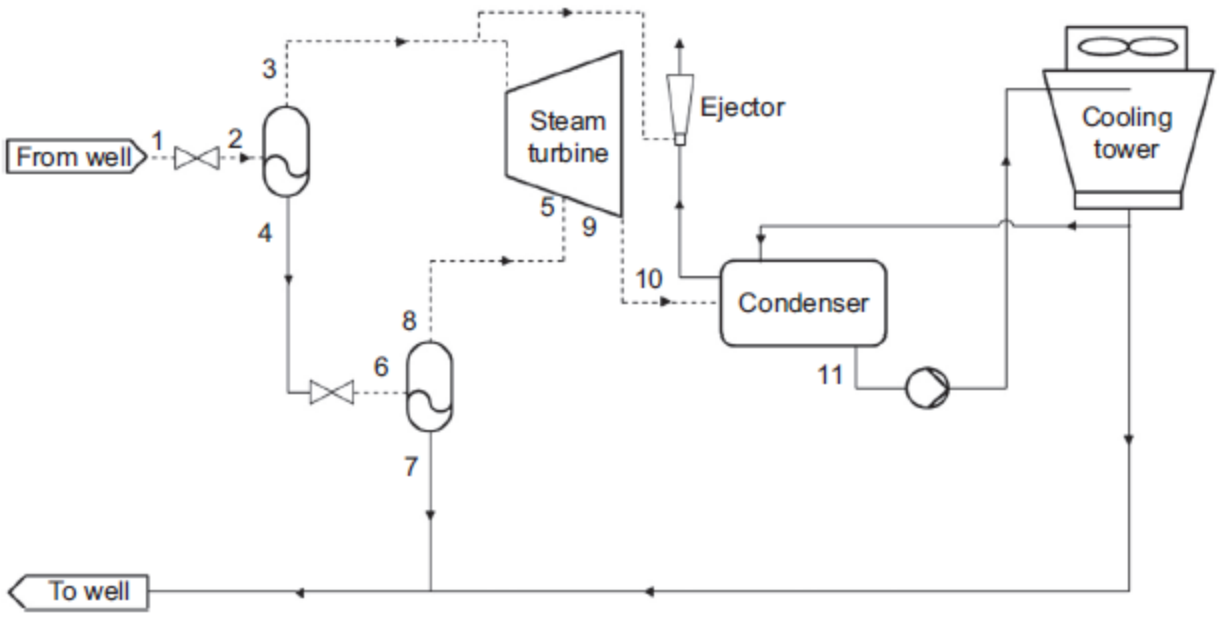

Figure 31: Double-flash cycle, typical plant simplified flow diagram [40].

Flash steam plants are the most important technology for electricity production with geothermal energy, they represent about two-thirds of the geothermal installed capacity in these days [16]. In the Table 4 it is presented a general overview of the status of flash steam plants in 2014.

Type	N° of units	% of the total (units)	Installed Capacity [MW]	% of the total (capacity)	MW/unit
Single-flash	185	32.3 %	5146	43.1 %	27.8
Double-flash	54	9.4 %	1889	15.8 %	35
Triple-flash	4	0.7 %	299	2.5 %	74.7

Table 4: Detail of the flash steam geothermal plants by number of units and installed capacity (December 2014) [7].

Binary Plants

Among the three main plant configurations for electricity generation, the binary plants are the one with the fastest growing in these days, principally because they are capable to exploit geothermal resources with low-to-medium temperature levels (80°C < T < 180°C) [39], which are the most frequently found in geothermal explorations. The upper limit of the temperature is usually governed by the stability of the working fluid, while the lower limit by technical-economic constraints (basically due to the size of the heat exchanger). Binary plant configurations can also be used in situations in which flashing of the geothermal fluid should be avoided (due to scaling risks for instance), in these cases the fluid is maintained as a pressurized liquid thanks to the implementation of a downhole pump below the flash point of the fluid.

Overall, binary-cycle plants are characterized by the utilization of a secondary fluid (also called working fluid) in the power cycle. It operates as a two closed-loops (from this concept comes the "binary" term in the name), one in which the geothermal fluid circulates through the production well, the heat exchanger and the re-injection well; and the second loop in which the working fluid circulates in a Rankine cycle. This configuration allows that neither the geothermal fluid nor the working fluid are in direct contact with the surface environment (except in the case of minor leakages). As a consequence, the environmental impact of these sort of power plants are theoretically zero, being the "cleanest" option for electricity production using geothermal resources.

The first binary plants used to use pure water as working fluid for the Rankine cycle, but the high temperatures needed for its vaporization or the risk of having liquid droplets during the expansion, among other disadvantages, cause the decrease in the utilization of water as secondary fluid.

Another type of binary plant that has been studied is the Kalina cycle. This system is generally designed as a regenerative superheated cycle, and its main feature is that the working fluid is a mixture of water and ammonia, which has the capacity to vaporize and condensate at different temperature but constant pressure [41]. This property allows the mixture to follow more efficiently the heat source curve in the temperature vs heat exchanged diagram than a pure substance [40], as it can be appreciated in the Figure 32:

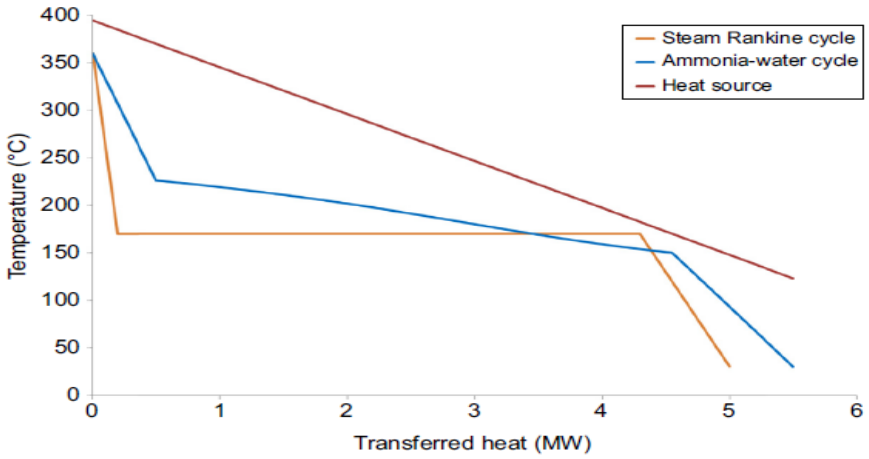

Figure 32: Comparison between T-Q diagrams of a Rankine and a Kalina cycle [40].

Even though the Kalina cycle in theory is more efficient and exhibits more advantages with respect to an Organic Rankine cycle, the significant higher complexity of the system and the technical problems that entails its implementation make difficult its commercial application.

Nowadays the most widespread and commonly used technology for geothermal binary plants are the Organic Rankine cycles (ORC). In these power plants the working fluid is an organic fluid with low boiling point and high vapor pressure at low temperatures [9], with respect to the properties of steam. As it can be seen in the Figure 33, the working fluid is heated and vaporized in the heat exchanger (thanks to the heat received from the geothermal fluid), then, the vapor is expanded in an axial turbine, cooled and condensed in the condenser and at the end, it is pressurized in its way to the heat exchanger to start the cycle again.

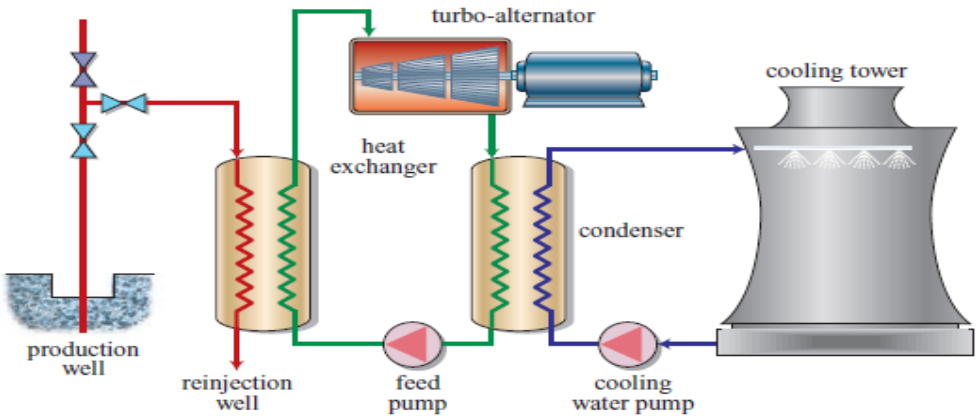

Figure 33: Diagram of a binary cycle plant for electricity generation [6].

One of the most important stages for the implementation of a binary plant is the selection of the working fluid and the working cycle. Taking into account the book of Macchi and Astolfi [40], the key parameters that must be considered for a proper design are:

- The conditions at the wellhead (liquid or liquid-vapor mixture);
- The enthalpy of the geothermal fluid (bottom-hole conditions);
- The non-condensable gases (NCG) content of the geothermal fluid;
- Chemical composition of the geothermal fluid;
- Size of the available resource (producible power);
- Condensation temperature/pressure and cooling media;
- Turbine technology selection;

Binary plants are usually built by modules, each module has a power capacity from about a few hundred kilowatts to a few megawatts; if the amount of power needed is too high for just one module, a group of a certain number of modules can be installed together to reach the required power. In this way the production cost is reduced, and the specific cost are independent from the size of the plant. The factor that most influence the cost of the plant is the temperature of the geothermal fluid, which affects the size of the heat exchanger, the cooling system and the turbine [6].

There are other configurations that grant ORC binary plants with the possibility to increase their energy conversion efficiency, one common variation with respect to the basic layout is to implement an ORC plant with two or three pressure levels, as it is described in the following pictures:

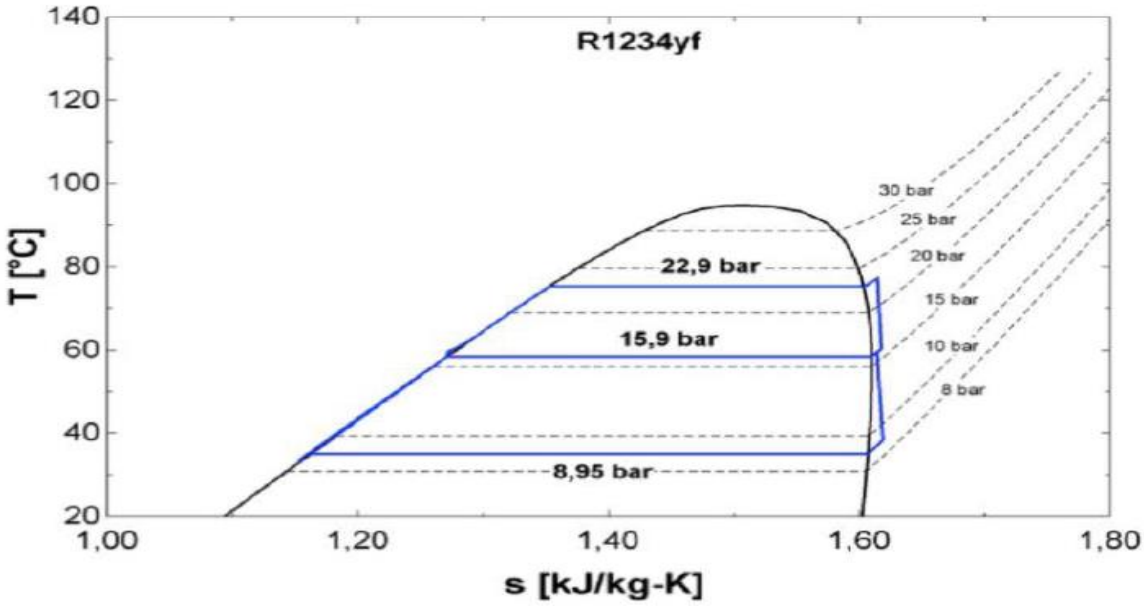

Figure 34: T-s diagram of a certain ORC binary plant with two pressure levels.

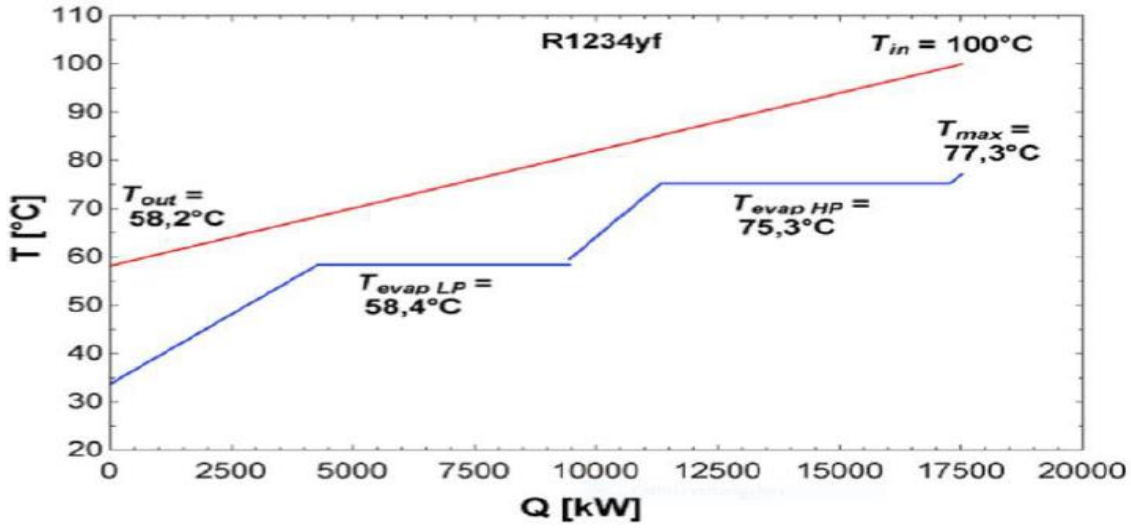

Figure 35: T-Q diagram of a certain ORC binary plant with two pressure levels.

Binary plants can also be used in combined-cycle or hybrid power plants. For a combined cycle for instance, if a system has a liquid dominated geothermal fluid at the wellhead, the vapor fraction could be exploited in a single-flash steam plant; while the liquid fraction that is separated in the flash unit could be circulated through a heat exchanger before being re-injected in the reservoir. In this way, the liquid fraction yields the remaining heat to a secondary fluid, which is circulated through a Rankine cycle. These configurations allow to achieve maximum energy conversion efficiencies.

3.3 Patents and Licenses

Some of the patents and licenses of the technology described in this work will be presented in this section, being specifically the ones related with the down-hole pump, the ORC plant in the surface, the working fluid of the plant, and the software's needed for the simulations. It is important to underline that for most of the equipment and technology used on a geothermal project (and practically on any project), there might be many different patents and licenses for one component, the important thing is to specify and understand the correct function in which that component is going to be used.

For instance, in the European Patent Office there is a patent with the title "ORC Binary Cycle Geothermal Plant and Process" [42]; this patent specifies all the components of an ORC Binary Plant, the connections between them and the function of each of these components. On the other hand, regarding the downhole pump, the oldest publications were published in the context of oil resources exploitations, in which these pumps were used for extracting the oil from the subsurface after the drilling process. A good example of these kind of pumps is the one described by the patent of Mendez in 1990, in which says: "The pump is mechanically driven by motor means whose diameter permits insertion through the well and whose output characteristics are suitable for driving the pump means. A single mounting bracket supports the motor means in a housing and prevents counter rotation of the motor stators. The motor means are immersed in a clean fluid inserted at the well surface and the clean fluid is maintained at the well hydrostatic pressure by a compensating piston" [43]. Is important to mention that the technology used for oil extraction is quite similar that the one used for geothermal projects; the main difference is that the materials of the pump used for geothermal purposes must be able to handle higher temperatures. One of the most important manufacturers of geothermal downhole pumps is Baker & Hughes.

In the case of the working fluid for the ORC cycle, there are also many patents for different utilizations, for instance the developed by Martin Schwiegel and company in 2008 [44], which specifies that perfluorinated hydrocarbons and/or partially perfluorinated polyethers and/or partially perfluorinated ketones may be used as working fluids in a thermal ORC process for combined electricity and heat generation, using thermal water as heat source. In the case of this thesis, the main working fluid used for the simulation and optimization of the reference case was an innovative refrigerant called HFO-1234ze; all the patents and licenses related with this fluid are owned by the company Honeywell [45].

Lastly but not least, as it was said before the software used for the simulation of the geothermal reservoir has open access and no license is needed; on the other hand, the software used for the simulation of the ORC plant request a proper license for its utilization. The company that provides these licenses and the owner of all the rights and patents of Aspen Plus v10 is Aspen Technology [46].

IV. Validation of the Model

The validation of the model will be performed analyzing four real and operating geothermal projects. Using as inputs the data obtained from the available literature related with these projects, the behavior of the model will be evaluated by comparing the results obtained with DoubletCalc and the target outputs found in the collected data from the literature. Taking into account the conditions and the assumptions considered for each study case, the model will be validated depending on how small the errors of the results with respect to the target outputs are.

It is worth mentioning that two of these study cases are located in the Netherlands (Honselersdijk and Den Haag), while the other two are in Belgium (Balmatt) and Austria (Altheim). For the two projects in the Netherlands, in addition to the analysis of the simulation employing the data from the literature that was found, another simulation was realized using a 3D web-based information system named ThermoGIS.

ThermoGIS was developed by the same creators of DoubletCalc v1.4.3 and DoubletCalc 2D (TNO) [15]. Given the maturity of the Netherlands in the oil and gas field, there is quite a lot information available about the subsurface characteristics, existing boreholes, drilling and exploration projects and so on. Thanks to this wide and accessible database, ThermoGIS is created with the main objective to support the geothermal energy community in assessing the feasibility of a geothermal system at practically any location within the Netherlands. The model provides a map of subsurface water reservoirs, from which is possible to estimate the most important parameters of the aquifer at a determined location, such as permeability, temperature, aquifer thickness, aquifer depth, optimized distance between production and injection wells, optimized downhole pump depth, optimized downhole pump pressure and so on. Using these parameters, ThermoGIS gives two kind of results, one estimated from its database and one calculated with an integrated version of DoubletCalc v1.4.3; the outputs calculated by ThermoGIS are the transmissivity [Dm], the geothermal power [MW] and the flow rate [m^3/h] of the potential geothermal doublet system [47]. The transmissivity (T) is the product of the hydraulic conductivity (K) and the reservoir thickness (L_R), and it measures the capacity to transmit a certain fluid (usually groundwater) among the whole extension of the reservoir thickness.

The main difference between the DoubletCalc integrated in ThermoGIS and the one that can be downloaded from the web page of NLOG [48] is that the uncertainty factor is handled in a different way. The version adopted in ThermoGIS is used deterministically, which means that the uncertainty considered by the normal version of DoubletCalc v1.4.3 is not taken into account and the percentiles 90, 50 and 10 must be run separately. For this reason and because, unlike DoubletCalc v1.4.3, many inputs cannot be modified in ThermoGIS (uncertainty of the reservoir properties, pump efficiency, pump depth, detailed well layout), it is expected some level of variation between the results obtained from DoubletCal v1.4.3 and ThermoGIS at a certain location.

Some of the inputs for the simulations of the study cases were not found or they did not have public access. To handle this inconvenient, for those parameters that were not available, their value was assumed considering the assumptions taken by ThermoGIS for the calculation of its integrated version of DoubletCalc [15]. These assumptions are reported in the Table 5, from which the most used for this thesis were the well trajectory curvature factor (to calculate the along hole depth of the well), the calculation segment length, the production and injection well skin, the casing roughness, the pump system efficiency and the aquifer kh/kv ratio. For the parameters that does not appear in this table and without a reference value from the literature, it was assumed the value used by the developers of DoubletCalc in the examples described in the manual of the software.

Technical parameters	**Value**	**Unit**
aquifer top depth	from map	m
aquifer thickness	from map	m
aquifer thickness uncertainty (SD)	from map	m
aquifer net-to-gross	from map	-
aquifer permeability	from map	mDarcy
uncertainty in natural logarithm permeability	from map	ln(mDarcy)
aquifer temperature	from 3D model	°C
aquifer water salinity	depth dependent	ppm
aquifer kh/kv ratio	1	-
return temperature	30	°C
minimum aquifer temperature	35	°C
distance between the two wells	optimized	m
pump system efficiency	0.6	-
production pump depth	500	m
pump pressure difference	optimized	bar
well trajectory curvature factor	1.1	-
calculation segment length	50	m
outer diameter (open production interval)	8.5	inch
inner diameter (casing)	8.5	inch
casing roughness	1.38	milli-inch
injector well skin	-1	-
production well skin	-1	-

Table 5: Assumptions taken by ThermoGIS for the utilization of the integrated version of DoubletCalc [15].

The analysis of the four study cases will be described in the upcoming paragraphs. It is worth mentioning that the parameters that had to be assumed by the author for each simulation (the target input was not found in the literature) are distinguished by its red color in the tables that report the inputs for every study case.

4.1 Balmatt

The first study case that will be analyzed is the Balmatt geothermal project, developed by The Flemish Institute of Technology (VITO) and located in Mol, Belgium. The main objective of the project is to produce geothermal fluid able to supply heat to the district area nearby and, if the conditions of the fluid are good enough, generate electricity using an ORC binary cycle.

The drilling process of the project begun in September of 2015, and it was planned to perforate until the top of the Lower Carboniferous Limestone Group at 2800 [m] vertical depth. However, some difficulties came out and the reservoir was encountered approximately 370 [m] deeper than the one that was estimated [49]. Because of this, some of the data available might vary from one document to another depending on the release date (before or after this particular event).

Two simulations were performed for this study case, the first one basing most of its parameters on a document released before the problems that were mentioned and the other one considering data from more recent documents.

4.1.1 Balmatt (1)

For the first simulation of the Balmatt project most of the inputs were assumed from a document released before the problems occurred during the drilling process [50]. The only parameters that were considered from more recent investigations were the depth of the wells and the well configuration [51]. In the following tables are presented the inputs used for the simulation of this study case:

Inputs Balmatt (1)			
Aquifer properties	**Minimum**	**Median**	**Maximum**
Permeability [mD]	41	391	3762
Net to gross	0.0588	0.0625	0.0667
Aquifer gross thickness [m]	750	800	850
Aquifer top at producer [m TVD]	2798	3109	3420
Aquifer top injector [m TVD]	3233	3592	3951
Water salinity [ppm]	100000	120000	140000
kh/kv ratio		1	
Surface Temperature [°C]		10	
Geothermal gradient [°C/m]		0.033	

Doublet and pump properties	
Exit Temperature at HX [°C]	35
Distance wells at aquifer level [m]	1200
Pump system efficiency	0.75
Production pump depth [m]	500
Pump pressure difference [bar]	60

Table 6: Inputs for the simulation of the study case 'Balmatt (1)' (aquifer, doublet and pump properties) [50].

Well properties (producer)					Well properties (injector)			
Outer diameter [inch]		7			Outer diameter [inch]		9.625	
Skin		0			Skin		0	
Penetration angle [deg]		42.6			Penetration angle [deg]		40	
Skin due penetration angle		-			Skin due penetration angle		-	
Segment	Pipe segment sections p [m AH]	Pipe segment depth p [m TVD]	Pipe inner diameter p [inch]	Pipe roughness p [milli-inch]	Pipe segment sections i [m AH]	Pipe segment depth i [m TVD]	Pipe inner diameter i [inch]	Pipe roughness i [milli-inch]
1	500	500	6.625	1.38	1395	1395	9.625	1.38
2	1395	1395	9.625	1.38	2322.1	2111	9.625	1.38
3	2970	2700	7	1.38	3951.2	3592	7	1.38
4	3419.9	3109	5	1.38				

Table 7: Inputs for the simulation of the study case 'Balmatt (1)' (well properties).

It is worth mentioning that the targets considered for this case were taken from the same document that was released in 2014 (before the problems in the drilling process). Therefore, it is possible to analyze how much vary the errors of the simulation changing just the configuration of the last part of the wells and depth of the production and injection wells.

Targets Balmatt (1)			
Monte Carlo cases	**P90**	**P50**	**P10**
Flow rate [m3/h]	140	259.77	583.32
Geothermal power [MW]	12.6	24.35	54.28
Aquifer Temp at producer [°C]	122	122	122

Table 8: Targets for the simulation of the study case 'Balmatt (1)' [50].

Outputs Balmatt (1)			
Monte Carlo cases	**P90**	**P50**	**P10**
Flow rate [m3/h]	143.70	239.00	407.50
Geothermal power [MW]	12.76	22.62	38.78
Aquifer Temp at producer [°C]	120.18	125.76	131.54

Table 9: Outputs obtained from the simulation of the study case 'Balmatt (1)'.

Error Balmatt 2017 (1) [%]			
Monte Carlo cases	**P90**	**P50**	**P10**
Flow rate	2.64	8.00	30.14
Geothermal power	1.27	7.10	28.56
Aquifer Temp at producer	1.49	3.08	7.82

Table 10: Error of the outputs obtained from the study case 'Balmatt (1)' with respect to its targets.

4.1.2 Balmatt (2)

For the second simulation of the Balmatt study case it was used a mix between the data from the poster report in 2014 [50] and the data available from more recent studies.

In the Table 11 the permeability, the net-to-gross ratio, the aquifer thickness, the kh/kv ratio, the surface temperature, the geothermal gradient, the pump system efficiency and the pump pressure difference were assumed from the poster report [50]. The production pump depth was calculated using the procedure that was explained at the beginning of this chapter. The salinity value was taken from a report published by VITO [52]. The exit temperature at the heat exchanger and the distance between wells at aquifer level were assumed considering a paper made by Ben Laenen [51].

Regarding the Table 12, most of the parameters were assumed from the same documents used for the previous case.

Inputs Balmatt (2)			
Aquifer properties	**Minimum**	**Median**	**Maximum**
Permeability [mD]	41	391	3762
Net to gross	0.0588	0.0625	0.0667
Aquifer gross thickness [m]	750	800	850
Aquifer top at producer [m TVD]	2798	3109	3420
Aquifer top injector [m TVD]	3233	3600	3951
Water salinity [ppm]	120000	165000	180000
kh/kv ratio		1	
Surface Temperature [°C]		10	
Geothermal gradient [°C/m]		0.033	

Doublet and pump properties	
Exit Temperature at HX [°C]	80
Distance wells at aquifer level [m]	1500
Pump system efficiency	0.75
Production pump depth [m]	736
Pump pressure difference [bar]	60

Table 11: Inputs for the simulation of the study case 'Balmatt (2)' (aquifer, doublet and pump properties) [50].

Well properties (producer)					Well properties (injector)			
Outer diameter [inch]		7			Outer diameter [inch]		9.625	
Skin		0			Skin		0	
Penetration angle [deg]		42.6			Penetration angle [deg]		40	
Skin due penetration angle		-			Skin due penetration angle		-	
Segment	Pipe segment sections p [m AH]	Pipe segment depth p [m TVD]	Pipe inner diameter p [inch]	Pipe roughness p [milli-inch]	Pipe segment sections i [m AH]	Pipe segment depth i [m TVD]	Pipe inner diameter i [inch]	Pipe roughness i [milli-inch]
1	736	736	6.625	1.38	1395	1395	9.625	1.38
2	1395	1395	9.625	1.38	2322.1	2111	9.625	1.38
3	2970	2700	7	1.38	3951.2	3592	7	1.38
4	3419.9	3109	5	1.38				

Table 12: Inputs for the simulation of the study case 'Balmatt (2)' (well properties).

Unlike the first case, the target results for this simulation are not presented with a Monte Carlo simulation. They were taken from recent studies in which the new well configuration is taken into account [52, 51]. For this reason, just the results obtained from the percentile 90 (P90) in the DoubletCalc simulation are used for the calculation of the error with respect to the target results. This because the percentile 90 represents the results with the highest probability of success.

Targets Balmatt (2)	
Flow rate [m3/h]	160
Geothermal Power [MW]	8
Aquifer Temp at producer [°C]	124

Table 13: Targets for the simulation of the study case 'Balmatt (2)'.

Outputs Balmatt (2)			
Monte Carlo cases	**P90**	**P50**	**P10**
Flow rate [m3/h]	155.60	246.80	385.60
Geothermal power [MW]	6.48	11.62	17.87
Aquifer Temp at producer [°C]	120.03	125.73	131.42

Table 14: Outputs obtained from the simulation of the study case 'Balmatt (2)'.

Error Balmatt (2) [%]	
Monte Carlo cases	**P90**
Flow rate	2.75
Geothermal Power	19.00
Aquifer Temp at producer	3.20

Table 15: Error of the outputs obtained from the study case 'Balmatt (2)' with respect to its targets.

4.2 Altheim

Altheim is a city of Austria with several medium-sized companies in its vicinities. It is located near the frontier with Germany and has a population of approximately 5000 inhabitants. The Altheim project was one of the first plants in Europe in exploits a low-enthalpy geothermal resource. The doublet system is been drilled until the Upper Jurassic formation, producing hot water from the Austrian part of the Molasse Basin at around 2300 [m] depth. At the first stages of the project in 1989, the main goal was to supply hot water for a district heating of about 1500 households, for which it was required a thermal power of approximately 10 to 15 [MW_{th}]. A few years later some studies were made, and the project was expanded implementing an electrical submersible pump in the production well (aiming to increase the flow rate to 100 [kg/s]) and adding a 1 [MW_{el}], ORC plant for electricity generation [53].

As it can be seen in the Table 16 and Table 17, it was possible to find most of the inputs required for the simulation in the literature that was available. The assumptions considered in the wells segments, the pump system efficiency and the net-to-gross ratio were estimated taking into account the suggested values in ThermoGIS and the manual of DoubletCalc, while the permeability of the formation was calculated by the author using the value of the hydraulic conductivity, presented on a report published by one of the companies involved in the project [54].

Inputs Altheim			
Aquifer properties	**Minimum**	**Median**	**Maximum**
Permeability [mD]	750	812.58	870
Net to gross	0.99	1	1.01
Aquifer gross thickness [m]	260	280	300
Aquifer top at producer [m TVD]	2075	2305	2536
Aquifer top injector [m TVD]	1949	2165	2382
Water salinity [ppm]	371	800	1300
kh/kv ratio		1	
Surface Temperature [°C]		11	
Geothermal gradient [°C/m]		0.038	

Doublet and pump properties	
Exit Temperature at HX [°C]	70
Distance wells at aquifer level [m]	1700
Pump system efficiency	0.75
Production pump depth [m]	290
Pump pressure difference [bar]	11.5

Table 16: Inputs for the simulation of the study case 'Altheim' (aquifer, doublet and pump properties).

Well properties (producer)					**Well properties (injector)**			
Outer diameter [inch]		8.5			Outer diameter [inch]		8.5	
Skin		0			Skin		0	
Penetration angle [deg]		0			Penetration angle [deg]		60	
Skin due penetration angle		-			Skin due penetration angle		-	
Segment	Pipe segment sections p [m AH]	Pipe segment depth p [m TVD]	Pipe inner diameter p [inch]	Pipe roughness p [milli-inch]	Pipe segment sections i [m AH]	Pipe segment depth i [m TVD]	Pipe inner diameter i [inch]	Pipe roughness i [milli-inch]
1	290	290	6.625	1.38	2128	1499	9.625	1.38
2	1827	1827	9.625	1.38	3078	2165	7	1.38
3	2305	2305	7	1.38				

Table 17: Inputs for the simulation of the study case 'Altheim' (well properties).

The Table 18 shows the targets for the simulation of the Altheim project. These were obtained principally from the papers made by Gerhard Pernecker [55, 56] and the reports published by MND [53] and ENGINE [54].

The error of the results with respect to the defined targets were calculated considering just the percentile 90 (P90), mainly due to the fact that the outputs presented in the P90 are the ones with the highest probability of success and the targets are not presented with a Monte Carlo distribution.

Targets Altheim	
Mass flow [kg/s]	82
Geothermal Power [MW]	11
Temperature at heat exchanger [°C]	106

Table 18: Targets for the simulation of the study case 'Altheim'.

Outputs Altheim			
Monte Carlo cases	**P90**	**P50**	**P10**
Mass flow [kg/s]	84.14	87.10	89.84
Geothermal power [MW]	9.87	11.95	14.18
Temperature at heat exchanger [°C]	99.09	103.90	108.78

Table 19: Outputs obtained from the simulation of the study case 'Altheim'.

Error Altheim [%]	
Monte Carlo cases	**P90**
Mass flow	2.61
Geothermal Power	10.27
Temperature at heat exchanger	6.52

Table 20: Error of the outputs obtained from the study case 'Altheim' with respect to its targets.

4.3 Honselersdijk

The geothermal project in the city of Honselersdijk was impulsed by Green Well Westland B.V. The main goal was to explore the geothermal potential of the area, in particular looking for the existence of hot water in the subsurface, expecting to use it to heat the Green houses of the participating companies.

The simulation of this project was performed for three different cases, the first and the second are two different potential scenarios proposed in a report published by one of the companies involved in the development of the drilling project and with public access in the web page of NLOG [48], while the third case was done by using the web map tool ThermoGIS that was discussed at the beginning of this section.

All the inputs and targets for the two first simulations of this study case were taken from the "Well proposals Honselersdijk" report published by PanTerra Geoconsultans B.V. [57]. In this document two different scenarios for the doublet system were simulated to compare and discuss the different results that can be obtained from each case. Unlike the two previous study cases, there are two additional target results that were taken from the outputs of this report, the coefficient of performance and the required pump power.

4.3.1 Honselersdijk (1)

The suggested doublet system of the first scenario aims to produce water from the Rijswijk and Delft Sandstone aquifers, at a top aquifer depth equal to 2322 [m]. The rest of the inputs are presented in the Table 21 and Table 22.

Inputs Honselersdijk (1)			
Aquifer properties	**Minimum**	**Median**	**Maximum**
Permeability [mD]	34	164	350
Net to gross	0.13	0.4	0.88
Aquifer gross thickness [m]	140	163	180
Aquifer top at producer [m TVD]	2090	2322	2554
Aquifer top injector [m TVD]	2080	2311	2542
Water salinity [ppm]	90000	100000	110000
kh/kv ratio		1	
Surface Temperature [°C]		10	
Geothermal gradient [°C/m]		0.031	

Doublet and pump properties	
Exit Temperature at HX [°C]	35
Distance wells at aquifer level [m]	1642
Pump system efficiency	0.61
Production pump depth [m]	300
Pump pressure difference [bar]	40

Table 21: Inputs for the simulation of the study case 'Honselersdijk (1)' (aquifer, doublet and pump properties).

Well properties (producer)					Well properties (injector)			
Outer diameter [inch]		8.5			Outer diameter [inch]		8.5	
Skin		0			Skin		0	
Penetration angle [deg]		35.3			Penetration angle [deg]		35.3	
Skin due penetration angle		-			Skin due penetration angle		-	
Segment	Pipe segment sections p [m AH]	Pipe segment depth p [m TVD]	Pipe inner diameter p [inch]	Pipe roughness p [milli-inch]	Pipe segment sections i [m AH]	Pipe segment depth i [m TVD]	Pipe inner diameter i [inch]	Pipe roughness i [milli-inch]
1	300	300	6.625	1.19	1097	1097	9.625	1.19
2	1097	1097	9.625	1.19	1992	1869	7	1.19
3	1967	1850	7	1.19	2570	2311	7	1.19
4	2584	2322	7	1.19				

Table 22: Inputs for the simulation of the study case 'Honselersdijk (1)' (well properties).

While the target results, the outputs of the simulation and the error of the outputs with respect to the targets are reported in the following tables:

Targets Honselersdijk (1)			
Monte Carlo cases	**P90**	**P50**	**P10**
Flow rate [m3/h]	39	82	142
Required pump power [kW]	71	149	258
Geothermal power [MWth]	1.7	4	7.3
COP	24	27	29
Aquifer Temp at producer [°C]	80	84	89

Table 23: Targets for the simulation of the study case 'Honselersdijk (1)'.

Outputs Honselersdijk (1)			
Monte Carlo cases	**P90**	**P50**	**P10**
Flow rate [m3/h]	40.3	81.5	147
Required pump power [kW]	73.3	148.5	267.8
Geothermal power [MW]	1.77	3.96	7.52
COP	23.7	26.7	29.3
Aquifer Temp at producer [°C]	80.6	84.49	88.43

Table 24: Outputs obtained from the simulation of the study case 'Honselersdijk (1)'.

Error Honselersdijk (1) [%]			
Monte Carlo cases	**P90**	**P50**	**P10**
Flow rate	3.33	0.61	3.52
Required pump power	3.24	0.34	3.80
Geothermal power	4.12	1.00	3.01
COP	1.25	1.11	1.03
Aquifer Temp at producer	0.75	0.58	0.64

Table 25: Error of the outputs obtained from the study case 'Honselersdijk (1)' with respect to its targets.

4.3.2 Honselersdijk (2)

The second scenario takes into consideration a deeper sandstone with respect to the previous case (same location but considering a deeper well that in the case (1). This means that the drilling process must be performed until a top aquifer depth equal to 2372 [m], using the Delft and the Pijnacker Sandstone as target aquifers for the geothermal exploitation. The other inputs needed for the simulation are shown in the Table 26 and Table 27.

Inputs Honselersdijk (2)			
Aquifer properties	**Minimum**	**Median**	**Maximum**
Permeability [mD]	81	157	350
Net to gross	0.24	0.36	0.88
Aquifer gross thickness [m]	400	450	500
Aquifer top at producer [m TVD]	2135	2372	2609
Aquifer top injector [m TVD]	2130	2367	2604
Water salinity [ppm]	90000	100000	110000
kh/kv ratio		1	
Surface Temperature [°C]		10	
Geothermal gradient [°C/m]		0.031	

Doublet and pump properties	
Exit Temperature at HX [°C]	35
Distance wells at aquifer level [m]	1467
Pump system efficiency	0.61
Production pump depth [m]	300
Pump pressure difference [bar]	40

Table 26: Inputs for the simulation of the study case 'Honselersdijk (2)' (aquifer, doublet and pump properties).

Well properties (producer)					**Well properties (injector)**			
Outer diameter [inch]		8.5			Outer diameter [inch]		8.5	
Skin		0			Skin		0	
Penetration angle [deg]		36.2			Penetration angle [deg]		36.2	
Skin due penetration angle		-			Skin due penetration angle		-	
Segment	Pipe segment sections p [m AH]	Pipe segment depth p [m TVD]	Pipe inner diameter p [inch]	Pipe roughness p [milli-inch]	Pipe segment sections i [m AH]	Pipe segment depth i [m TVD]	Pipe inner diameter i [inch]	Pipe roughness i [milli-inch]
1	300	300	6.625	1.19	1097	1097	9.625	1.19
2	1097	1097	9.625	1.19	1896	1865	7	1.19
3	1889	1860	7	1.19	2552	2368	7	1.19
4	2558	2372	7	1.19				

Table 27: Inputs for the simulation of the study case 'Honselersdijk (2)' (well properties).

While the target results, the outputs of the simulation and the error of the outputs with respect to the targets are reported in the following tables:

Targets Honselersdijk (2)			
Monte Carlo cases	**P90**	**P50**	**P10**
Flow rate [m3/h]	129	190	271
Required pump power [kW]	236	345	493
Geothermal power [MWth]	7.2	11.1	16
COP	29	32	34
Aquifer Temp at producer [°C]	86	90	95

Table 28: Targets for the simulation of the study case 'Honselersdijk (2)'.

Outputs Honselersdijk (2)			
Monte Carlo cases	**P90**	**P50**	**P10**
Flow rate [m3/h]	135.7	198.8	291.9
Required pump power [kW]	247.2	362.2	531.7
Geothermal power [MW]	7.63	11.34	17.32
COP	29.4	31.7	34.1
Aquifer Temp at producer [°C]	86.46	90.54	94.66

Table 29: Outputs obtained from the simulation of the study case 'Honselersdijk (2)'.

Error Honselersdijk (2) [%]			
Monte Carlo cases	**P90**	**P50**	**P10**
Flow rate	5.19	4.63	7.71
Required pump power	4.75	4.99	7.85
Geothermal power	5.97	2.16	8.25
COP	1.38	0.94	0.29
Aquifer Temp at producer	0.53	0.60	0.36

Table 30: Error of the outputs obtained from the study case 'Honselersdijk (2)' with respect to its targets.

4.3.3 Honselersdijk (ThermoGIS)

For the third simulation of this study case, the inputs shown in the Table 31 were obtained from the web map tool ThermoGIS [15]; in which the target aquifer and the production well were located in the map to get the desired parameters. On the other hand, regarding the inputs shown in the Table 32, the ones that are needed to specify the segments of the production and injection well cannot be obtained from ThermoGIS. For this reason, these parameters were assumed by the author, based on the data acquired from the "Final Well Report" of the project [58].

Inputs Honselersdijk (ThermoGIS)			
Aquifer properties	**Minimum**	**Median**	**Maximum**
Permeability [mD]	131	534	2229
Net to gross	0.99	1	1.01
Aquifer gross thickness [m]	186	225	264
Aquifer top at producer [m TVD]	2254	2504	2754
Aquifer top injector [m TVD]	2241	2490	2739
Water salinity [ppm]	105186.7	116853.3	128520
kh/kv ratio		1	
Surface Temperature [°C]		10	
Geothermal gradient [°C/m]		0.031	

Doublet and pump properties	
Exit Temperature at HX [°C]	30
Distance wells at aquifer level [m]	1035
Pump system efficiency	0.6
Production pump depth [m]	500
Pump pressure difference [bar]	44

Table 31: Inputs for the simulation of the study case 'Honselersdijk (ThermoGIS)' (aquifer, doublet and pump properties).

Well properties (producer)					**Well properties (injector)**			
Outer diameter [inch]		8.5			Outer diameter [inch]		8.5	
Skin		0			Skin		0	
Penetration angle [deg]		44.7			Penetration angle [deg]		44.7	
Skin due penetration angle		-			Skin due penetration angle		-	
Segment	Pipe segment sections p [m AH]	Pipe segment depth p [m TVD]	Pipe inner diameter p [inch]	Pipe roughness p [milli-inch]	Pipe segment sections i [m AH]	Pipe segment depth i [m TVD]	Pipe inner diameter i [inch]	Pipe roughness i [milli-inch]
1	500	500	6.625	1.38	1097	1097	8.5	1.38
2	1097	1097	8.5	1.38	2051.5	1865	8.5	1.38
3	2046	1860	8.5	1.38	2739	2490	8.5	1.38
4	2754.4	2504	8.5	1.38				

Table 32: Inputs for the simulation of the study case 'Honselersdijk (ThermoGIS)' (well properties).

In the Table 33 are reported the targets results taken from the research in ThermoGIS. One group of targets is from the database of the tool and the other from the calculation of the integrated version of DoubletCalc. In the Table 34 and Table 35 can be seen the outputs of the simulation performed in DoubletCalc v1.4.3 and its respective errors with respect to the targets.

Targets Honselersdijk (ThermoGIS)						
	From database			**From integrated DoubletCalc**		
Monte Carlo cases	**P90**	**P50**	**P10**	**P90**	**P50**	**P10**
Flow rate [m3/h]	475	500	500	204	502	641
Geothermal power [MWth]	29.5	31	31	12.5	31.4	40.2
Aquifer Temp at producer [°C]	89	89	89	89	89	89

Table 33: Targets for the simulation of the study case 'Honselersdijk (ThermoGIS)'.

Outputs Honselersdijk (ThermoGIS)			
Monte Carlo cases	**P90**	**P50**	**P10**
Flow rate [m3/h]	390.30	476.80	563.80
Geothermal power [MW]	24.89	31.17	37.17
Aquifer Temp at producer [°C]	86.85	91.13	95.42

Table 34: Outputs obtained from the simulation of the study case 'Honselersdijk (ThermoGIS)'.

Error Honselersdijk (ThermoGIS) [%]						
	From database			**From integrated DoubletCalc**		
Monte Carlo cases	**P90**	**P50**	**P10**	**P90**	**P50**	**P10**
Flow rate	17.83	4.64	12.76	91.32	5.02	12.04
Geothermal power	15.63	0.55	19.90	99.12	0.73	7.54
Aquifer Temp at producer	2.42	2.39	7.21	2.42	2.39	7.21

Table 35: Error of the outputs obtained from the study case 'Honselersdijk (ThermoGIS)' with respect to its targets.

As it can be seen in the Table 33, the results of the integrated DoubletCalc and the database of ThermoGIS differ considerably between each other (except for the percentile 50). As it was mentioned at the beginning of this section, this is explained by the fact that the DoubletCalc version adopted in ThermoGIS is used deterministically, which means that the uncertainty considered by the normal version of DoubletCalc v1.4.3 is not taken into account and the percentiles 90, 50 and 10 are run separately. On the other hand, in DoubletCalc the uncertainty is set in a triangle distribution for a number of parameters, even when putting the minimum estimate at 0, this means that the P90 value cannot be less than 45% percent of the P50 value. For this reason, many inputs cannot be modified in ThermoGIS (uncertainty of the reservoir properties, pump efficiency, pump depth, detailed well layout). Therefore, some level of variation must be expected between the results obtained from DoubletCal v1.4.3 and ThermoGIS at a certain location.

4.4 Den Haag

The last study case that will be presented is a geothermal district heating system at the Leyweg in the city of Den Haag. The project was designed to produce approximately 5 [MW_{th}], which will provide heating for about 6000 houses [59]. The doublet system has a target depth of around 2200 [m] and 50 [m] thickness, arriving until an upper Jurassic sandstone layer called 'Delft sandstone', which has been the objective of numerous oil and gas exploration projects in the last century [60].

In this study case two simulations will be presented, the first one based on the parameters found in the available literature and the second one using the parameters obtained from ThermoGIS.

4.4.1 Den Haag (1)

The inputs for the first case presented in the Table 36 and Table 37 were obtained mainly from the 'End well report' of the project [61], the 'Well testing report' [62] and the 'Water/Gas samples report' [63]; all of these reports have public access and are available at the web page of NLOG [48]. For most of the data in the Table 36, either the minimum, median or maximum value had to be assumed by the author considering a variation of a 10% with respect to the available parameters.

Inputs Den Haag (1)			
Aquifer properties	**Minimum**	**Median**	**Maximum**
Permeability [mD]	100	500	1000
Net to gross	0.99	1	1.01
Aquifer gross thickness [m]	50	75	200
Aquifer top at producer [m TVD]	1971	2190	2409
Aquifer top injector [m TVD]	1603	1781	1959
Water salinity [ppm]	72000	80000	88000
kh/kv ratio		1	
Surface Temperature [°C]		11	
Geothermal gradient [°C/m]		0.031	

Doublet and pump properties	
Exit Temperature at HX [°C]	40
Distance wells at aquifer level [m]	1137
Pump system efficiency	0.61
Production pump depth [m]	488
Pump pressure difference [bar]	40

Table 36: Inputs for the simulation of the study case 'Den Haag (1)' (aquifer, doublet and pump properties).

Well properties (producer)					Well properties (injector)			
Outer diameter [inch]		7			Outer diameter [inch]		7	
Skin		0			Skin		0	
Penetration angle [deg]		46			Penetration angle [deg]		46	
Skin due penetration angle		-			Skin due penetration angle		-	
Segment	Pipe segment sections p [m AH]	Pipe segment depth p [m TVD]	Pipe inner diameter p [inch]	Pipe roughness p [milli-inch]	Pipe segment sections i [m AH]	Pipe segment depth i [m TVD]	Pipe inner diameter i [inch]	Pipe roughness i [milli-inch]
1	488	488	6.625	1.38	1190	1127	10.75	1.38
2	1248	1200	10.75	1.38	2163	1781	7	1.38
3	2522	2190	7	1.38				

Table 37: Inputs for the simulation of the study case 'Den Haag (1)' (well properties).

The target results for the simulation are reported in the Table 38. These were obtained principally from the paper done by Mottaghy, Pechnig, Buik and Simmelink [59], in which it is worth mentioning that most of the values were an approximation of the desired outputs of the project.

Regarding the error of the results with respect to the targets, as the objectives are not presented with a Monte Carlo distribution, just the results of the percentile 90 (P90) were taken into account. This because it contains the results with the highest probability of success.

Targets Den Haag (1)	
Flow rate [m^3/h]	175
Geothermal Power [MW]	5
Aquifer Temp at producer [°C]	75

Table 38: Targets for the simulation of the study case 'Den Haag (1)'.

Outputs Den Haag (1)			
Monte Carlo cases	**P90**	**P50**	**P10**
Flow rate [m^3/h]	165.00	264.60	361.10
Geothermal power [MW]	6.84	11.30	16.25
Aquifer Temp at producer [°C]	76.56	80.29	84.14

Table 39: Outputs obtained from the simulation of the study case 'Den Haag (1)'.

Error Den Haag (1) [%]	
Monte Carlo cases	**P90**
Flow rate	5.71
Geothermal Power	36.80
Aquifer Temp at producer	2.08

Table 40: Error of the outputs obtained from the study case 'Den Haag (1)' with respect to its targets.

4.4.2 Den Haag (ThermoGIS)

As it was said, ThermoGIS was used to find the inputs for the second case. To do this, the production and injection wells of the Den Haag project were located in the web map of ThermoGIS, in which the respective target aquifer was selected. In the Table 41 and Table 42 are presented the parameters found by ThermoGIS, from which it can be observed that they have a certain degree of variation with respect to the previous case; this is mainly due to the assumptions taken by ThermoGIS and the data available from its database. In addition, as in the previous study case, the inputs for the well segments is not given by ThermoGIS, therefore, these parameters were assumed by the author considering the data available in the related literature.

Inputs Den Haag (ThermoGIS)			
Aquifer properties	**Minimum**	**Median**	**Maximum**
Permeability [mD]	211	925	3992
Net to gross	0.99	1	1.01
Aquifer gross thickness [m]	124	188	249
Aquifer top at producer [m TVD]	1655	1839	2023
Aquifer top injector [m TVD]	1511	1679	1847
Water salinity [ppm]	77233.33	85820	94406.67
kh/kv ratio		1	
Surface Temperature [°C]		10	
Geothermal gradient [°C/m]		0.031	

Doublet and pump properties	
Exit Temperature at HX [°C]	30
Distance wells at aquifer level [m]	1137
Pump system efficiency	0.6
Production pump depth [m]	500
Pump pressure difference [bar]	35

Table 41: Inputs for the simulation of the study case 'Den Haag (ThermoGIS)' (aquifer, doublet and pump properties).

Well properties (producer)					Well properties (injector)			
Outer diameter [inch]		8.5			Outer diameter [inch]		8.5	
Skin		0			Skin		0	
Penetration angle [deg]		44.9			Penetration angle [deg]		44.9	
Skin due penetration angle		-			Skin due penetration angle		-	
Segment	Pipe segment sections p [m AH]	Pipe segment depth p [m TVD]	Pipe inner diameter p [inch]	Pipe roughness p [milli-inch]	Pipe segment sections i [m AH]	Pipe segment depth i [m TVD]	Pipe inner diameter i [inch]	Pipe roughness i [milli-inch]
1	500	500	6.625	1.38	1190	1127	8.5	1.38
2	1248	1200	8.5	1.38	1846.9	1679	8.5	1.38
3	2022.9	1839	8.5	1.38				

Table 42: Inputs for the simulation of the study case 'Den Haag (ThermoGIS)' (well properties).

As in the previous subsection, the outputs obtained from the simulation performed in DoubletCalc v1.4.3 are compared with the both targets available, one from the database of ThermoGIS and the other from the results of the calculation done by the DoubletCalc version integrated in ThermoGIS.

Targets Den Haag (ThermoGIS)						
	From database			From integrated DoubletCalc		
Monte Carlo cases	**P90**	**P50**	**P10**	**P90**	**P50**	**P10**
Flow rate [m3/h]	438	500	501	161	503	644
Geothermal power [MWth]	18.1	20.7	20.8	6.5	20.7	26.6
Aquifer Temp at producer [°C]	68	68	68	68	68	68

Table 43: Targets for the simulation of the study case 'Den Haag (ThermoGIS)'.

Outputs Den Haag (ThermoGIS)			
Monte Carlo cases	**P90**	**P50**	**P10**
Flow rate [m3/h]	380.90	475.70	557.30
Geothermal power [MW]	16.19	20.69	24.82
Aquifer Temp at producer [°C]	66.77	69.96	73.14

Table 44: Outputs obtained from the simulation of the study case 'Den Haag (ThermoGIS)'.

Error Den Haag (ThermoGIS) [%]						
	From database			From integrated DoubletCalc		
Monte Carlo cases	**P90**	**P50**	**P10**	**P90**	**P50**	**P10**
Flow rate	13.04	4.86	11.24	136.58	5.43	13.46
Geothermal power	10.55	0.05	19.33	149.08	0.05	6.69
Aquifer Temp at producer	1.81	2.88	7.56	1.81	2.88	7.56

Table 45: Error of the outputs obtained from the study case 'Den Haag (ThermoGIS)' with respect to its targets.

As it was discussed in the previous study case, the differences that can be appreciated between the results obtained from the integrated version of DoubletCalc and from the database of ThermoGIS in the Table 43 are explained by the fact that the versiond of DoubletCalc adopted by ThermoGIS does not consider the probabilistic approach of DoubletCalc v1.4.3.

4.5 Conclusions

Taking into account all the assumptions that had to be made, the errors obtained are quite acceptable and the model can be considered validated by these study cases.

The highest errors were found in the comparison between the results of the "ThermoGIS" simulations and the target results from the integrated DoubletCalc calculation, in particular the percentile 90. This was mainly because what was said before, the calculation of the integrated version of DoubletCalc does not consider the uncertainties in the same way than DoubletCalc v1.4.3; in fact, it can be seen that in both cases in which ThermoGIS was used, the percentile 90 from the calculation of the integrated DoubletCalc differs very much from the values obtained from the database of the tool and from the DoubletCalc v1.4.3 simulation. For this reason, it is considered more suitable to use the ThermoGIS database for parameters assessment in future reservoir simulations with DoubletCalc v1.4.3. Other point that should be remarked is that for both the Den Haag and the Honselersdijk "ThermoGIS" simulations, the lowest errors are the one of the P50 for all the three target results, having the both cases a maxim of about 5 % in the flow rate.

On the other hand, the lowest errors were obtained in the first two cases of the Honselersdijk simulation, in which the facts of being geothermal projects located in the Netherlands, having all the inputs available for the simulation and that the target outputs were presented with a Monte Carlo distribution had a very important influence in the success of the analysis.

Without considering the errors of the integrated version of DoubletCalc that was already discussed, the first simulation of the Den Haag project presents a considerably high error for the geothermal power (36.80 %). This is mainly because the target result for this parameter was taken from a rough estimation. Being said that, if the rough estimation was 5 [MW] and the result of the simulation of the P90 is equal to 6.84 [MW], it can be said that the error is not very representative, and that the simulation could be consider acceptable.

Regarding the Atlheim project it can be said that the results are very satisfactory. Taking into account that it is a project located outside the Netherlands territory, the targets are not presented with a Monte Carlo distribution and one of the most important inputs (permeability) was assumed by the author (the assumptions were based on similar rock formations), the errors obtained for the P90 are quite small with respect to what was expected before the simulation.

Finally, the other simulation that was performed considering a project outside the Netherlands territory was for the study case in Balmatt, which in general presents low errors for all the three simulations. The second simulation (Balmatt 2017(1)) was the one with the lowest errors and the third simulation (Balmatt 2017 (2)) the one with the highest. The main causes of errors is due to the fact that the inputs and targets of the simulation of 2014 were set before the changes in the well configuration (the depth increased from 2800 [m] to 3100 [m] approximately); therefore, as it occurred with the third simulation, some old inputs had to be used to simulate and estimate the newest targets.

V. Simulation and optimization of the ORC Binary Plant

In this chapter is going to be described the simulation and optimization of both a specific geothermal reservoir and the respective ORC plant for the production of electricity. For the simulation of the geothermal reservoir and the doublet system was used the software DoubletCalc v1.4.3, which was described in the previous chapter, while for the case of the ORC plant was used a commercial software called Aspen Plus.

Some of the outputs from the simulation of the geothermal reservoir were used for the simulation of the ORC plant, in this way it can be seen how the two models can be coupled and used together for the simulation of the overall geothermal plant.

5.1 Reservoir Simulation

As it can be implied from the previous chapter, the availability of the data needed for the inputs of DoubletCalc v1.4.3 is a key issue for the simulation of the geothermal plant. Is because of this fact that the selection of the location that will be used for the simulation of the doublet system is one of the most important steps on this thesis.

After considering many potential geothermal projects from the data available in the literature and the suitable locations that could be simulated with the help of the web map tool ThermoGIS that was discussed in the previous chapter, it was selected as reference case the Altheim geothermal project.

The Altheim geothermal project was used in the previous chapter as a study case for the validation of the model of DoubletCalv v1.4.3. The selection of this study case for the simulation of the geothermal plant was the most appropriate among the options that were into consideration, almost all the inputs needed for the DoubletCalc simulation are available (except the net-to-gross ratio and the pipe roughness), both the targets for the reservoir and the ORC plant simulation are also available and there is very useful data for the ORC plant simulation.

5.1.1 Description of the chosen location and target results

As it was said during the validation of the model of DoubletCalc v1.4.3, the Altheim geothermal project is located in the 'Upper Austria' District, close to the German/Bavarian Border. The city has a population of about 5000 habitants and the main objective of the project is to provide district heating for a certain number of households, for which the thermal energy required is approximately 11 [MW]. Some years after the plant started its production, the project was expanded implementing an electrical submersible pump in the production well (aiming to increase the flow rate to 100 [lt/s]) and adding a 1 [MWel], ORC plant for electricity generation [45].

Figure 36: Power house of the ORC plant of the Altheim geothermal project [56]

The Altheim project exploits a low-enthalpy geothermal resource located in the Austrian part of the Molasse Basin, in the Upper Jurassic formation at 2300 [m] depth. At the right side of the Figure 37 it can be appreciated a panoramic view of the city of Altheim, while at the left side it is shown the exact location of the city on a map.

Figure 37: Altheim, a Geothermal Project in the Upper Austrian Molasse [45]

As it was said before, the most important goal of this project is to produce hot geothermal water for being utilized in district heating for the community. At the first stages of the project the objective was to supply enough thermal energy for 1500 households approximately.

In 1994 the project was expanded and an electrical submersible pump (ESP) was installed in the production well at 290 [m] depth. The ESP aimed to increase the current mass flow rate from 46 [kg/s] to 100 [kg/s], but at the end the mass flow rate and the temperature of the geothermal water at surface level was around 82 [kg/s] and 106 [°C] respectively, which are the target results that were taken into consideration for the reservoir simulation [53]. The expansion of the geothermal plant also allowed the implementation of an ORC plant for power production, manufactured by Turboden and able to produce 1 [MWel] approximately [54].

During winter and some weeks of autumn and spring, the produced geothermal water is divided into two streams, one for the district heating and the other for the ORC plant. On the other hand, during summer, when the district heating is not needed, all the geothermal water goes to the ORC plant and its electric production reach its maximum. After the ORC plant, the geothermal water outflow is used for the local school and indoor swimming pool heating system, providing a thermal energy of about 1 [MW_{th}] [55]. To ensure that there will be thermal energy available for the local school and the swimming pool, and to avoid potential problems such as scaling formation, the temperature of the geothermal water at the outlet of the ORC plant is set to be equal to 70 [°C. The following picture shows a general layout of the Altheim geothermal project:

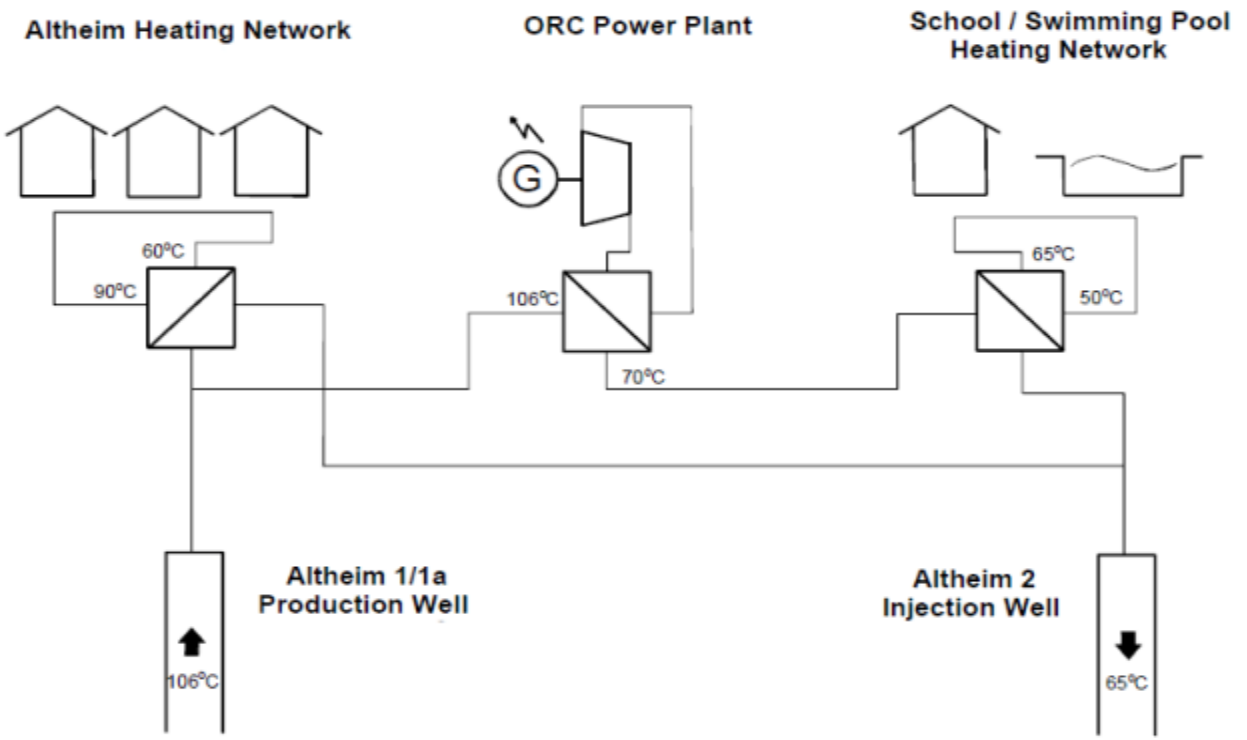

Figure 38: Schematic of the power plant and district heating system of the Altheim geothermal project [47].

5.1.2 Assumptions and parameters used for the simulation of the reference case

All the values used for the simulation of the geothermal reservoir can be seen in the Table 16 and Table 17, presented in the Chapter 4. Fortunately, most of the inputs needed for the simulation were available in the literature.

It is worth mentioning that the value of the permeability was calculated by the author using the value of the hydraulic conductivity that was found in the literature. The Equation (2.2), presented back in the Chapter 2, was used for the calculation of the permeability, in which the following values were assumed for each parameter:

- $K = 2.75 \times 10^{-5}$ [m/s];
- $\rho = 971.76$ [kg/m^3];
- $\mu = 2.78 \times 10^{-4}$ [kg/(m·s)];
- $g = 9.81$ [m/s^2];

The hydraulic conductivity was taken from the ENGINE report [54], while the density and the viscosity at reservoir level were taken from a preliminary test simulation performed on DoubletCalc v1.4.3. The calculated permeability is equal to 8.02×10^{-13} [m^2] = 812,58 [mD], which was assumed as the median value for the simulation, and even if it seems to be too high, it is a value within the range for hydrothermal exploitations and it could be expected for a reservoir located in the Molasse Basin.

Regarding the rest of the inputs used for the simulation, the only ones that were assumed by the author are the wells segments and the net-to-gross ratio, which were estimated taking into consideration the suggested values in ThermoGIS and the manual of DoubletCalc.

5.1.3 Results from DoubletCalc v1.4.3

The target results of the simulation are the real operating values of the geothermal plant that were found in the literature, these are the mass flow rate of geothermal water that supplies the doublet system (82 [kg/s]), the geothermal power that can be produced (11 [MW]) and the temperature of the geothermal power at the wellhead (104 [°C]). In the Tables 18, 19 and 20, presented in the Chapter 4, are displayed the target results, the obtained results and the error of the results with respect to the targets.

Back in the Chapter 4, the error was calculated taking into account the results obtained from the percentile 90 in the DoubletCalc simulation, which are the results with the highest probability of success. However, considering that the results obtained from the percentile 50 are also quite similar to the targets and have a small error compared with them, the values used for the simulations done on Aspen Plus were the ones from the percentile 50. This decision was taken mainly because the fingerprint graph that can be generated with DoubletCalc considers the results from the percentile 50. The fingerprint graph gives quite useful information for the analysis of the doublet system, such as the behavior of the required pump power curve changing the value of the down-hole pump pressure difference; besides that, the data of this graph can be used for the analysis of the overall geothermal plant after coupling the DoubletCalc and the Aspen Plus simulations.

Using the inputs shown in the Table 16 and Table 17 for the simulation of the geothermal reservoir on DoubletCalc v1.4.3 and considering this scenario as the base case for later simulations, the results obtained and the corresponding fingerprint graph are presented in the Table 46 and in the Figure 39 respectively.

Outputs Altheim			
Monte Carlo cases	**P90**	**P50**	**P10**
Aquifer kh net [Dm]	214.54	227.75	239.82
Mass flow [kg/s]	84.14	87.14	89.84
Pump volume flow [m3/h]	314.2	326.3	337.9
Required pump power [kW]	133.8	139	143.9
Geothermal power [MW]	9.87	11.95	14.18
COP	73.7	86.1	98.7
Aquifer pressure at prod. [bar]	212.42	224.61	236.7
Aquifer pressure at inj. [bar]	199.78	211.23	222.66
Pressure dif. at prod. [bar]	1.62	1.71	1.8
Pressure dif. at inj. [bar]	1.48	1.56	1.65
Aquifer Temp at producer [°C]	99.09	103.9	108.78
Temperature at HX [°C]	97.88	102.6	107.44
Pressure at HX [bar]		10.71	

Table 46: Results of the DoubletCalc v1.4.3 simulation for the Altheim base case scenario.

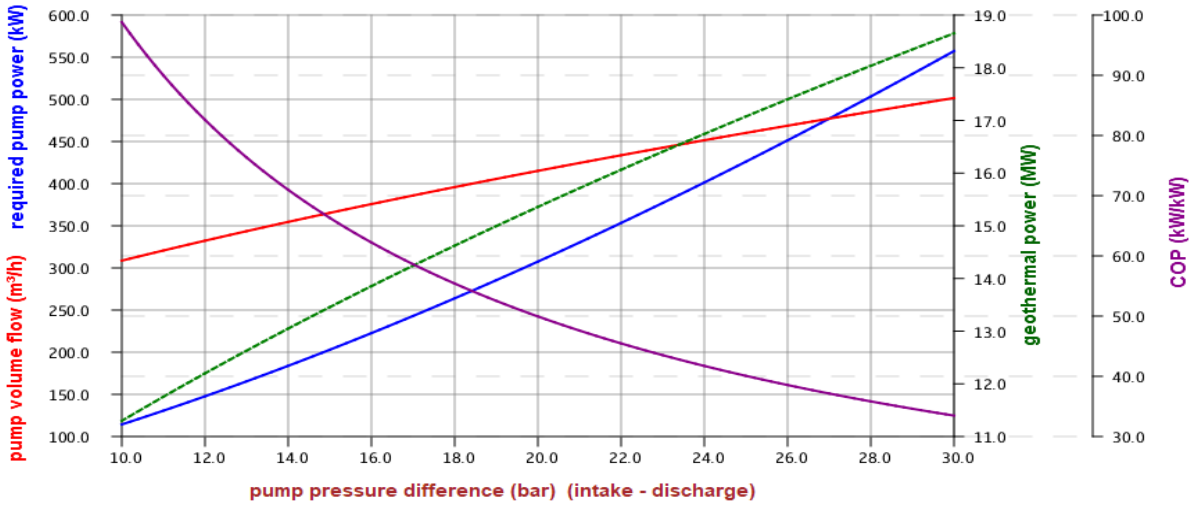

Figure 39: Fingerprint graph of the DoubletCalc v1.4.3 simulation for the Altheim base case scenario.

5.2 Simulation and optimization of the Organic Rankine Cycle

Like it was said at the beginning of this work, binary plants cover around the 12% of the installed power in the world among the geotherm applications for electricity production [33]; however, they represent almost half of the installed systems. Even though the Altheim geothermal project counts with a simple saturated ORC plant, in this thesis will be analyzed two different configurations: a simple saturated ORC plant and a saturated recuperative ORC plant. Different working fluids have been taken into consideration, all of them chosen from those most used in the literature. The parameters and constraints used for the modeling of the implants have been taken from various papers, which contain a detailed review of several ORC implants [64, 65, 66, 67, 68, 69]; the most used paper for this part of the thesis was the one made by M. Astolfi and P. Bombarda [69], from which, besides the parameters and constraints for the modeling of the plant, it was also assumed the utilization of the REFPROP model for the simulation of the thermodynamic properties on Aspen Plus.

5.2.1 Simulation of the reference case and assumptions for the optimization of the ORC plant

The reference case for this part of the thesis is based on the real Altheim geothermal project, and it was defined using the data available from the literature. The Table 47 shows some of the most relevant parameters of the reference case that were used for the simulation and optimization the ORC plant. It is worth mentioning that, even though at the beginning the ORC plant was designed as a simple saturated cycle, adopting as working fluid Perfluoro-n-Pentane (C_5F_{12}), after some time the working fluid was soon replaced by an azeotropic mixture.

Assumptions	
Working fluid	Perfluoro-n-Pentane
Cooling medium	Water
Down-hole pump pressure difference	11.5 [bar]
Mass flow rate (cooling water)	340 [kg/s]
Mass flow rate of geothermal fluid	82 [kg/s]
Target Power Produced (approximate)	1 [MW]
T_{eva} of the working fluid	77.6 [°C]
T_{cond} of the working fluid	28.3 [°C]
Temperature of the cooling water	10 [°C]
Target Power Produced (approximate)	1 [MW]

Table 47: Relevant parameters of the reference case.

Using the data from the Table 47 it was performed a simulation of the ORC plant of the Altheim geothermal project. The simulation of the ORC plant was carried out using the 'Design Spec' function, this option allows the user to set a target value for a previously specified parameter; the software does this changing the value of another indicated parameter until it finds the exact pair of values that match the condition imposed by the user. To find the evaporation pressure, the condensation pressure and the mass flow rate of the working fluid were defined three 'Design Spec' (Ds) functions:

- Ds-1: Target condition: $T_{eva} = 77.6$ [°C]; varying the evaporation pressure.
- Ds-2: Target condition: $T_{cond} = 28.3$ [°C]; varying the discharge pressure of the turbine (condensation pressure).
- Ds-3: Target condition: $T_{geo,out} = 70$ [°C]; varying the mass flow rate of the working fluid.

The results of the simulation of the ORC plant can be appreciated in the Table 48 and in the Figure 40. It is worth noticing that the power produced by the simulated ORC plant (993 [kW]) is quite similar to the target value taken from the literature (around 1 [MW]).

$\dot{W}_{net,turb}$ [kW]	$\dot{W}_{net,pump}$ [kW]	$\dot{W}_{net,ORC}$ [kW]	$\dot{Q}_{in}$ [kW]	η_I [%]
993.134	37.125	956.009	12405.100	7.707

Table 48: Results of the simulation of the reference case on Aspen Plus.

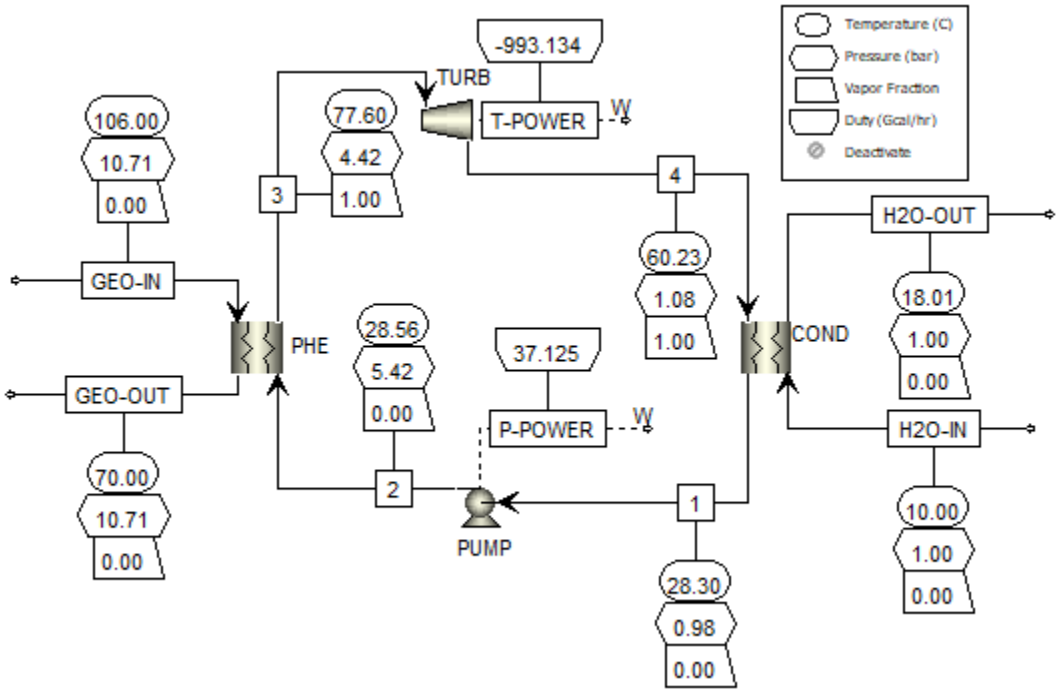

Figure 40: ORC plant of the reference case simulated on Aspen Plus.

Having conducted this performance evaluation as a references case, further simulations were performed by means of Aspen Plus selecting different fluids as working fluid. For every simulation, the results obtained from the DoubletCalc simulation were considered as initial and boundary conditions; in this way the feasibility and reliabilty of coupling the two models can be stated

Therefore, besides some of the parameters of the Table 47, there are certain parameters required for the optimization of the ORC plant that must be taken from the simulation of the doublet system on DoubletCalc v1.4.3; these values are presented in the Table 49 and correspond to the results of the percentile 50 of the reference case.

Pressure at the primary heat exchanger	10.71	[bar]
Mass flow rate	87.14	[kg/s]
Temperature at the heat exchanger	102.62	[°C]

Table 49: Data taken from the DoubletCalc simulation (results of the percentile 50 of the reference case).

These parameters act as initial and boundary conditions for the optimization of the ORC plant, and they could be considered as the link needed for the coupling of the geothermal reservoir model (DoubletCalc v1.4.3) with the ORC plant model (Aspen Plus).

It is well known that for every design or simulation of an ORC plant it is required to define the proper conditions for the optimum operation of the thermodynamic cycle. A higher evaporation pressure implies a higher enthalpy jump on the turbine, which means a higher power produced; on the other hand, a higher evaporation pressure also implies a lower mass flow rate, which decreases the power produced; for this reason, it is necessary to find the optimum values for the most efficient operation of the ORC plant. Being said that, the Table 50 contains the values assumed from the available literature for the optimization of the ORC plant. The parameters used for the optimization of the plant are the pinch point temperature difference in the condenser and in the primary heat exchanger, in this way the thermal energy exchanged is maximized without affecting the correct operation of the plant.

Another assumption that is worth mentioning is the time of the year and the respective ambient temperature; as it was said before, the geothermal water produced is divided into two streams during certain months of the year, one stream for district heating and the other one for electricity generation. For this reason, and for sake of simplicity, it was assumed that the time of the year was summer (no district heating) and consequently all the produced geothermal water was employed for electricity generation.

Time of the year	Summer	[-]
T_{amb}	20	[°C]
η_{pump}	0.75	[-]
$\eta_{pump,el,mec}$	0.95	[-]
$\eta_{turb,is}$	0.85	[-]
$\eta_{turb,el,mec}$	0.97	[-]
$\Delta T_{pp,cond}$	2	[°C]
$\Delta T_{pp,PHE}$	3	[°C]
$\Delta P_{cond,wf}$	0.1	[bar]
$\Delta P_{PHE,wf}$	1	[bar]
Fixed fraction of cooling power for the water loop	1.5	%
Fixed amount of consumption for the other auxiliaries	7	[kW]

Table 50: Assumptions for the simulations of the ORC plant [69, 64, 65].

5.2.2 Selection of the Working Fluid

The selection of the working fluids for the optimization of the ORC plant was defined after two steps. The first one consisted on the collection of the most used working fluids in cases like the one studied in this thesis, taking as reference the previously mentioned papers. The following list contains the most employed working fluids taken from the literature:

- Iso-Pentane
- Iso-Butane
- n-Pentane
- n-Butane
- R245fa
- Ammonia
- Perfluoro-n-Pentane (C5F12)
- R236fa
- R236ea
- Butane
- Perfluoro butane (C4F10)

The most repeated working fluids were chosen from the previous list, in order for being used on the optimization of the ORC plant. Each one of the chosen fluids are presented with their respect characteristics in the Table 51. In addition to the chosen fluids from the list, it was also considered for the simulations a relatively new working fluid called HFO-1234ze(E).

Working Fluid	MM [g/mol]	T_{cr} [°C]	P_{cr} [bar]
R245fa	134	154	36.51
R236fa	152.04	124.92	32
Iso-Butane	58.12	135.9	36.8
Iso-Pentane	72.15	187.25	33.8
R236ea	152.04	139.3	32.4
Butane	58.12	152	37.96
HFO-1234ze(E)	114	109.4	36.36

Table 51: Working fluids considered for the simulations of the ORC plant.

Each one of these fluids was used for the optimization of the ORC plant but juts one of them was chosen for further analysis regarding the coupling of the two simulation models. The selection of the working fluid was based on the current environmental and security regulations that must be respected in these kinds of applications. Therefore, according to a report published by Honeywell [70], which is a document based on the original trilogue agreement, the most appropriate working fluid between the ones described on the Table 51 is the HFO-1234ze(E). Among its principal characteristics that make this fluid so attractive with respect to the others is its classification as 'Non-Flammable', a GWP < 1 and an ODP = 0 [45].

Although the selected fluid was the HFO-1234ze(E), the optimization of the ORC plant (simple and recuperative) was performed for every working fluid on the Table 51. Furthermore, a second law efficiency analysis was done for every case in order to compare the behavior of the ORC plant in different scenarios. The assumptions and results of the second law analysis will be discussed in the following sections, while the optimization curves and the respective values of the optimum point of each of the 'non-selected' working fluids can be seen in the Appendix E and Appendix F.

5.2.3 Optimization of the simple saturated ORC plant

The layout of this case is shown in the Figure 41, which was taken from the interface of the dedicated section on Aspen Plus for the depiction of the desire system. As it can be appreciated, the geothermal fluid enters the preliminary heat exchanger and heats the working fluid until saturation conditions, then the working fluid is expanded in the turbine, cooled in the condenser until saturation conditions and pumped to the primary heat exchanger starting the cycle again. For both the primary heat exchanger and the condenser was selected a "Multi-stream Heat Exchanger" between the options available in Aspen Plus.

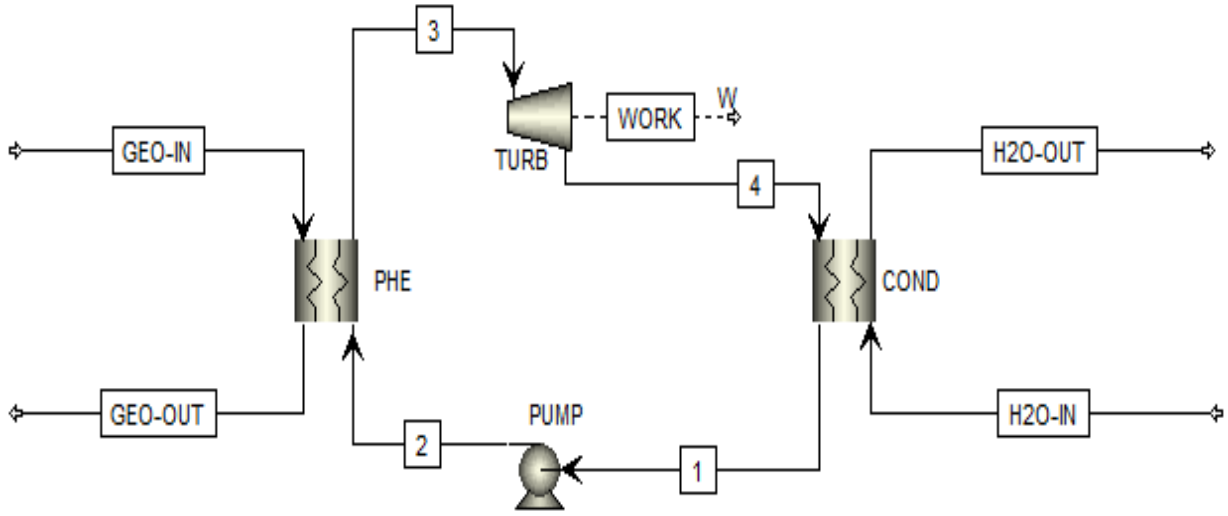

Figure 41: Layout of the simple saturated ORC plant.

The optimizations performed in Aspen Plus for this case were carried out using the 'Design Spec' function. As it was said before, this option allows the user to set a target value for a previously specified parameter. To find the optimal mass flow rate of the working fluid and the optimal discharge pressure of the turbine (condensation pressure), two 'Design Spec' (Ds) functions were defined:

- Ds-1: Target condition: $\Delta T_{pp,PHE} = 3\ [°C]$; varying the mass flow rate of the working fluid.

- Ds-2: Target condition: $\Delta T_{pp,cond} = 2\ [°C]$; varying the discharge pressure of the turbine (condensation pressure).

Then it was used a sensitivity analysis varying the evaporation pressure to find the point in which the ORC plant produces its maximum power (optimum point), this procedure was repeated for every fluid presented in the Table 51. For this configuration were analyzed two different scenarios for the optimization of the ORC plant, one with a $T_{geo,out}$ lower limit equal to 70 [°C] and another one without any temperature limit for $T_{geo,out}$. The Table 52 and the Figure 42 show the most important values of the optimum point for each case and the curve of the sensitivity analysis for the HFO-1234ze(E) respectively. The tables and curves for the rest of the fluids of the Table 51 can be observed in the Appendix E.

	P_{eva} [bar]	P_{cond} [bar]	$T_{geo,out}$ [°C]	Mass flow [kg/s]	$\dot{W}_{net,ORC}$ [kW]
No $T_{geo,out}$ lim.	16.50	4.62	56.14	87.32	1515.61
$T_{geo,out} \geq 70[°C]$	22.00	4.13	71.20	56.62	1278.96

Table 52: Optimized values of the simulation of the simple saturated ORC plant using HFO-1234ze(E) as working fluid.

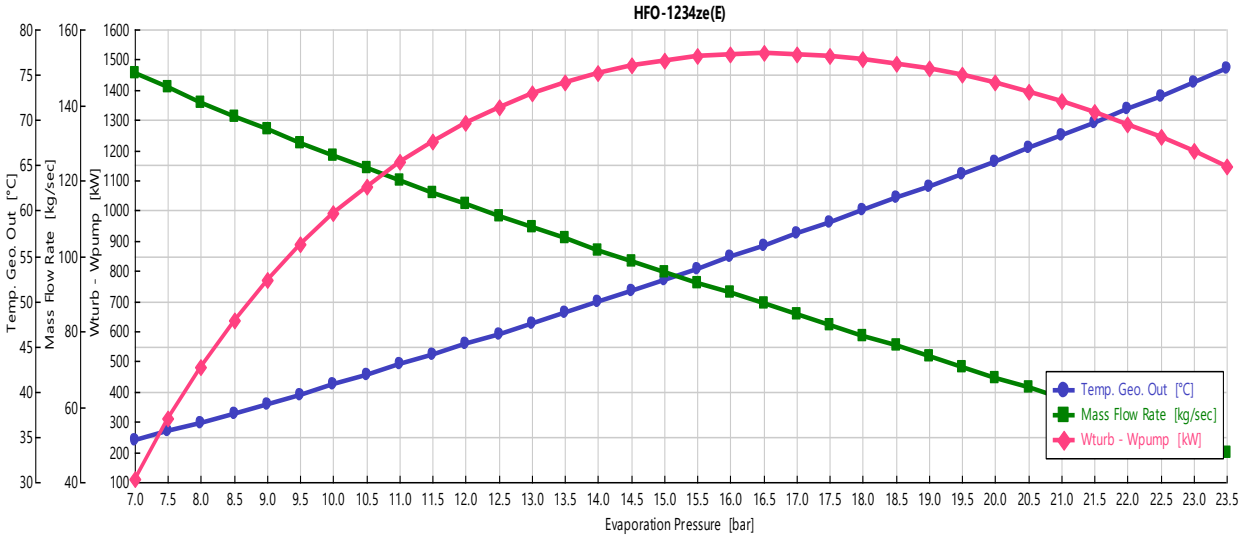

Figure 42: Graph of the optimization of the simple saturated ORC plant using HFO-1234ze(E) as working fluid.

In the Table 52 it can be seen how not imposing a limit to the outlet temperature of the geothermal fluid implies a higher net power than the case with the temperature limit. The case without the temperature limit also has a lower evaporation pressure and a higher mass flow rate than the other case. If there were no operation constraints with the $T_{geo,out}$ limit, all the parameters that have been mentioned should be taken into account for a proper economic analysis to choose the most convenient option for the ORC plant.

Simple saturated cycle without the limit on $T_{geo,out}$

As it was said, the analysis was carried out for the seven different working fluids considered. The variation of the results obtained for the net power of the ORC plant with respect to the evaporation pressure is displayed in the Figure 43.

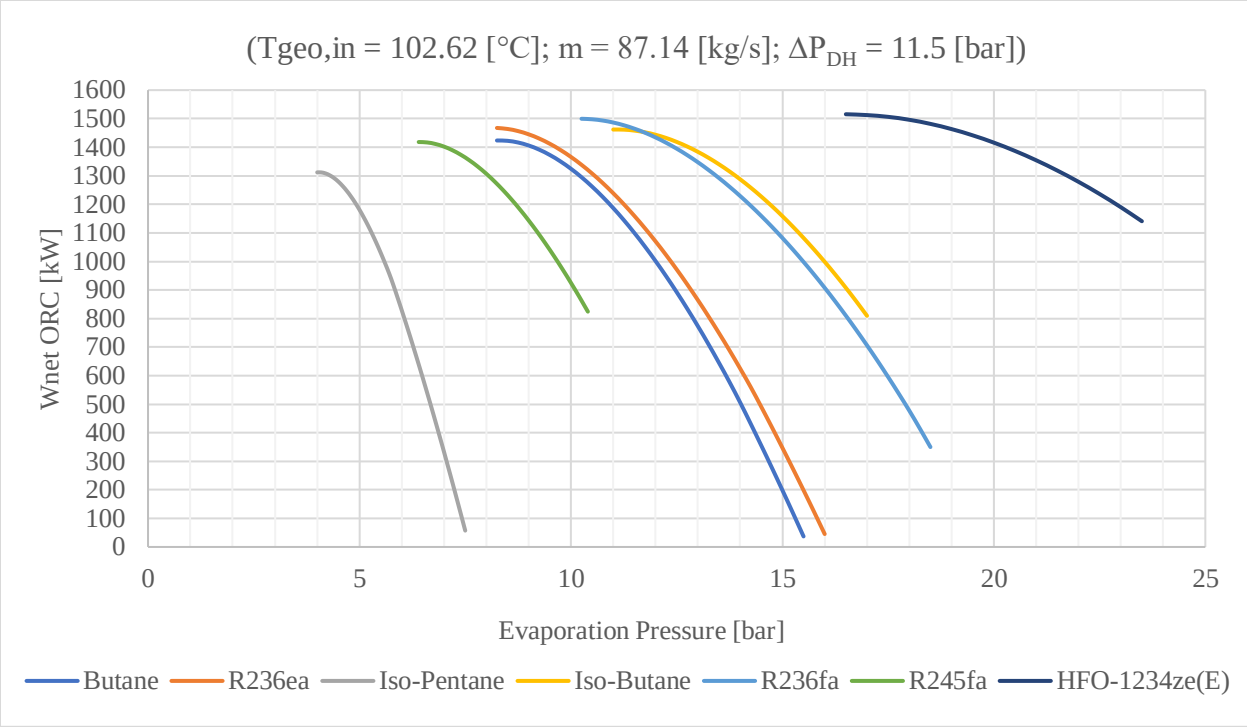

Figure 43: Variation of the net power of the ORC plant with respect to the evaporation pressure without $T_{geo,out}$ limit

In this case the highest net power is obtained using the HFO-1234ze(E) (not by much difference though), but at the same time is probably more expensive than the other options due to its high evaporation pressure. On the other hand, the lowest net power is obtained with the Iso-Pentane, but unlike the HFO-124ze(E), its evaporation pressure is the lowest among all the fluids, which probably makes the Iso-Pentane a cheaper option compared with the other working fluids.

Simple saturated cycle with the limit on $T_{geo,out}$

For the case with the temperature limit for $T_{geo,out}$ all the values from the sensitivity analysis with $T_{geo,out}$ lower than 70 [°C] were neglected. As a matter of fact, it can be seen that the Figure 44 is equal to the Figure 43 but without the values with $T_{geo,out}$ below 70 [°C]. Being said that, the readers can observe that the trend regarding the evaporation pressure does not change from the Figure 43. In general, all the options should operate at higher evaporation pressures, the HFO-1234ze(E) still is the option that operates at the highest P_{eva} and the Iso-Pentane the one at the lowest. On the other hand, unlike the previous case in which the HFO-1234ze(E) was the option that produces the highest net power, now it can be notice how the Iso-Butane, Butane, R245fa and R236fa seems to produce higher net power than the HFO-1234ze(E).

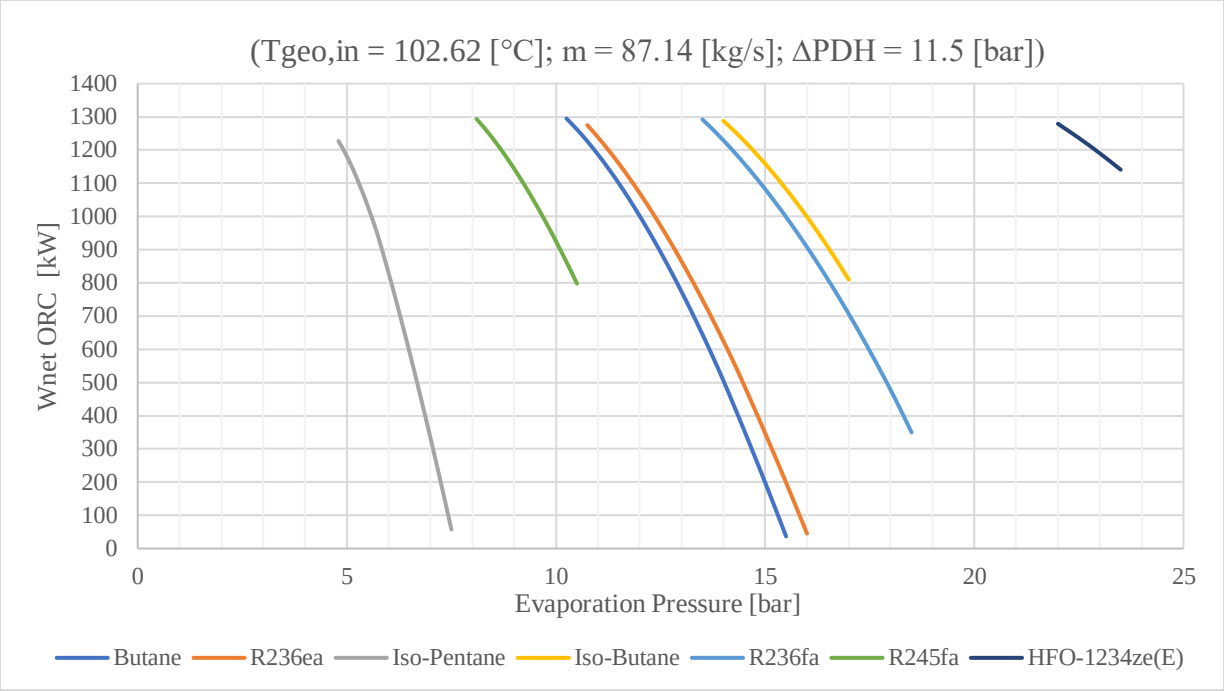

Figure 44: Variation of the net power of the ORC plant with respect to the evaporation pressure with $T_{geo,out}$ limit

5.2.4 Optimization of the saturated recuperative ORC plant

This configuration was considered to analyze the performance of the ORC plant in different scenario. The layout of this case is shown in the Figure 45, the only difference from the simple saturated cycle is the addition of the recuperator after the turbine. This configuration allows to recover part of the thermal energy contained in the outlet stream of the turbine and used for the preheating of the working fluid before entering the primary heat exchanger. As in the previous case, it was selected a "Multi-stream Heat Exchanger" for the recuperator.

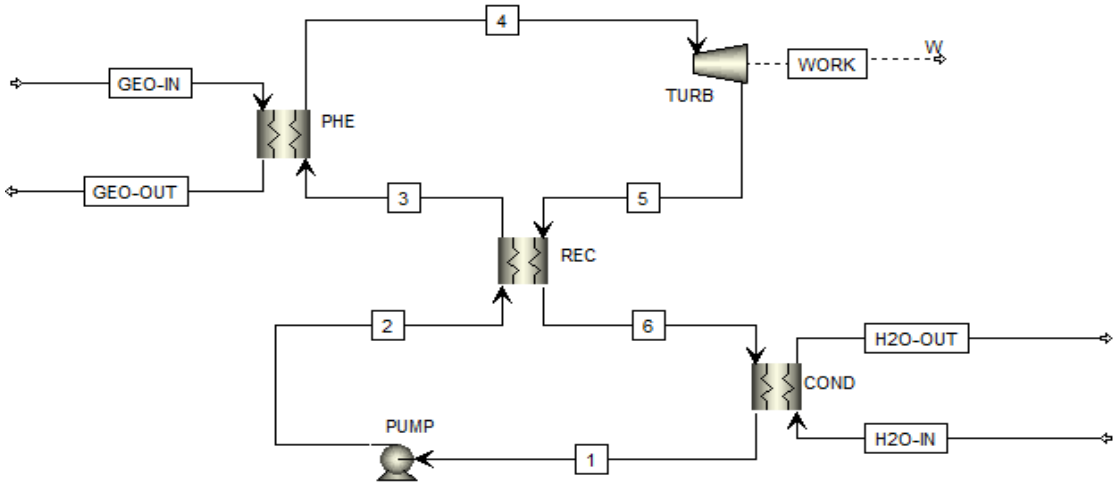

Figure 45: Layout of the saturated recuperative ORC plant.

The same assumptions taken from the previous case were used for the optimization of the ORC plan in this case. The most important addition was a new 'Design Spec' function for the recuperator:

- Ds-3: Target condition: $\Delta T_{pp,rec} = 5\ [°C]$; varying the temperature change of the cold side of the recuperator.

It was also assumed a $\Delta P = 0.5\ [bar]$ in the cold side of the recuperator, taken from the paper of M. Astolfi and P. Bombarda [69].

For this configuration it was considered just one case for the optimization of the plant, in which the outlet temperature of the geothermal fluid must be equal or higher than 70 [°C] (with $T_{geo,out}$ limit). All the results from the sensitivity analysis with $T_{geo,out} < 70\ [°C]$ were neglected. As for the previous configuration, the Table 53 and the Figure 46 show the most important values of the optimum point for this case and the curve of the sensitivity analysis for the HFO-1234ze(E) respectively. The tables and curves for the rest of the fluids of the Table 51 using this ORC plant configuration can be observed in the Appendix F.

P_{eva} [bar]	P_{cond} [bar]	Mass flow [kg/s]	$T_{geo,out}$ [°C]	$\dot{W}_{net,ORC}$ [kW]
22	4.17	59.42	70.02	1314.56

Table 53: Optimized values of the simulation of the saturated recuperative ORC plant using HFO-1234ze(E) as working fluid.

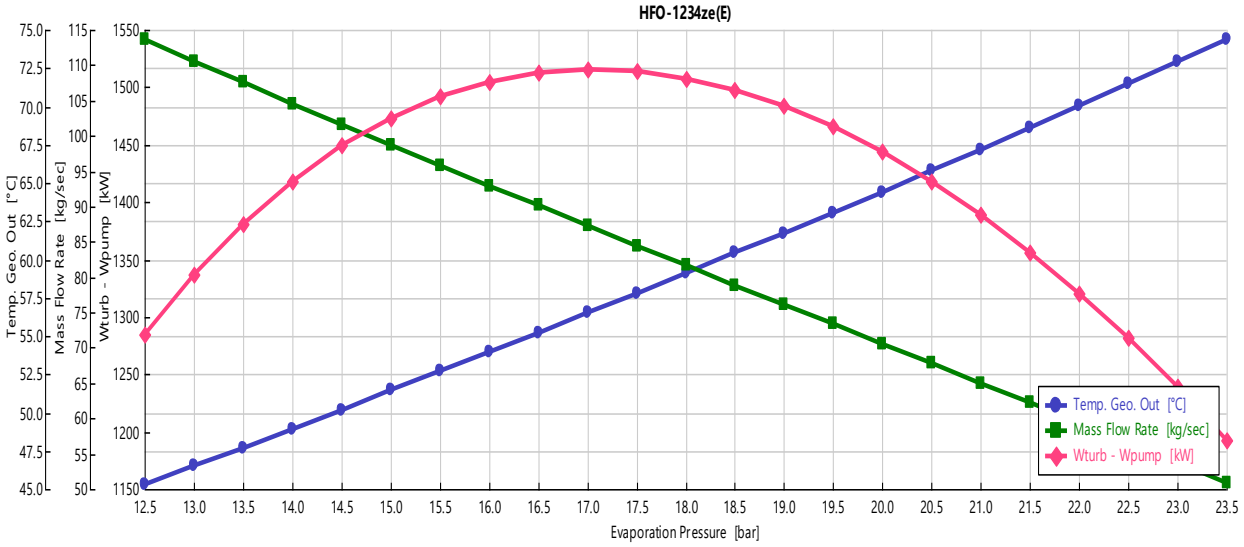

Figure 46: Graph of the optimization of the saturated recuperative ORC plant using HFO-1234ze(E) as working fluid.

For this configuration it is also presented a graph comparing the behavior of the net power of the ORC plant with respect to the evaporation pressure for each of the analyzed fluids. It is worth mentioning that in this graph all the results of $\dot{W}_{net,ORC}$ that correspond to a $T_{geo,out}$ lower than 70 [°C] were neglected.

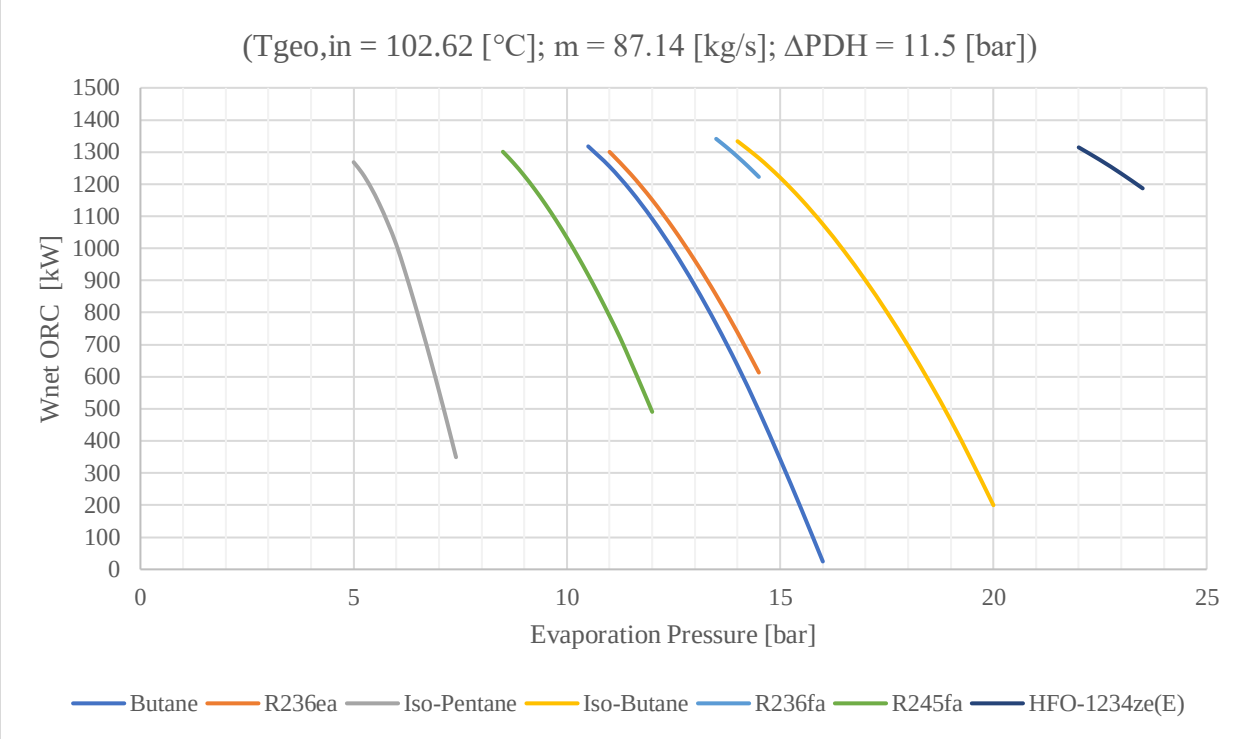

Figure 47: Variation of the net power of the ORC plant with respect to the evaporation pressure for the saturated recuperative ORC plant with $T_{geo,out}$ limit.

From this picture in this case the highest net power is obtained using the R236fa and the Iso-Butane, while the lowest net power appears to be produced by the Iso-Pentane again. The trend of the evaporation pressure is maintained like in the previous configuration, being the HFO-1234ze(E) the one that operates at the highest evaporation pressure and the Iso-Pentane the one that operates at the lowest.

5.3 Second law analysis of the optimized ORC plants

As it was said, a second law efficiency analysis was done for every case for all the working fluids shown in the Table 51. Before presenting the equations used for this analysis, it is necessary to calculate the reversible work that can be obtained from the source of heat, which in this case is the geothermal fluid. The reversible work corresponds to the maximum amount of power that can be produced by a system in reversible conditions with respect to a certain reference state. In the case without the temperature limit at the outlet of the primary heat exchanger the reversible work was calculated using an exergy approach, using the conditions of the geothermal fluid at the inlet of the primary heat exchanger and considering that was cooled down to the reference state at a temperature of 20 [°C]. On the other hand, for the case with the temperature limit, the reversible work was calculated assuming that the geothermal fluid was cooled down to 70 [°C]. The equations (5.1) and (5.2) describe how the reversible work was calculated for the case without and with the temperature limit respectively:

$$\dot{W}_{rev} = \dot{m}_{geo}\left(\left(h_{in,geo} - h_{0,geo}\right) - T_0\left(s_{in,geo} - s_{0,geo}\right)\right) \tag{5.1}$$

$$\dot{W}_{rev} = \dot{m}_{geo}\left(\left(h_{in,geo} - h_{lim,geo}\right) - T_0\left(s_{in,geo} - s_{lim,geo}\right)\right) \tag{5.2}$$

Where the symbols ‘0’ and ‘lim’ indicates the values at reference state and at conditions with the temperature limit. Using the reversible work and the net power produced by the ORC plant in each case, the second law efficiency was calculated as follows:

$$\eta_{II} = \frac{\dot{W}_{net,ORC}}{\dot{W}_{rev}} \tag{5.3}$$

In which the net power produced by the ORC plant is equal to the difference between the net power produced by the turbine minus the net power required by the feed pump of the ORC plant:

$$\dot{W}_{net,ORC} = \dot{W}_{turb} - \dot{W}_{pump} \tag{5.4}$$

For the performance analysis of the ORC plant were also considered the following equations:

$$\eta_I = \frac{\dot{W}_{net,ORC}}{\dot{Q}_{in}} \tag{5.5}$$

$$\eta_{th,rec} = \frac{\dot{Q}_{in}}{\dot{Q}_{in,max}} \tag{5.6}$$

$$\eta_{rec} = \eta_{th,rec} \cdot \eta_I \tag{5.7}$$

With $\eta_{th,rec}$ and η_{rec} the thermal recovery efficiency and total recovery efficiency respectively, $\dot{Q}_{in}$ the thermal energy supplied by the geothermal water in the primary heat exchanger and $\dot{Q}_{in,max}$ the maximum thermal energy that can be recovered from the geothermal water depending the specifications of the case.

As it was said before, according to the available literature, the outlet temperature of the geothermal water from the primary heat exchanger in theory should be equal or higher than 70 [°C], in this way it can be ensured that there will be thermal energy available for the local school and the swimming pool, and also potential problems related with salt precipitation on the pipes and heat exchanger surfaces could be avoided. However, as it was said before, for the optimization of the simple saturated ORC plant were considered two possible cases, one with a $T_{geo,out}$ lower limit equal to 70 [°C] and another without any temperature limit for $T_{geo,out}$. Taking this constraint into consideration, there is a big variation between the second law efficiency value of the two cases; this is mainly because in the case without the temperature limit, $\dot{Q}_{in,max}$ and $\dot{W}_{rev}$ are calculated assuming that the geothermal water was cooled down to the ambient temperature, while for the case with the temperature limit, $\dot{Q}_{in,max}$ and $\dot{W}_{rev}$ are calculated cooling the geothermal water just until 70 [°C]. Doing this, the values of $\dot{Q}_{in,max}$ and $\dot{W}_{rev}$ will be obviously higher in the case without temperature limit, so consequently the heat recovery efficiency and the second law efficiency will be lower than the case with temperature limit.

It is very important to have in mind that the introduction of the cycle efficiency is not intended to be taken as an optimization parameter for the ORC plant; the discussions around these parameters on this thesis are just presented as a tool for the interpretation and comparison between the results obtained for the diverse simulations.

5.3.1 Simple saturated cycle without $T_{geo,out}$ limit

The Table 54 shows the second law efficiency analysis that was done for this case. This calculation confirms what was said before, the option using the HFO-1234ze(E) is the one that produce the highest net power for the ORC plant. In this case, without any temperature limit for the outlet geothermal water, $\dot{Q}_{in,max}$ and the $\dot{W}_{rev}$ were calculated assuming a $T_{geo,out}$ like if the geothermal fluid was cooled down to the ambient temperature. As it could be expected, taking this assumption into consideration, the heat introduced to the system and the maximum heat that can be recovered are very high, which provokes low values for the second law efficiency.

Working Fluid	$\dot{W}_{rev}$ $[kW]$	$\dot{W}_{net,ORC}$ $[kW]$	η_I [%]	$\eta_{th,rec}$ [%]	η_{rec} [%]	η_{II} [%]
Iso-Pentane	3585.910	1311.980	8.833	49.296	4.354	36.587
Iso-Butane	3585.910	1461.987	8.974	54.068	4.852	40.770
Butane	3585.910	1423.695	9.066	52.120	4.725	39.702
R245fa	3585.910	1418.269	9.085	51.814	4.707	39.551
R236fa	3585.910	1499.683	8.940	55.673	4.977	41.822
R236ea	3585.910	1467.544	9.030	53.936	4.871	40.925
HFO-1234ze(E)	3585.910	1515.606	8.927	56.345	5.030	42.266

Table 54: Second law efficiency analysis for the simple saturated ORC plant without $T_{geo,out}$ limit.

5.3.2 Simple saturated cycle with $T_{geo,out}$ limit

The second law efficiency analysis that was calculated for this case is presented in the Table 55. As it was noticed in the Figure 44, the results shown on the table confirmed that the Iso-Butane, Butane, R245fa and R236fa produce higher net power than the HFO-1234ze(E), being the Butane the options that produces the highest net power and the Iso-Pentane the one that produces the lowest. In this case, taking into consideration the temperature limit for the outlet geothermal water, $\dot{Q}_{in,max}$ was calculated assuming that the geothermal water was cooled down to 70 [°C]. The same was assumed for the calculation of the reversible work ($\dot{W}_{rev}$), considering the exergy difference between the state at the inlet of the primary heat exchanger and the outlet at $T_{geo,out} = 70\ [°C]$. As it could be expected, taking this assumption into consideration, the heat introduced to the system and the maximum heat that can be recovered are almost the same, which provokes a recovery efficiency value near to the unit and consequently higher second law efficiency value than the previous case.

Working Fluid	$\dot{W}_{rev}$ $[kW]$	$\dot{W}_{net,ORC}$ $[kW]$	η_I [%]	$\eta_{th,rec}$ [%]	η_{rec} [%]	η_{II} [%]
Iso-Pentane	2189.067	1227.265	10.567	97.370	10.290	56.063
Iso-Butane	2189.067	1287.849	11.177	96.608	10.797	58.831
Butane	2189.067	1295.017	11.084	97.958	10.858	59.158
R245fa	2189.067	1293.383	11.020	98.400	10.844	59.084
R236fa	2189.067	1292.143	11.048	98.057	10.833	59.027
R236ea	2189.067	1274.759	11.098	96.304	10.688	58.233
HFO-1234ze(E)	2189.067	1278.959	11.132	96.324	10.723	58.425

Table 55: Second law efficiency analysis for the simple saturated ORC plant with $T_{geo,out}$ limit.

5.3.3 Saturated recuperative ORC plant

The Table 56 shows the second law efficiency that was done for this configuration. As it was noticed in the Figure 47, the R236fa and the Iso-Butane are the options that produce the highest $\dot{W}_{net,ORC}$. In this configuration it was also considered the temperature limit for the outlet geothermal water, so just like the previous case, the $\dot{Q}_{in,max}$ and $\dot{W}_{rev}$ were calculated assuming that the geothermal water was cooled down to 70 [°C].

It can be observed comparing the results presented in the Table 56 and in the Table 55 that the addition of the recuperator helps the ORC plant to reach higher values for the $\dot{W}_{net,ORC}$ and the second law efficiency, mainly because the recuperator allows to exploit more efficiently the thermal power available from the geothermal water. However, having the same considerations than the previous case, is important to highlight that the improvement on the net power produced is quite small compared to the simple cycle with temperature limit. Normally, it would be expected that the addition of the recuperator provokes a considerable boost on the net power produced by the plant that compensate in a certain way the economic investment. In this case the temperature of the geothermal fluid is not high enough to allow the cycle recover sufficient thermal energy and make the economic investment worthy. For this reason, the selection of the configuration of the ORC plant, in a real case scenario, must be decided after proper economic and performance analysis.

Working Fluid	$\dot{W}_{rev}$ [kW]	$\dot{W}_{net,ORC}$ [kW]	η_I [%]	$\eta_{th,rec}$ [%]	η_{rec} [%]	η_{II} [%]
Iso-Pentane	2189.06663	1268.326	10.770	98.739	10.634	57.939
Iso-Butane	2189.06663	1333.734	11.348	98.540	11.182	60.927
Butane	2189.06663	1317.719	11.364	97.215	11.048	60.195
R245fa	2189.06663	1300.921	11.449	95.267	10.907	59.428
R236fa	2189.06663	1341.079	11.484	97.910	11.244	61.263
R236ea	2189.06663	1300.419	11.784	92.524	10.903	59.405
HFO-1234ze(E)	2189.06663	1314.556	11.028	99.942	11.021	60.051

Table 56: Second law efficiency analysis for the saturated recuperative ORC plant with $T_{geo,out}$ limit.

5.3.1 Analysis of the second law efficiency losses for the simple saturated ORC plant

Since the reference case assumed in this thesis correspond to a simple saturated ORC plant, based on the real Altheim geothermal project, it was also analyzed the second law efficiency losses for every component of the optimized simple saturated ORC plant. Neglecting the possible operation requirements from the local school and the swimming pool, this evaluation was performed just for the simple saturated cycle without temperature limit, since it is the case that produces the highest net power among all the cases.

To calculate the second law efficiency with this approach, taking into account the losses due to the irreversibilities of all the components that compose the ORC plant, it is necessary to calculate first the reversible work that can be obtained from the source of heat as it was done for the previous analysis. As it was already seen, for this case the reversible work was calculated using the conditions of the geothermal fluid at the inlet of the primary heat exchanger and considering that was cooled down to the reference state at a temperature of 20 [°C]. Having calculated the reversible work, the second law efficiency loss of every component of the plant can be calculated using the following equation:

$$\Delta\eta_{II,i} = \frac{\dot{W}_{loss}}{\dot{W}_{rev}} \tag{5.8}$$

Then, the second law efficiency of the cycle can be obtained as follows:

$$\eta_{II} = 1 - \sum \Delta\eta_{II,i} \tag{5.9}$$

Where $\Delta\eta_{II,i}$ correspond to the second law efficiency losses of a certain component 'i'. For this case were taken into account seven second law efficiency losses within the cycle, the losses in the condenser, pump, turbine, primary heat exchanger, reinjected geothermal fluid and the electrical-mechanical losses (both for the pump and for the turbine). The equations used for the calculation of all these losses are presented in the following paragraphs.

The second law efficiency losses in the condenser are cause mainly by two irreversibilities: one due to the heat transfer and the other due to the mixing of the coolant discharged by the condenser into the environment. The Equation (3.10) describes how this loss was calculated:

$$\Delta\eta_{II,cond} = \frac{T_0\left(\dot{m}_{wf}\left(s_{out,cond} - s_{in,cond}\right) + \frac{\dot{Q}_{cond}}{T_0}\right)}{\dot{W}_{rev}} \tag{5.10}$$

The efficiency loss associated with the pump are caused by the fluid dynamic irreversabilities that take place inside this component. Generally, these losses are small compared to those of other elements of the plant and their importance rises proportional with the maximum cycle pressure.

$$\Delta\eta_{II,pump} = \frac{T_0\dot{m}_{wf}}{\dot{W}_{rev}}\left(s_{out,pump} - s_{in,pump}\right) \tag{5.11}$$

The losses in the turbine are caused by the same kind of irreversibilities than the ones in the pump. The following equation describes the efficiency losses produced due to expansion of the working fluid in the turbine:

$$\Delta\eta_{II,turb} = \frac{T_0\dot{m}_{wf}}{\dot{W}_{rev}}\left(s_{out,turb} - s_{in,turb}\right) \tag{5.12}$$

The efficiency losses in the primary heat exchanger are associated with the production of irreversibility due to two phenomena: the heat introduction to the cycle from the geothermal fluid to the working fluid and the pressure drops. The efficiency losses in this component were calculated as follows:

$$\Delta\eta_{II,PHE} = \frac{T_0\left(\dot{m}_{wf}\left(s_{out,PHE} - s_{in,PHE}\right) + \dot{m}_{geo}\left(s_{out,geo} - s_{in,geo}\right)\right)}{\dot{W}_{rev}} \tag{5.13}$$

The electrical and mechanical losses correspond to the dissipation of totally lost energy from the conversion of the mechanical energy into electric energy. These losses must be calculated both for the pump and the turbine of the ORC plant:

$$\Delta\eta_{II,pump,el,mec} = \frac{\dot{W}_{gross,pump}\left(\frac{1}{\eta_{pump,el,mec}} - 1\right)}{\dot{W}_{rev}} \quad (5.14)$$

$$\Delta\eta_{II,turb,el,mec} = \frac{\dot{W}_{gross,turb}\left(1 - \eta_{pump,el,mec}\right)}{\dot{W}_{rev}} \quad (5.15)$$

The reinjection losses can be considered as an 'stack' efficiency loss, which is caused by the heat transfer of the geothermal fluid at the outlet conditions of the primary heat exchanger with the environment at temperature T_0.

$$\Delta\eta_{II,reinj} = \frac{\dot{m}_{geo}\left(\left(h_{out,geo} - h_{0,geo}\right) - T_0\left(s_{out,geo} - s_{0,geo}\right)\right)}{\dot{W}_{rev}} \quad (5.16)$$

All the values needed for the calculation of these losses and the later second law efficiency of the ORC plant were taken from the results obtained from the optimization performed on Aspen Plus. The Table 57 shows the results obtained from this analysis:

$\Delta\eta_{II,cond}$	4.048	[%]
$\Delta\eta_{II,pump}$	0.826	[%]
$\Delta\eta_{II,turb}$	8.123	[%]
$\Delta\eta_{II,PHE}$	22.191	[%]
$\Delta\eta_{II,pump\ el,mec}$	1.415	[%]
$\Delta\eta_{II,turb,el,mec}$	0.174	[%]
$\Delta\eta_{II,reinj}$	20.987	[%]
η_{II}	42.234	[%]

Table 57: Second law efficiency losses of the simple saturated ORC plant without temperature limit

From these results it can be clearly appreciated that the most important losses are the ones related with the heat introduction and the heat rejection from the system, being the highest the primary heat exchanger efficiency loss, followed by the reinjection losses. This was expected due to the high irreversibilities that are associated with the heat introduction to the system and the heat rejection to the environment that take part on these components. It is also important to mention that the value obtained from the calculation of the second law efficiency is consistent with the one calculated using the previous approach, proving in this way that the two procedures were carried

out correctly and the efficiency losses that were taken into account are exactly the ones that need to be considered. for this analysis.

5.4 Analysis of the geothermal plant considering the coupling of the two simulation models

To study the behavior and the performance of the overall geothermal plant, the coupling of the two models was analyzed with two different approaches. First, it was studied a graph that represents the influence of the permeability on the mass flow rate, the required down-hole pump power and the net power produced by the geothermal plant. In this graph the value of the down-hole pump pressure difference was maintained constant at the value of the reference case (11.5 [bar]) and just the permeability was varied.

The second approach consist on replicate the fingerprint graph that can be obtained from DoubletCalc v1.4.3. In this graph were examined the influence of the down-hole pump pressure difference on the mass flow rate of geothermal fluid produced, the required down-hole pump power and the net power produced by the geothermal plant (net power of the ORC plant minus the power consumed by the auxiliaries, the water loop of the condenser and the down-hole pump). There are four different fingerprint graphs presented on this thesis, one for the optimized simple saturated ORC plant, one considering the permeability value of the previous case multiplied by 0.5, then another one with the permeability multiplied by 0.25 and finally one with a permeability multiplied by 0.1; in this way it can be appreciated the influence of one of the most important parameters of the geothermal reservoir on the performance of the plant changing the down-hole pump pressure difference.

As it was mentioned, the case that was studied in this part of the thesis is the optimization of the simple saturated cycle without the temperature limit, since it has the same configuration of the real Altheim geothermal plant and is the option that produces the highest net power. However, if the readers want to see the graphs for the simple saturated cycle and the saturated recuperative cycle with the temperature limit, these are presented on the Appendix G and Appendix H respectively.

Like it was said in the previous paragraphs, the net power produced by the geothermal plant was calculated like in the Equation (5.17), in which the power required by the downhole pump was taken from the DoubletCalc simulation, the power consumed by the auxiliaries was assumed as 7 [kW] and the power consumed by the water loop is equal to the 1.5 [%] of the heat exchanged in the condenser.

$$\dot{W}_{net,plant} = \dot{W}_{net,ORC} - \dot{W}_{DH} - \dot{W}_{water\ loop} - \dot{W}_{aux} \tag{5.17}$$

5.4.1 Simple saturated ORC plant without temperature limit

The Figure 48 shows the influence of the permeability of the geothermal reservoir on the produced mass flow rate, the required power by the down-hole pump, the net power produced by the ORC plant and the net power produced by the geothermal plant. For this analysis were considered all the inputs used for the DoubletCalc simulation of the reference case except by the permeability, which was varied according to the data shown in the graph, maintaining a constant down-hole pump pressure difference of 11.5 [bar].

This graph was done making a DoubletCalc simulation for every permeability value that can be seen on the graph, from these simulations were taken the required down-hole pump power, the temperature at surface level, the pressure at surface level and the produced mass flow rate. These last three parameters were used for the optimization of the simple saturated ORC plant performed on Aspen plus, which was repeated for every point of the graph taking from every simulation the value of the net power produced by the ORC plant. Then, the net power produced by the geothermal plant was calculated and all the four parameters were graphed with respect to the permeability variation.

From the graph it can be observed practically the same trend for all the four curves, which indicates a permanent decrease when the permeability is reduced. It could be said that the decrease starts to be more pronounced more less after a permeability equal to 212.6 [mD]. Therefore, it can be said that for this case, if the permeability value is lower than this point, the geothermal reservoir would not be considered attractive for electric generation applications.

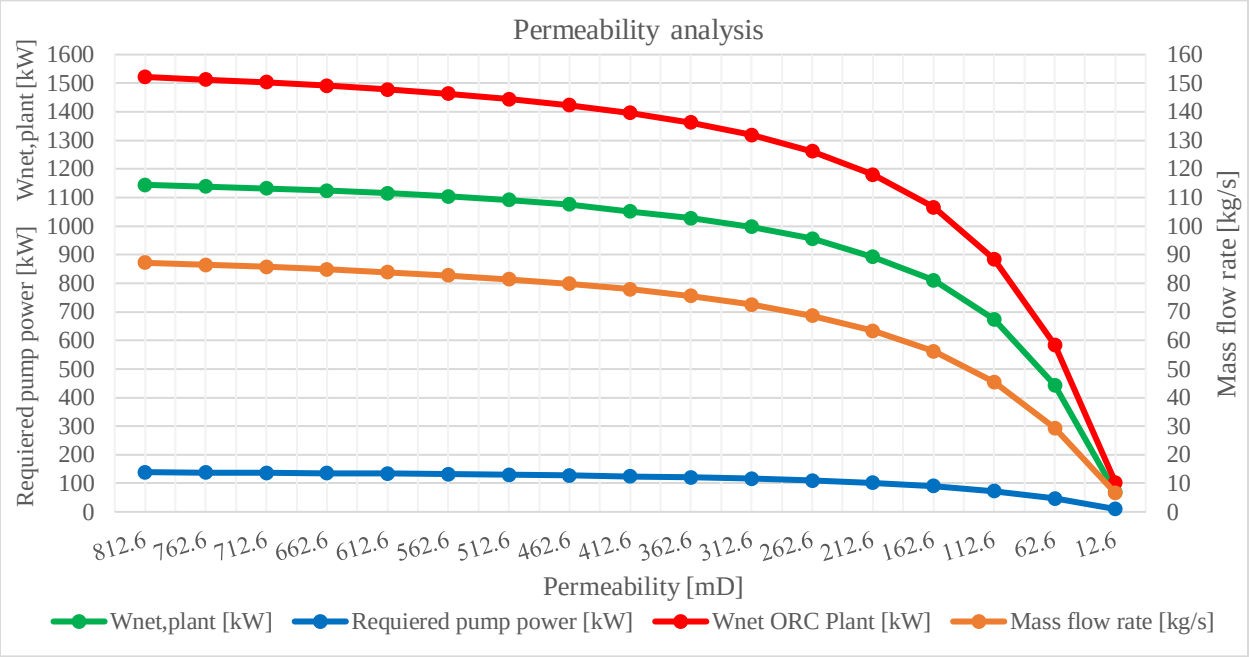

Figure 48: Permeability analysis for the simple saturated ORC plant without temperature limit.

Seeing that the permeability has a big impact on the net power produced by the geothermal plant at constant downhole pump pressure difference, it was also studied a case in which the permeability is maintained constant and the down-hole pump pressure difference is changed.

The Figure 49 represent the fingerprint graph for the reference case scenario, corresponding to the optimization of the simple saturated ORC plant without temperature limit. This graph was done making a DoubletCalc simulation for every down-hole pump pressure difference and taking for every simulation the calculated require down-hole pump power, the temperature of the geothermal fluid at surface level, the pressure of the geothermal fluid at surface level and the mass flow rate of the geothermal fluid produced. Then, the temperature, pressure and mass flow rate of the geothermal fluid were used to perform an optimization of the simple saturated ORC plant on Aspen Plus for every point of the graph and taking from the results the net power produced by the ORC plant. Having all the results needed from the two simulation software's, the net power produced by the geothermal plant was calculated as the difference between the net power produced by the ORC plant and the required power by the down-hole pump.

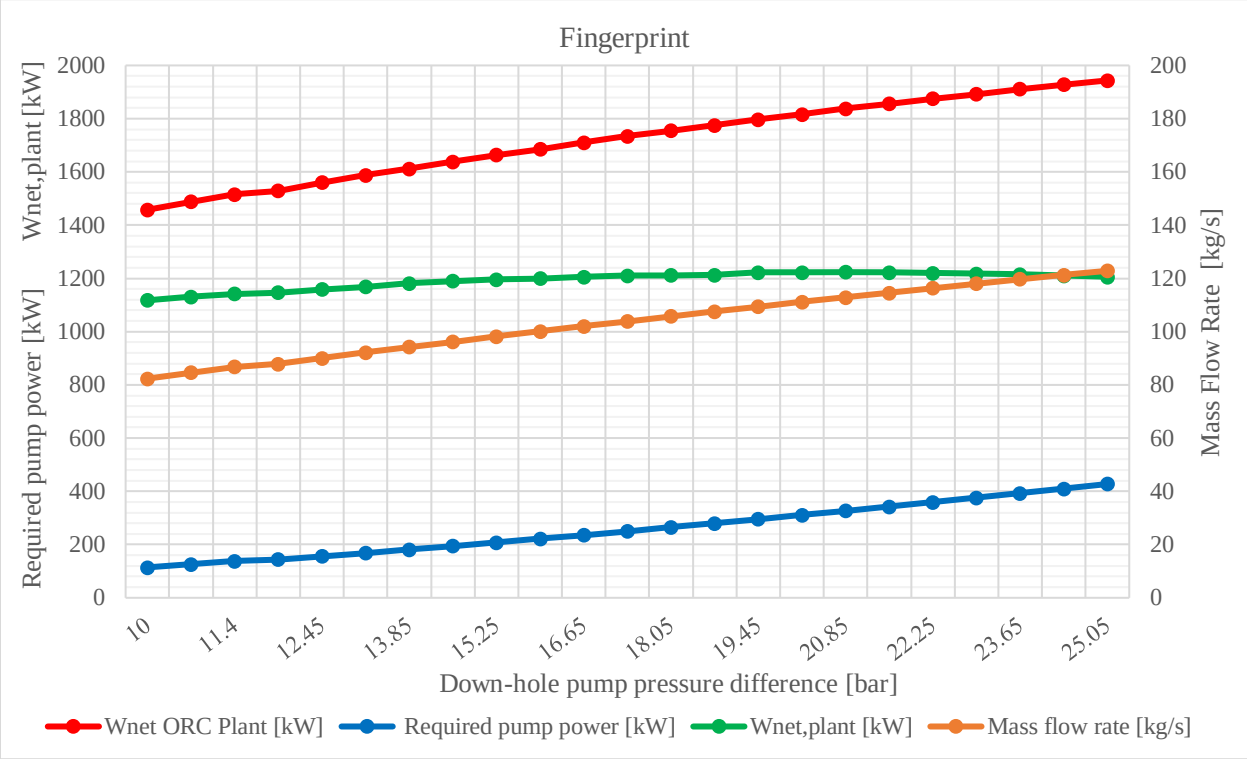

Figure 49: Fingerprint graph of the reference case scenario for the simple saturated ORC plant without temperature limit.

From the Figure 49 it can be seen that the net power of the ORC plant, the mass flow rate and the require down-hole pump power increase proportionally with the increase of the down-hole pump pressure difference, while the net power produced by the geothermal plant seems to have a maximum in a certain point but in general its behavior is relatively constant. The maximum decrease that it can be observed from the maximum net power produced to the lowest net power produced is 8,6 [%] approximately, which is quite low and practically does not imply much difference, in terms of net power produced, between operate at a down-hole pump pressure difference of 10 [bar] or 25 [bar]. One other thing that is worth noticing is that the value of the net power produced by the geothermal plant a bit higher than the value of the real Altheim geothermal project (around 1 [MW]). This difference is mainly due to the fact that this analysis was performed for the optimized case without temperature limit. However, the results suggest an acceptable output for the coupling of the two simulation software's.

The following three figures represent the fingerprint graph for three different permeability values with respect to the reference case scenario. It can be appreciated from these graphs that the power required by the down-hole pump for producing the same mass flow rate value than the reference case increases at lower permeability values, because of this, the net power produced by the geothermal plant decreases compared with the reference case. It can be also observed from these graphs that at lower permeability values, the maximum of the net power produced by the geothermal plant it can be seen clearer than for the reference case, in which the trend was almost constant.

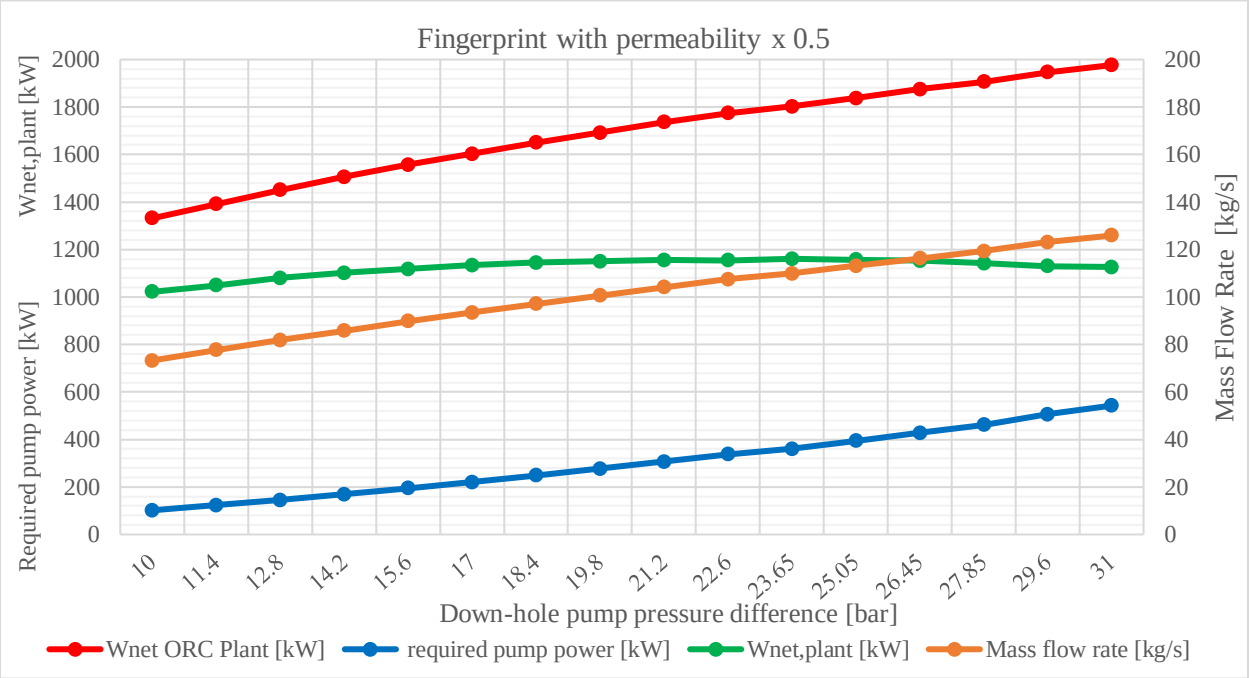

Figure 50: Fingerprint graph of the scenario with permeability x 0.5 for the simple saturated ORC plant without temperature limit.

Taking as point of comparison a target mass flow rate produced within the range of 115 and 130 [kg/s] (which is represented by the last points on every fingerprint graph), it can be seen from the Figure 49 that the down-hole pump of the base case supplies a pressure difference of 25 [bar] and needs around 400 [kW] for producing this value of mass flow rate, which implies a net power produced equal to 1200 [kW] approximately. On the other hand, considering the half of the permeability that was used for the reference case, the Figure 50 indicates that in this case produces a net power near the 1100 [kW] for the target mass flow rate, operating with a down-hole pump pressure difference of 31 [bar] and about 550 [kW] of require down-hole pump power. Also, in this case the difference between the maximum and the minimum net power produced implies a decrease of about 12 [%], which suggest that at lower permeabilities the trend of the net power produced curve by the geothermal plant will not be as 'constant' as the reference case and the maximum point will be see clearer.

In the Figure 51 it can be appreciated that it is necessary a down-hole pump pressure difference of 40 [bar] to be able to produce the target mass flow rate for the case with a permeability value multiplied by 0.25. Because of this considerable increase on the pump pressure difference, the require down-hole pump power almost doubles the value of the previous case, with a require power of 700 [kW]. Having this high required pump power, the net power produced by the geothermal plant decreased almost 250 [kW] with respect to the reference case, having a value of about 970 [kW].

It is also important to notice that for this case the trend of the net power produced curve it cannot be considered as constant anymore, since it can be clearly spotted the maximum point of the curve. The decrease between the maximum and the minimum net power produced in this case is around 19 [%], which is clearly not negligible and limit the operation of the plant to a certain down-hole pump pressure difference to maximize the production.

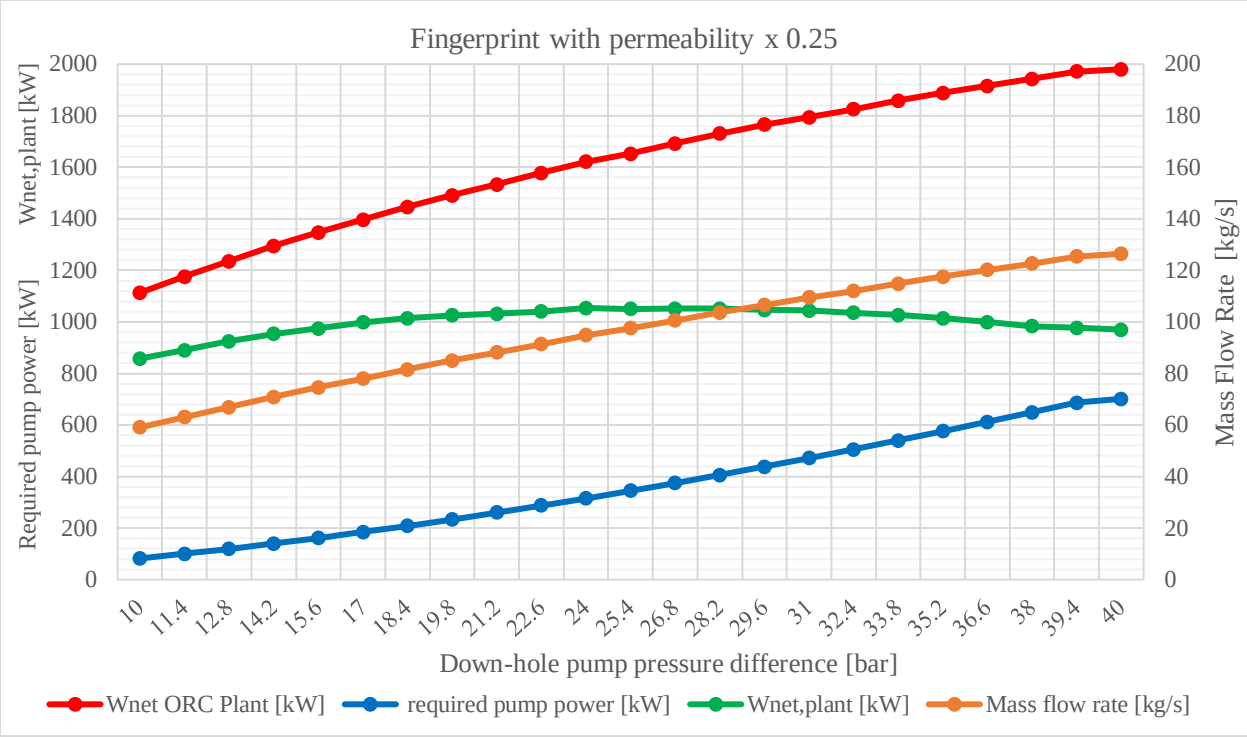

Figure 51: Fingerprint graph of the scenario with permeability x 0.25 for the simple saturated ORC plant without temperature limit.

Finally, the case with a permeability value multiplied by 0.1 shown in the Figure 52 is the clearest representation of the importance of this parameter in a geothermal plant among the fingerprint graphs previously discussed. For instance, the net power produced in this case for the first point of the graph with a pressure difference of 14 [bar], it is almost half of the value that the one obtained in the reference case with the same down-hole pressure difference. As a matter of fact, to be able to produce the target mass flow rate within the range of 115 and 130 [kg/s], this case needs a down-hole pressure difference of 60 [bar], almost three times the value needed in the reference case. To be able to supply this pressure difference, the down-hole pump requires around 950 [kW], which implies a net power produced of 600 [kW], practically half of the net power produced in the reference case. Making the same analysis than from the previous cases comparing the maximum and the minimum net power produced, this case presents a decrease of 25 [%] approximately, a considerable amount that cannot be neglected and restrict the plant to operate under certain conditions.

With these results it is obvious that it would be impossible to operate the plant in these conditions, both because of the performance of the plant and the high investment cost that would imply a down-hole pump with the characteristics needed for this case. The required power by the down-hole pump is almost equal to the net power produced by the real Altheim geothermal project, while the net power produced in this case is almost half of the target value of the real geothermal plant.

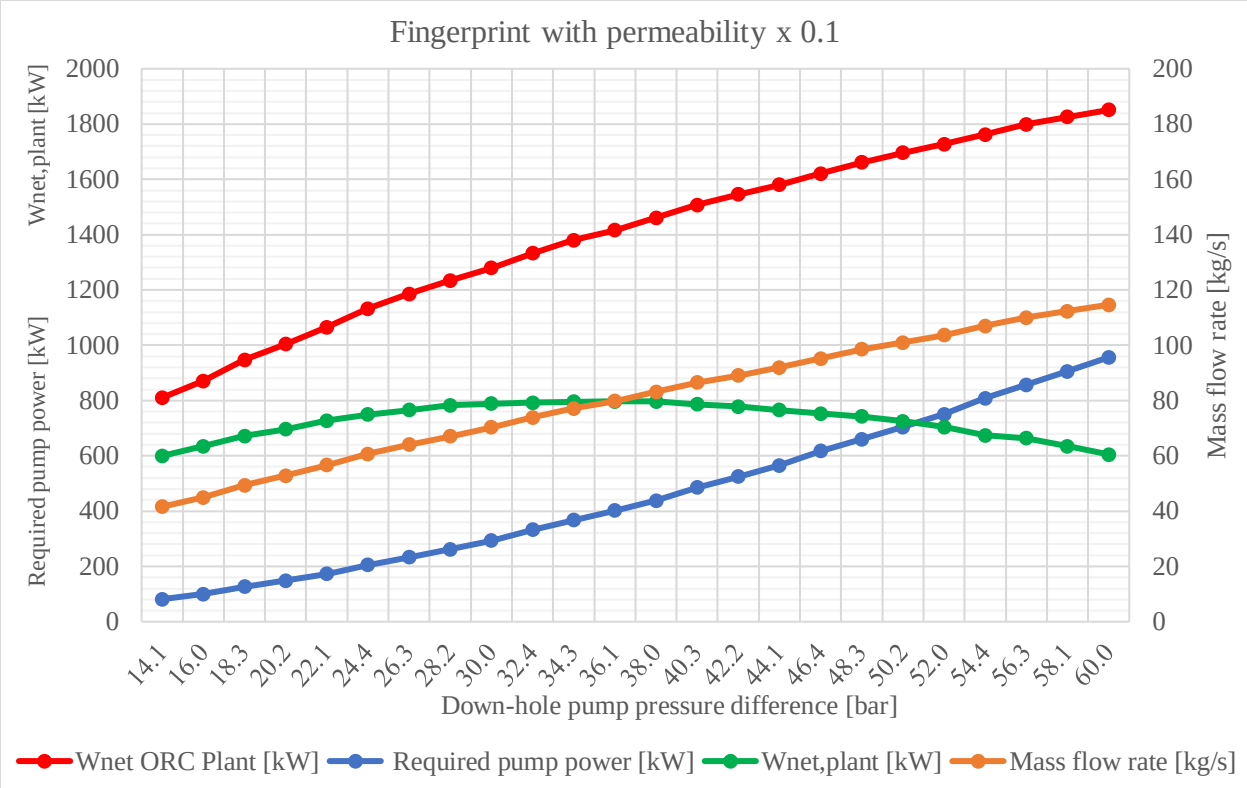

Figure 52: Fingerprint graph of the scenario with permeability x 0.1 for the simple saturated ORC plant without temperature limit.

VI. Conclusions

In these days, the principal constraint for the expansion of the geothermal energy on the world energy market is the high uncertainty that exist in a geothermal project is around the exploration and drilling processes; this problem implies a high economic risk compared with other traditional renewables resources like solar or wind. The geothermal energy has an immense potential of being one of the most important sources of renewable energy in the future, but it is fundamental the development of new techniques or tools that enable an efficient assessment of the most relevant subsurface parameters for a reliable preliminary simulation of the reservoir.

After a proper explanation of the most relevant governing equations of the geothermal reservoirs and the model of DoubletCalc v1.4.3, it has been seen how an open source software like the one utilized during this thesis allow the users to produce reliable simulations of homogeneous geothermal reservoirs. The reliability of the DoubletCalc model have been proved through the validation of the model, in which the results of the simulation of four real geothermal projects have been compared with the data available from the literature, obtaining small errors with respect to the target results of the reference cases.

One of the four study cases used for the validation of the DoubletCalc model was selected as reference case for the simulation and optimization of the ORC binary plant, which were performed using a commercial software called Aspen Plus. The study case selected was the Altheim geothermal project located in Austria, mainly because was the one with more data available for the simulation of the ORC plant and the results obtained in the validation of the DoubletCalc model were quite good. The simulation of the reservoir was realized on DoubletCalc v1.4.3 using the data available from the literature. Some of the results obtained from the reservoir simulation were used as initial and boundary conditions for the later simulation and optimization on Aspen Plus, specifically the mass flow rate of geothermal fluid produced, the temperature and the pressure of the geothermal fluid at surface level.

The optimization of the ORC plant was performed using seven different working fluids, which were chosen from the most commonly used in these kinds of applications. Three different cases were taken into account for the optimization, two utilizing a simple saturated ORC plant and one utilizing a saturated recuperative ORC plant. The difference between the two cases for the simple cycle was the consideration of a minimum temperature limit of 70 [°C] for the geothermal fluid at the outlet of the primary heat exchanger for one of the cases, while for the recuperative cycle was contemplated just one case considering the temperature limit.

The optimization was carried out imposing target values taken from the literature for the pinch point temperature difference in the primary heat exchanger, the condenser and in the recuperator varying the mass flow rate, the condensation pressure and the temperature change in the cold side of the recuperator respectively. Then, a sensitivity analysis varying the evaporation pressure was done to find the optimum point in each case. A graph of the net power produced by the ORC plant versus the evaporation pressure was realized for each case, considering all even working fluids on the graph.

With the results of the optimization, a second law efficiency analysis was executed for every working fluid and for every case. For this analysis it was used an approach utilizing the net power produced by the ORC plant and the reversible work that could be produced, which was calculated considering that the geothermal fluid was cooled down to ambient temperature in the case without temperature limit and down to 70 [°C] in the case with the temperature limit. The results of the optimization and the second law efficiency analysis were presented for all three cases and for the seven working fluids. From the results it can be appreciated that the simple cycle without temperature limit is the option that produces the highest net power, but at the same time is the one with the lowest efficiency. On the other hand, the results of the simple and recuperative cycle with the temperature limit are very similar; the recuperative cycle has slightly better results, but the temperature of the geothermal fluid is not high enough to make the recuperative cycle an option worth of consideration taking into account the high economic investment that implies the addition of a recuperator.

From the seven working fluid that were studied it was selected the optimization performed using the HFO-1234ze(E) for further analysis, mainly because among all the fluids selected, the HFO-1234ze(E) is the only that completely meet the current environment and security regulations for these kinds of applications. From the optimizations using HFO-1234ze(E) it was chosen the simple saturated ORC plant without temperature limit for further investigations, principally because it has the same configuration of the real Altheim plant and is the option that produces the highest net power among the three cases that were studied.

For this case it was performed a second law efficiency analysis, calculating the most relevant second law efficiency losses of the plant and calculating the second law efficiency with a different approach than before. The results of this analysis shown that the most important losses are provoked by the heat introduction to the system and the heat rejection to the environment, and these are located in the primary heat exchanger and the outlet geothermal fluid stream. The result of the second law efficiency is consistent with the one calculated with the net power produced by the ORC plant and the reversible work, which indicates that the two procedures were carried out correctly.

Finally, it was analyzed the coupling of the two simulation models used in this thesis. To do that it was again selected the simple saturated cycle without temperature limit using HFO-1234ze(E) as working fluid. The coupling of the two models was analyzed using two kind of graphs, the first one was realized varying the permeability of the geothermal reservoir with respect to the mass flow rate produced, the require down-hole pump power, the net power produced by the ORC plant and the net power produced by the overall geothermal plant (net power of the ORC plant minus required power by the down-hole pump), maintaining a constant value for the down-hole pump pressure difference. For the second graph was maintained constant the permeability value and it was varied the down-hole pump pressure difference with respect to the mass flow rate produced, the required down-hole pump power, the net power produced by the ORC plant and the net power produced by the geothermal plant.

The results of the first graph indicate that decreasing the permeability there is a constant decrease of all the other variables, and after a certain value of permeability the geothermal reservoir is not worthy of exploitation for electricity production. The second graph was analyzed for four different values of permeability, one base case that corresponds to the optimization of the simple cycle without temperature limit, one with half of the permeability, one with a quarter of the permeability and one with a permeability multiplied by 0.1. The base case shows that the trend of the net power produced curve is almost constant and there is not a significant change between different operation values for the down-hole pump pressure difference. However, decreasing the permeability it can be seen clearly that the trend of the curve shows a maximum and there is a considerable difference between the maximum net power produced and the minimum power produced. Therefore, if the permeability of a geothermal reservoir is low, then it exists an optimum value for the flow rate of the produced geothermal fluid that maximize the plant performance. Because of this, for low permeability values it is necessary to do a performance analysis to find the best operation value for the down-hole pump pressure difference.

Future investigations related with the topic of this thesis could be the introduction of the model of DoubletCalc 2D into the simulation of the ORC plant. As it was previously presented, DoubletCalc 2D allows the user to simulate the development of the geothermal reservoir in time, which would be an interesting addition to the simulation. DoubletCalc 2D, unlike DoubletCalc v1.4.3, presents also the possibility to simulate heterogeneous reservoirs, which would expand the field of potential simulations and would allow to consider reservoirs with fractures or enhanced geothermal systems. It would be also interesting to analyze different configurations for the ORC plant, such as a two-pressure level plant for instance, or to simulate and optimize a geothermal plant in which the addition of a recuperator implies a considerable boost in the net power produced. However, probably the most directly related future work that could be developed would be to analyze the performance of the selected geothermal plant (Altheim geothermal project) during a whole year; this because in this thesis it was assumed that the time of the year was summer and all of the geothermal fluid produced was used only for the generation of electricity, but during winter for instance, a not negligible part of the produced mass flow rate should go to the district heating of the city.

References

[1] J. van Wees , A. Kronimus , M. van Putten, M. Pluymaekers , H. Mijnlieff, P. van Hooff , A. Obdam and L. Kramers, "Geothermal aquifer performance assessment for direct heat production – Methodology and application to Rotliegend aquifers," *Netherlands Journal of Geosciences*, vol. 91 – 4, pp. 651 - 665, 2012.

[2] H. Mijnlieff, A. Obdam, . J. van Wees, M. Pluymaekers and . J. Veldkamp, "DoubletCalc 1.4 manual: English version for DoubletCalc 1.4.3.," TNO, Utrecht, Netherlands, 2014.

[3] A. Verruijt, Theory of Groundwater Flow, Macmillan, 1970.

[4] E. Lubimova, "Thermal history of the Earth. In: The Earth's Crust and Upper Mantle," *American Geophysics Un*, Vols. Geophysics Monographs, Series 13, pp. 63-77, 1968.

[5] F. Stacey and D. Loper, "Thermal history of the Earth: a corollary concerning non-linear mantle rheology," *Phys. Earth. Planet. Inter*, vol. 53, pp. 167-74, 1988.

[6] M. H. Dickson, M. Fanelli and P. Manetti, "Geothermal energy," Istituto di Geoscienze e Georisorse, Pisa, Italy.

[7] R. DiPippo, Geothermal power plants: Principles, applications, case studies and environmental impact. 4th ed., North Dartmouth, MA, USA: Butterworth-Heinemann, 2015.

[8] Islandsbanki, "US Geothermal Energy Market Report.," 2011.

[9] M. H. Dickson and M. Fanelli, Geothermal Energy: Utilization and Technology, UNESCO Publishing, 2003.

[10] M. Hochstein, "Classification and assessment of geothermal resources," in *M.H. Dickson and M. Fanelli (eds.), Small Geothermal Resources: A Guide to Development and Utilization*, New York, UNITAR, 1990, pp. 31-57.

[11] B. Goldstein, G. Hiriart, R. Bertani, C. Bromley, L. Gutiérrez-Negrín, E. Huenges, H. Muraoka, A. Ragnarsson, J. Tester and V. Zui, "Geothermal Energy. In IPCC Special Report on Renewable Energy Sources and Climate," Cambridge University Press, Cambridge, United Kingdom and New York, NY, USA, 2011.

[12] "geothermal," Geothermal Resources Council, [Online]. Available: https://geothermal.org/what.html.

[13] D. White , "Characteristics of geothermal resources," in *In: P. Kruger and C. Otte (eds.), Geothermal Energy* , Stanford University Press, 1973, pp. 69-94.

[14] K. Nicholson, Geothermal Fluids, Berlin: Springer Verlag, 1993.

[15] "ThermoGis," Netherlands Organisation for Applied Scientific Research (TNO), [Online]. Available: https://www.thermogis.nl/en.

[16] International Energy Agency, "Technology Roadmap, Geothermal Heat and Power," Paris, France, 2011.

[17] W. A. Duffield and J. H. Sass, Geothermal Energy—Clean Power from the Earth's Heat, Reston, Virginia, U.S.: U.S. Geological Survey, 2003.

[18] "geothermal energy," Internation Geothermal Association, [Online]. Available: https://www.geothermal-energy.org/explore/what-is-geothermal/.

[19] N. Aksoy, "Optimization of downhole pump setting depths in liquid-dominated geothermal systems: A case study on the Balcova-Narlidere field, Turkey," *Geothermics*, 2007.

[20] H. Darcy, The public fountains of the City of Dijon: experience and application, principles to follow and formulas to be used in the question of the distribution of water, [Brown G, Cateni B, Trans. 1999], Original published in 1856.

[21] H. Wang, Theory of Linear Poroelasticity with Applications to Geomechanics and Hydrogeology, Princeton University Press, 2000.

[22] L. Dake, "Fundamentals of reservoir engineering," in *Developments in Petroleum Science 8.*, Elsevier, 1978.

[23] E. Egbele, I. Ezuka and M. Onyekonwu, "Net-To-Gross Ratios: Implications in Integrated Reservoir Management Studies," in *Annual SPE International Technical Conference and Exhibition*, Abuja, Nigeria, 2005.

[24] H. Beggs and J. Brill, "A study of two-phase flow in inclined pipes," *Petroleum Technology*, pp. 607-617, 1973.

[25] P. Bombarda and M. Gaia, "Binary Systems with Geothermal Fluid Pressurization to Avoid Flashing: Energy Evaluation of Down-hole Pump Cooling below Geothermal Fluid Temperature," in *World Geothermal Congress*, Antalya, Turkey, 2005.

[26] S. Frick , S. Regenspurg, S. Kranz, H. Milsch, A. Saadat, H. Francke, W. Brandt and E. Huenges, "Geochemical and Process Engineering Challenges for Geothermal Power Generation," in *Chemie Ingenieur Technik (83)*, Weinheim, Germany, 2011.

[27] M. Batzle and Z. Wang, "Seismic properties of pore fluids. Geophysics," *Geophysics*, vol. 57, pp. 1396-1408, 1992.

[28] A. Garcia-Gutierrez , G. Espinosa-Paredes and I. Hernandez-Ramirez, "Study on the flow production characteristics of deep geothermal wells," *Geothermics,* vol. 31, pp. 141-167., 2001.

[29] D. Straathof, "Cost of Deep Geothermal Energy in Netherlands," Utrecht University, Energy research centre of the Netherlands, Utrecht, Ntherlands, 2012.

[30] L. Kramers , J. van Wees , M. Pluymaeke, A. Kronimus and T. Boxem, "Direct heat resource assessment and subsurface information systems for geothermal aquifers; the Dutch perspective," *Netherlands Journal of Geosciences,* vol. 91 – 4, pp. 637 - 649, 2012.

[31] S. Ehrenberg, P. Nadeau and Ø. Steen, "Petroleum reservoir porosity versus depth: Influence of geological age," *American Association of Petroleum. Geologists Bulletin,* vol. 93, pp. 1281-1296., 2009.

[32] "iea," International Energy Agency, [Online]. Available: https://www.iea.org/topics/renewables/geothermal/.

[33] J. W. Lund, R. Bertani and T. L. Boyd, "Worldwide Geothermal Energy Utilization 2015," *Geothermal Resources Council Transactions,* vol. 39, no. Geothermal overviews, 2015.

[34] P. Contil, G. Passaleva and R. Cataldi, "A Prudent View of Geothermal Development in Italy by 2030," in *European Geothermal Congress*, Strasbourg, France, 2016.

[35] A. Lahsen, "Chilean geothermal resources and their possible utilization," *Geothermics,* vol. 17, no. 2-3, pp. 401-410, 1988.

[36] A. Hauser, "Catastro y caracterización de las fuentes de aguas minerales y termales de Chile," Servicio Nacional de Geología y Minería, Santiago, Chile, 1997.

[37] Ministerio de Energía, "Ministerio de Energía, Gobierno de Chile," 17 Junio 2019. [Online]. Available: http://www.energia.gob.cl/energias-renovables.

[38] Ministerio de Energía, "Proyectos en Construcción e Ingresados al SEIA a julio 2016. Unidad Gestión de Proyectos.," Santiago, Chile, 2016.

[39] "geoelect," [Online]. Available: http://www.geoelec.eu/about-geothermal-electricity/.

[40] E. Macchi and M. Astolfi, Organic Rankine Cycle (ORC) Power Systems Technologies and Applications, Woodhead Publishing.

[41] A. Kalina, "Combined Cycle System with Novel Bottoming Cycle," *ASME,* Vols. Paper 84-GT-173, 1984.

[42] C. Spadacini, D. Rizzi and G. L. Xodo, "ORC Binary Cycle Geothermal Plant and Process". Europe Patent EP3368750, 5 september 2018.

[43] L. Mendez, "Downhole Pump Abstratct of the Disclousure A". Canada Patent 2008152, 28 October 1990.

[44] M. Schwiegel, F. Flohr and C. Meurer, "Working Fluid for an ORC process, ORC Process and ORC Apparatus". Europe Patent EP1929129, 11 June 2008.

[45] Honeywell International Inc., "The Environmental Alternative to Traditional Refrigerants, Solstice® ze Refrigerant (HFO-1234ze)," Heverlee, Belgium, 2015.

[46] Aspen Technology, "aspentech," Aspen Technology, [Online]. Available: https://www.aspentech.com/.

[47] J. van Wees , L. Kramers, J. Juez-Larré , A. Kronimus , H. Mijnlieff, D. Bonté, S. van Gessel, A. Obdam and H. Verweij, "ThermoGIS: An Integrated Web-Based Information System for Geothermal Exploration and Governmental Decision Support for Mature Oil and Gas Basins," in *Proceedings World Geothermal Congress 2010*, Bali, Indonesia, 2010.

[48] "NLOG, Netherlands Oil and Gas," Netherlands Organisation for Applied Scientific Research (TNO), [Online]. Available: https://www.nlog.nl/en.

[49] S. Bos and B. Laenen, "Development of the first deep geothermal doublet in the Campine Basin of Belgium," Flemish Institute for Technological Research (VITO), Mol, Belgium, 2017.

[50] B. Laenen , M. Broothaers, V. Harcouët-Menou and S. Loveless, "The Balmatt Deep Geothermal Project in Northern Belgium," Energy Ville, Genk, Belgium, 2014.

[51] S. Bos, B. Laenen and V. Harcouet-Menou, "The Balmatt Demonstration Deep Geothermal Project in Belgium," in *80th EAGE Conference and Exhibition 2018*, Copenhagen, Denmark, 2018.

[52] B. Laenen, "Materials & Technologies for performance imporvement for cooling systems in power plants (MATChING)," The Flemish Institute of Technology (VITO), 2017.

[53] MND, "Altheim in Upper Austria – an example of cascaded geothermal energy use," in *Geothermal Workshop Veli Lošinj*, 2014.

[54] ENGINE, "Geothermal Power Plant Altheim," ENGINE- Geothermal lighthouse projects in Europe, Altheim, Austria, 2008.

[55] G. Pernecker and S. Uhlig, "Low enthalpy power generation with ORC-Turbogenerator, The Altheim Project, Upper Austria," in *International summer school on direct application of geothermal energy*.

[56] G. Pemecker, "Altheim geothermal plant for electricity production by ORC-turbogenerator," Centre d'hrydrogiologie, Universitd de Neuchatel, Editions Peter Lang, Altheim, Austria, 1999.

[57] A. Bender, "Well proposals Honselersdijk," PanTerra Geoconsultans B.V., Leiderdorp, Netherlands, 2011.

[58] Green Well Westland, T & A Survey and Geoservices: A Schlumberger Company, "FINAL WELL REPORT Well: Hon-GT-01 & Hon-GT-01-ST1," Honselersdijk, Netherlands, 2011.

[59] D. Mottaghy, R. Pechnig, N. Buik and E. Simmelink, "3-D Numerical Models for Temperature Prediction and Reservoir Simulation," in *World Geothermal Congress*, Bali, Indonesia, 2010.

[60] H. Simmelink and V. Vandeweijer, "Geothermie Den Haag Zuid-West, 2e fase geologisch onderzoek," TNOrapport, Utrecht, Netherlands, 2008.

[61] R. te Gussinklo Ohmann, "End of well report HAG GT 01," Aardwarmte Den Haag, Northern Dutch Drilling Company and Well Project Management International, Den Haag, Netherlands, 2011.

[62] F. Schoof and B. Pittens, "Well testing report HAG GT-01 (Producer)," Aardwarmte Den Haag, IF Technology and Well Engineering Partners, Den Haag, Netherlands, 2010.

[63] P. Geoconsultants, "Water/Gas Samples HAG-GT1 Well," PanTerra Geoconsultants, Den Haag, Netherlands, 2010.

[64] P. Bombarda and M. Gaia, "Geothermal binary plants utilising an innovative non-flammable, azeotropic mixture as working fluid," in *28th NZ Geotherlmal Workshop*, 2006.

[65] P. Bombarda, M. Gaia and C. Pietra, "Integration of Geothermal Liquid Dominated Sources and Waste Heat Sources for Electricity Production," in *World Geothermal Congress* , Bali, Indonesia, 2010.

[66] P. Bombarda, M. Gaia, C. Invernizzi and C. Pietra, "Comparison of Enhanced Organic Rankine Cycles for Geothermal Power Units," in *World Geothermal Congress*, Melbourne, Australia, 2015.

[67] Z. Kai, Z. Mi, W. Yabo, S. Zhili, L. Shengchun and N. Jinghong, "Parametric Optimization of Low Temperature ORC System," in *The 7th International Conference on Applied Energy*, 2015.

[68] H. M. Hettiarachchi, M. Golubovic, W. M. Worek and Y. Ikegami, "Optimum design criteria for an Organic Rankine cycle using low-temperature geothermal heat sources," *Energy,* vol. 32, p. 1698–1706, 2007.

[69] M. Astolfi, M. C. Romano, P. Bombarda and E. Macchi, "Binary ORC (organic Rankine cycles) power plants for the exploitation of mediumelow temperature geothermal sources e Part A: Thermodynamic optimization," *Energy,* vol. 66, pp. 423-434, 2014.

[70] Honeywell International Inc., "The new F-gas regulation," Amsterdam, Netherlands, 2015.

[71] M. Pluymaekers, H. Veldkamp and J. van Wees, "DoubletCalc 2D: a free geothermal flow simulator," in *European Geothermal Congress,* Strasbourg, France, 2016.

[72] J. Veldkamp, M. Pluymaekers and J. van Wees, "DoubletCalc 2D 1.0 User Manual," Netherlands Organisation for Applied Scientific Research (TNO), Utrecht, Netherlands, 2015.

[73] L. Grunberg, "Properties of sea water concentrations," *Third International Symposium on Fresh Water from the Sea,* vol. 1, pp. 31-39, 1970.

[74] E. Rogers and M. Economides, The skin due to slant of deviated wells in permeability-anisotropic reservoirs. SPE 37068, 1996.

[75] T. Boyd, W. Glassley, E. Littlefield and J. Renner, "Geothermal Basics: Q&A," Geothermal Energy Association, 2012.

[76] M. J. Blunt, Reservoir Engineering, Lecture Notes, London: Department of Earth Science and Engineering, Imperial College London.

[77] D. Stegers, S. Edelman and K. Pieterse, "Geological study into the geothermal potential near fault zones in the Roer Valley Graben and West Netherlands Basin," Kennisagenda Aardwarmte, Amsterdam, Netherlands, 2018.

[78] D. Bonté , J. Van Wees and J. Verweij, "Subsurface temperature of the onshore Netherlands: new temperature dataset and modelling.," *Netherlands Journal of Geosciences ,* Vols. 91-4, pp. 491-515, 2012.

[79] P. Swamee and A. Jain , "Explicit equations for pipe flow problems," *J Hydraul Eng,* pp. 102-657 ASCE, 1976.

[80] M. van Putten, J. van Wees, D. Straathof, P. Lako, L. Kramers and M. Pluymaekers, "Finding a way to optimize drilling depths in clastic aquifers for geothermal energy," *Geothermics.*

[81] M. Pluymaekers , L. Kramers , J. van Wees, A. Kronimus , S. Nelskamp, T. Boxem and D. Bonté, "Reservoir characterisation of aquifers for direct heat production: Methodology and

screening of the potential reservoirs for the Netherlands," *Netherlands Journal of Geosciences,* Vols. 91 - 4, pp. 621 - 636 , 2012.

[82] E. Petitclerc, B. Laenen , D. Lagrou and H. Hoes, "Geothermal Energy Use, Country Update for Belgium," in *European Geothermal Congress*, Strasbourg, France, 2016.

Appendix A: DoubletCalc 2D: A potential tool for future investigations

DoubletCalc 2D allows the users to simulate the behavior of the temperature, pressure and mass flow rate around two or more geothermal wells in two dimensions over time. The main difference of this software with respect to DoubletCalc v1.4.3 is that its model does not considered a probabilistic approach and that its able to simulate heterogeneous aquifers with discontinuities like natural faults, high spatial variations in the reservoir properties, cooling of the host rock and spatial and temporal development of temperature, pressure and viscosity in the reservoir [71].

Unlike DoubletCalc v1.4.3, DoubletCalc 2D gives all its results at reservoir depth level, neglecting all temperature and pressure losses in the production and injection pipes. Consequently, this software does not provide a detailed simulation of the doublet system above the reservoir level.

The developers of these two open source tools (TNO) advice the users to realize a previous simulation with DoubletCalc v1.4.3 before using DoubletCalc 2D. In this way the target doublet system can be simulated in a specific time (steady conditions), and some of the outputs obtained can be used as inputs for the simulation in DoubletCalc 2D; in which the behavior of the target doublet system is analyzed with respect time.

The parameters needed from the simulation in DoubletCalc v1.4.3 are the pump volume flow (or the pressure difference at the producer well (well excess pressure)) and the initial temperature (temperature of the producer at reservoir level). On the other hand, there are some inputs that have to be the same in both simulations; these parameters are:

- Depth of the aquifer [m];
- Aquifer gross thickness [m];
- Aquifer net-to-gross ratio [-];
- Permeability of the reservoir [mD];
- Salinity of the geothermal fluid [ppm];
- The exit temperature at the heat exchanger (well (inj) temperature) [°C];
- Distance between producer and injector wells at aquifer level [m];
- The well outer diameter (for producer and injector) [in];
- Well skin (for producer and injector) [-];

The interface that appear when the user selects to open a new project or to load a previous project is the one showed in the Figure 53, in which the values that can be seen are the ones used to run the example of the software manual [72] .

In the following three figures are reported the input screens of DoubletCalc 2D. The most important differences that can be noticed with respect to DoubletCalc v1.4.3 are:

- More options to describe the subsurface characteristics of the region of interest (suitable to simulate heterogeneous reservoirs with natural faults);
- There is no need neither option to specify the uncertainties of certain parameters before the simulation (no probabilistic approach);
- There is a section to indicate the inputs related with the time step simulation;
- The software requires the user to define the dimension of the cross section of the region of interest at reservoir depth level, in which the number of nodes of the grid must be specified;
- It is possible to consider the natural cooling of the reservoir and the subsidence phenomena in the simulation;
- There is an option to choose the format of the outputs obtained from the simulation;

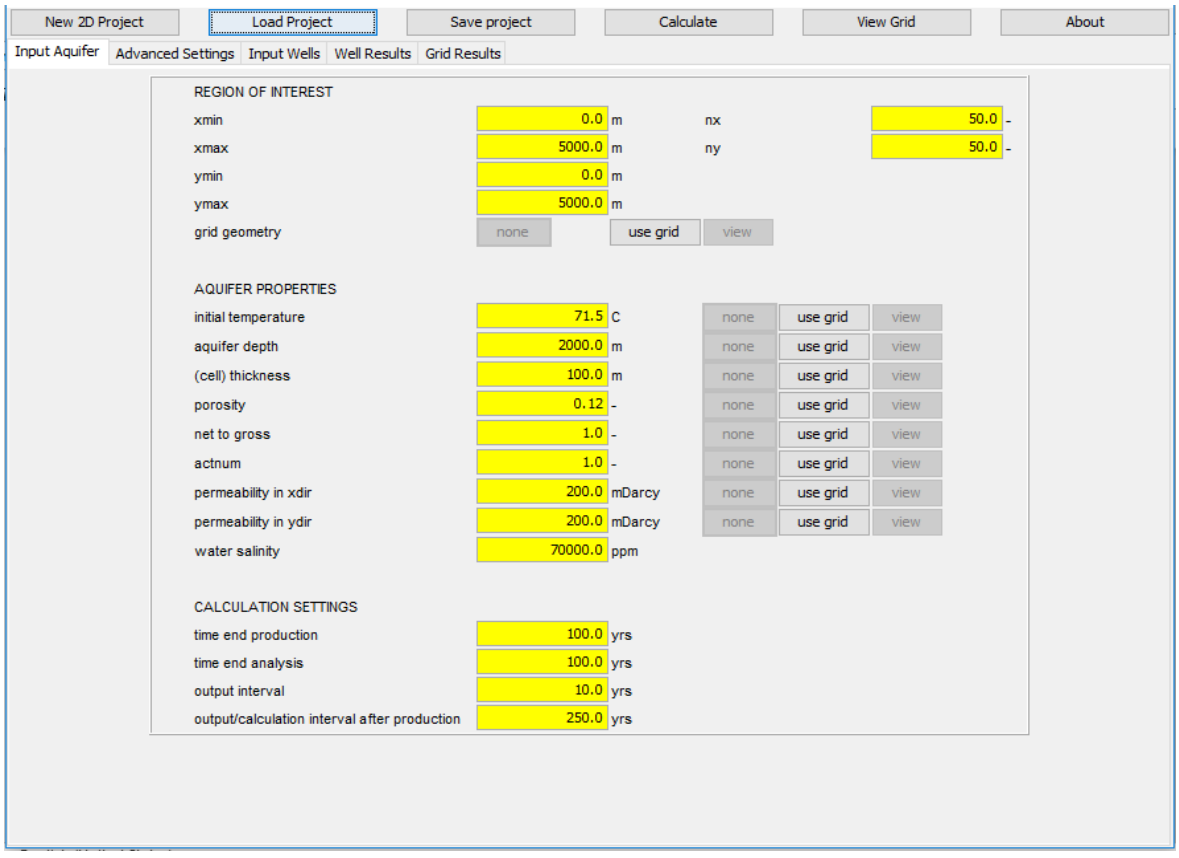

Figure 53: Aquifer specifications on the input screen of DoubletCalc 2D [72].

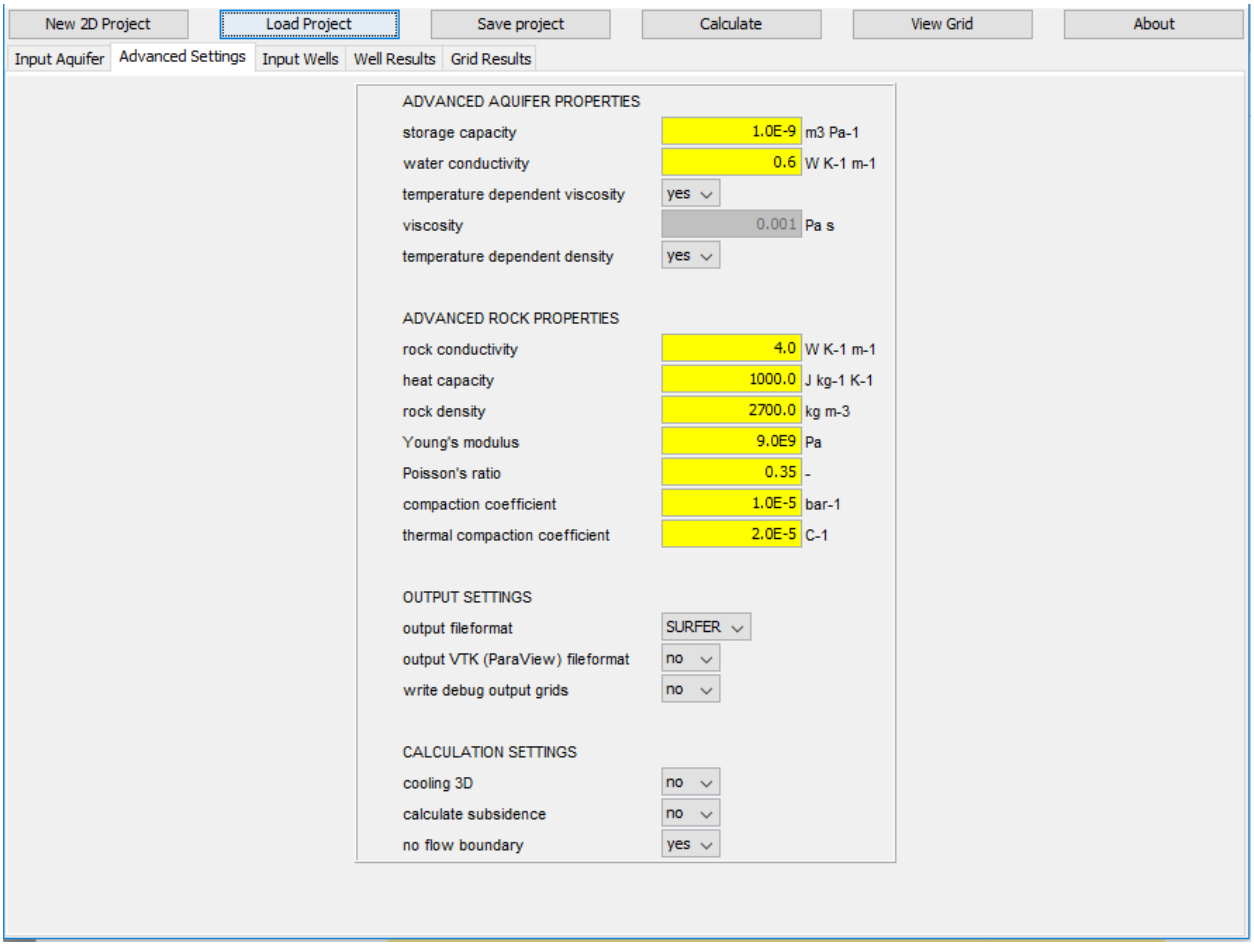

Figure 54: Advanced settings on the input screen of DoubletCalc 2D [72].

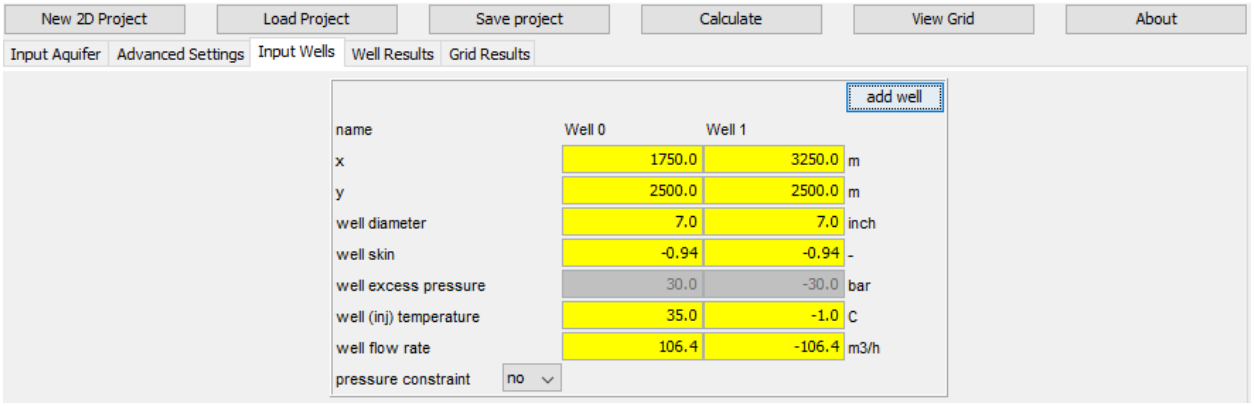

Figure 55: Well specifications on the input screen of DoubletCalc 2D [72].

Taking into account all the differences between the two tools, it is obvious that the outputs will differ quite a lot with respect to its applications. In the following three pictures are shown the outputs that can be obtained from DoubletCalc 2D. As it was said before, the main difference compared with DoubletCalc v.1.4.3 is that DoubletCalc 2D simulates the parameters of the doublet system at reservoir depth level (just bottom hole values) over time.

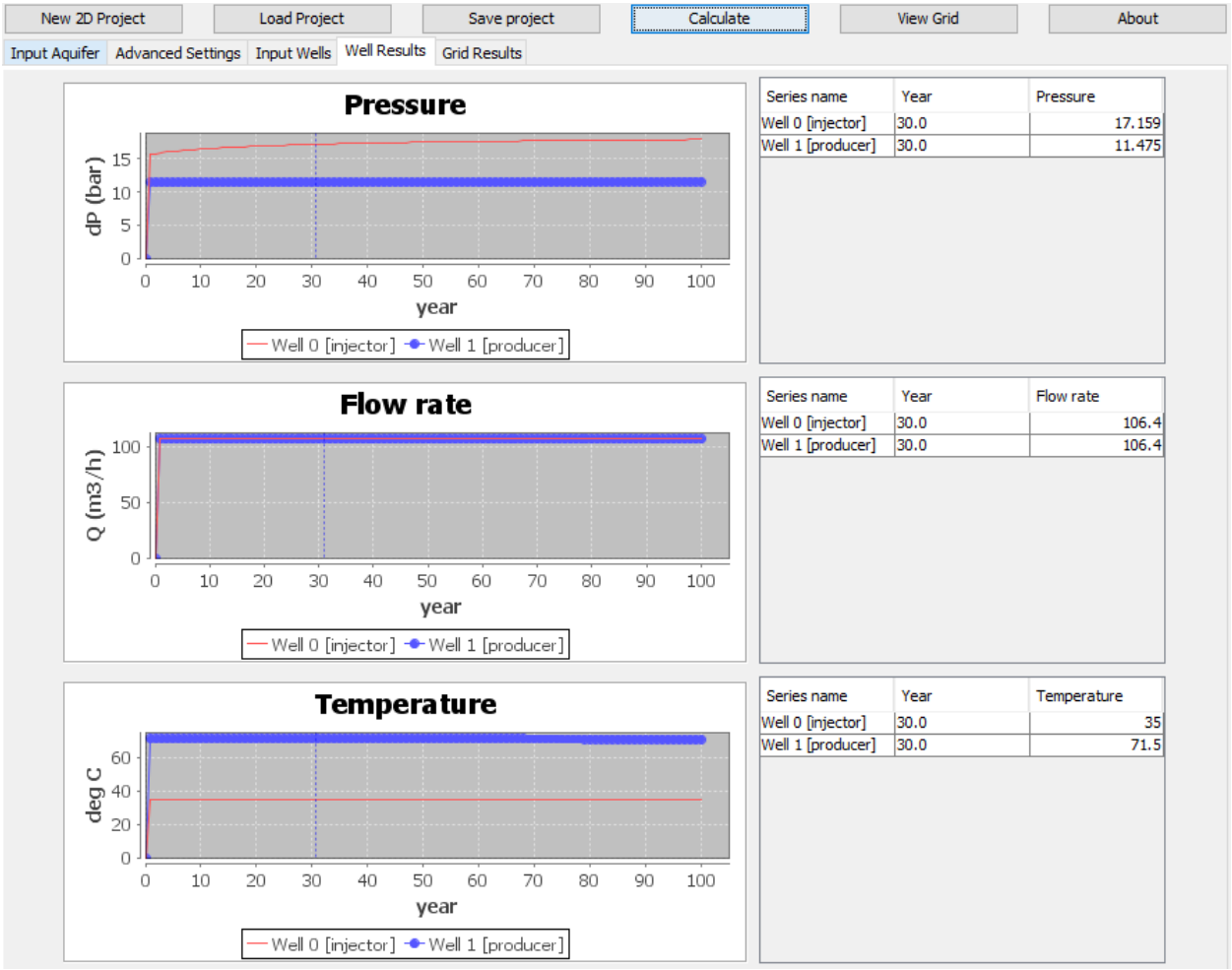

Figure 56: Output screen of DoubletCalc 2D [72].

The first output screen that is shown to the user after the simulation is the one presented in the Figure 56. In this interface there are three graphs, everyone showing the variation of a certain parameter (for the producer and the injector wells) with respect to time (total time and time step defined in the Input Aquifer tab). The first graph shows the variation of the pressure difference between aquifer and producer/injector well at aquifer level, the second graph shows the variation of the flow rate and the third graph shows the variation of the temperature. On the right side of each graph the user can see the values of the parameters in a specific year of interest. The data shown in the graphs can be exported to CSV file for further studies.

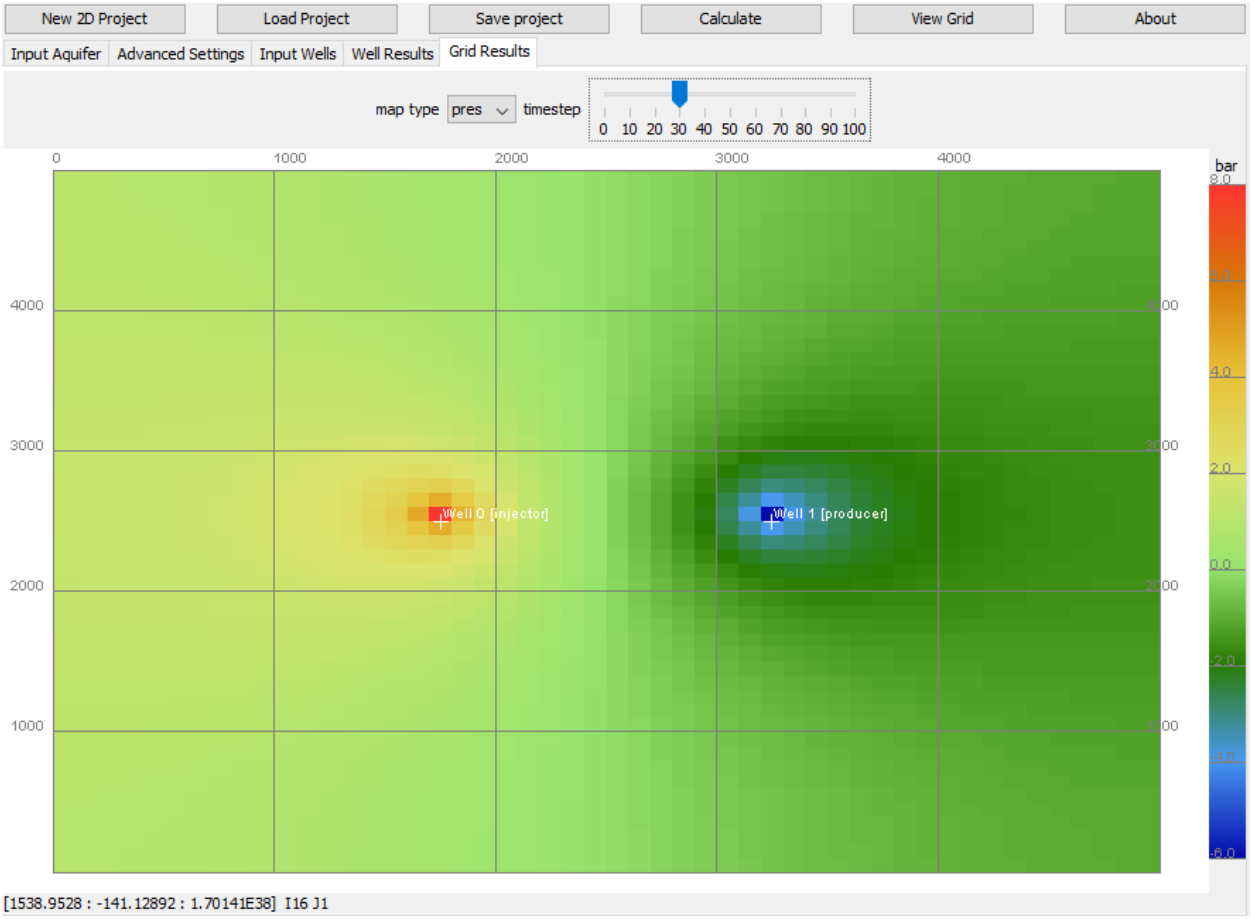

Figure 57: Grid results screen of DoubletCalc 2D [72].

In the Figure 57 is exposed the 'Grid Results' screen. This interface enables the user to see the region of interest with all its grid cells after the calculation, either for the pressure or for the temperature (both of them calculated per time step). Moving the cursor around the grid, the value of the pressure (or temperature) for the selected time step is shown for a certain grid cell (depending on which XY coordinate the cursor is located).

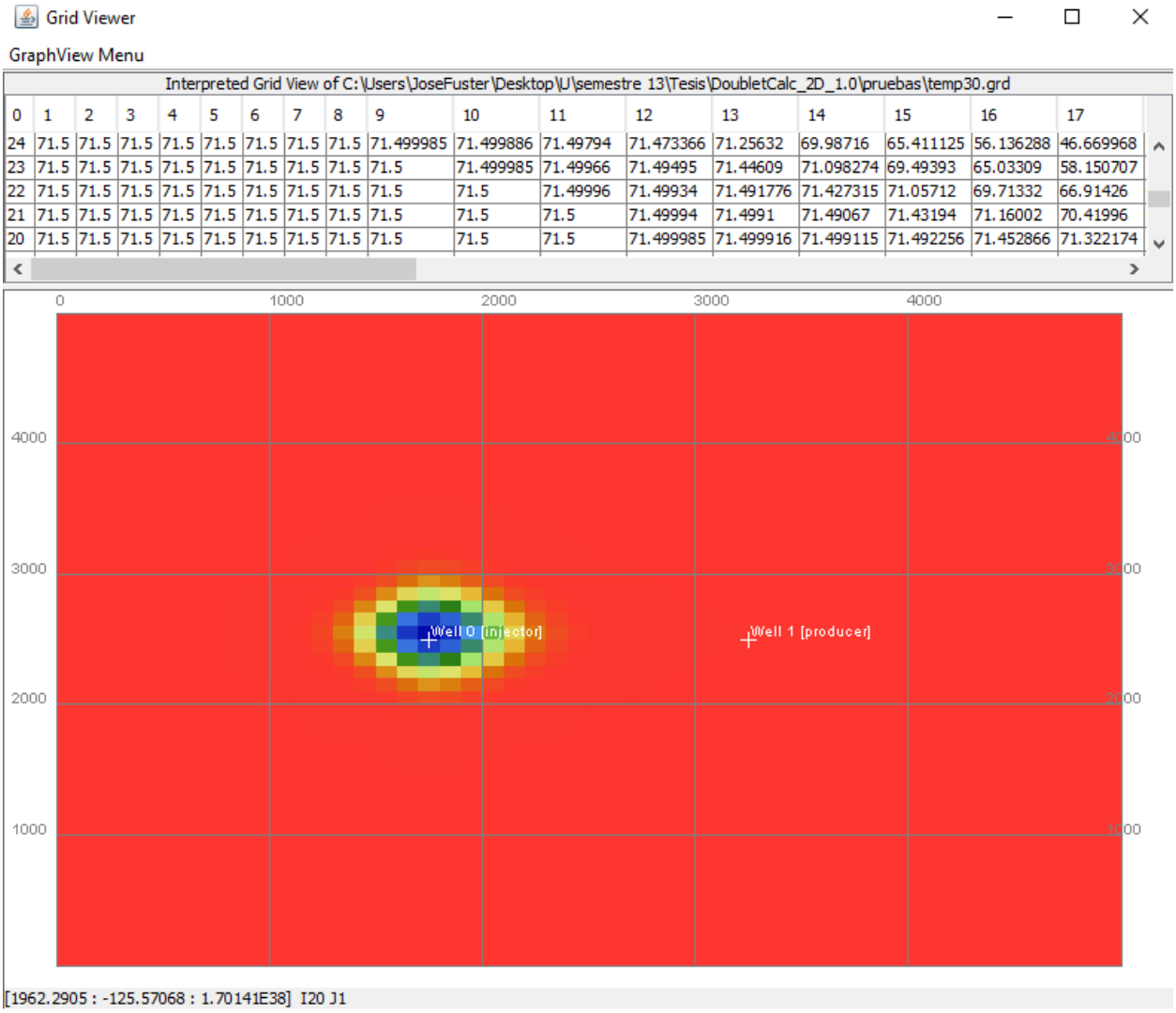

Figure 58: Grid viewer screen of DoubletCalc 2D [72].

Finally, in the Figure 58 is exhibited the 'Grid Viewer' screen, which is another option available in the software to analyze the results of the simulation. This tool enables the user to select a grid at a specific time (either for the temperature or for the pressure distribution). At the bottom part of the interface it is shown the grid with its respective production and injection well. On the other hand, at the top of the interface it can be seen the numerical values of each grid cell of the region of interest with its respective value of temperature (or pressure), depending on the position of the cursor on the grid.

Appendix B: Calculation to locate the flash point in a liquid-only flow [7, 19].

For cases in which it is desired to maintain an only-liquid flow at all times within the production well, is very useful to know in what exact location it will occur the flashing of the fluid. Being said that, the value that has to be calculated is the vertical distance from the inlet of the well, at reservoir level, to the point in which the fluid starts to flash into the vapor phase. The first step is to consider the volumetric flow rate as a function of the mass flow rate and the density:

$$\dot{V} = \frac{\dot{m}}{\rho} \tag{B.1}$$

Taking as reference the Figure 16 and assuming the equation for the drawdown pressure proposed by DiPippo [7], in which the skin factor and the net-to-gross ratio are neglected:

$$\Delta P = P_R - P_1 = \frac{\mu \ln\left({}^{r_R}/_{r_W}\right)}{2\pi k L_R \rho_R} \times \dot{m} = C_D \times \dot{m} \tag{B.2}$$

With C_D being the drawdown coefficient. Thus, the pressure at the inlet of the well at reservoir level can be found from the reservoir pressure, the mass flow rate, and the drawdown coefficient:

$$P_1 = P_R - C_D \dot{m} \tag{B.3}$$

The flash of the geothermal fluid will start when the pressure inside the well drops until it reaches the saturation pressure of the fluid. Accordingly, at the flash point the pressure will be:

$$P_F = P_{sat}(T_R) \tag{B.4}$$

Combining the Equation (2.5) and (2.6) from the Chapter 2:

$$P_1 - P_2 = \rho g L_W + \frac{8 f \rho \dot{V}^2 L_W}{\pi^2 D^5} \tag{B.5}$$

Taking this last equation and replacing P_1 in the Equation (B.2) it is obtained the following expression:

$$P_2 = P_R - \left[\frac{\mu}{\rho_R}\right]\left[\frac{1}{k L_R}\right]\left[\frac{\ln\left({}^{r_R}/_{r_W}\right)}{2\pi}\right]\dot{m} - \left[\frac{1}{\rho}\right]\left[\frac{8}{\pi^2}\right]\left[\frac{f L_W}{D^5}\right]\dot{m}^2 - g\rho L_W \tag{B.6}$$

The previous equation is taking into account the whole well though, so the P_2 and the L_W must be replaced for the proper values to obtain the equation in terms of saturation conditions:

$$P_{sat}(T_R) = P_R - \left[\frac{\mu}{\rho_R}\right]\left[\frac{1}{kL_R}\right]\left[\frac{\ln(r_R/r_W)}{2\pi}\right]\dot{m} - \left[\frac{1}{\rho}\right]\left[\frac{8}{\pi^2}\right]\left[\frac{fL_F}{D^5}\right]\dot{m}^2 - g\rho L_F \qquad \text{(B.7)}$$

In this way it is present the term L_F in the equation, which correspond to the distance from the inlet of the well up to the flash point. Then the only step missing is the clearing of the Equation (B.7) with respect to L_F:

$$L_F = \frac{P_R - P_{sat}(T_R) - C_D\dot{m}}{\rho g + C_2\dot{m}^2} \qquad \text{(B.8)}$$

where a new term C_2 has been defined as:

$$C_2 = \left[\frac{1}{\rho}\right]\left[\frac{8}{\pi^2}\right]\left[\frac{f}{D^5}\right] \qquad \text{(B.9)}$$

It is worth mentioning that the depth of the flash point from the surface is not equal to L_F, but to (L_W – L_F). Also, from Equation (B.8), the reader can notice that the value (or the length) of the flash point gets smaller as the mass flow rate gets larger. Thus, one can presume that at sufficiently high flow rates the flash point could reach the feed zone of the well and even move into the formation.

Appendix C: Properties of the geothermal fluid assumed in DoubletCalc v1.4.3 [2].

Density

The density of the geothermal fluid is calculated suing the relations proposed by Batzle and Wang (1992) [27], in which the density is defined as a function of the temperature (T), pressure (P) and salinity (s), salinity (s):

$$\rho_{fw} = 1 + 10^{-6}(-80T - 3.3T^2 + 0.00175T^3 + 489P - 2TP + 0.016T^2P - 1.3 \times 10^{-5}T^3P - 0.333P^2 - 0.002T^2P) \quad \text{(C.1)}$$

$$\rho = \rho_{fw} + s\{0.668 + 0.44s + 10^{-6}[300P - 2400Ps + T(80 + 3T - 330s - 13P + 47Ps)]\} \quad \text{(C.2)}$$

Where:

- ρ_{fw} = fresh water density [kg/m^3]
- ρ = salt water density [kg/m^3]
- P = pressure [MPa]
- s = salt content (salinity) [ppm/1,000,000] or [kg/kg]
- T = temperature [°C]

Viscosity

As the density, the viscosity of the geothermal fluid is also calculated using the Batzle and Wang equations [27]:

$$\mu = 0.1 + 0.333s + (1.65 + 91.9s^3)\exp(-[0.42(s^{0.8} - 0.17)^2 + 0.045]T^{0.8}) \quad \text{(C.3)}$$

With:

- μ = water viscosity [cP]
- s = salt content (salinity) [ppm/1,000,000] or [kg/kg]
- T = temperature [°C]

Heat capacity

The heat capacity (Cp) of the geothermal fluid is approximated using the polynomials described by Grundberg (1970) [73]. In this relation the heat capacity depends on the temperature (T), the pressure (P) and the salinity (s):

$$\begin{aligned} Cp = {} & (+5.328 - 9.760 \times 10^{-2} s + 4.040 \times 10^{-4} s^2) \\ & + (-6.913 \times 10^{-3} + 7.351 \times 10^{-4} s - 3.150 \times 10^{-6} s^2) T \\ & + (+9.600 \times 10^{-6} - 1.927 \times 10^{-6} s + 8.230 \times 10^{-9} s^2) T^2 \\ & + (+2.500 \times 10^{-9} + 1.666 \times 10^{-9} s - 7.125 \times 10^{-12} s^2) T^3 \end{aligned} \quad \text{(C.4)}$$

With:

- Cp = water heat capacity [kJ/(kg×K)]
- s = salt content (salinity) of the water [g/kg]
- T = temperature [°K]

Salinity

There are two states or conditions that can be considered for the analysis of the geothermal fluid's salinity:

- Static: Initial equilibrium state in the subsurface (stationary conditions).
- Dynamic: During the production in the doublet system.

The salinity of the geothermal fluid (s) in static conditions is defined as a function of the depth (d):

$$s(d) = s_{aq} \times \frac{d}{d_{top,p} + 0.5 L_R} \quad \text{(C.5)}$$

- s_{aq} = salinity of the aquifer brine [kg/kg] or [ppm]
- $d_{top,p}$= depth of the top of the aquifer at the production well [m TVD]
- L_R = aquifer thickness at the production well [m]

From the previous formula it can be inferred that at surface level, s = 0. Being said that, for the calculation of the hydrostatic pressure it is assumed that the salinity increases linearly with the depth from zero (at surface level), until the specified value at the target depth of the reservoir. Therefore, the salinity of the geothermal fluid in dynamic conditions (during production) is assumed to be equal to that of the reservoir brine in every point within the doublet system:

$$s = s_{aq} \quad \text{(C.6)}$$

Appendix D: Consequences of perforating the reservoir obliquely [2].

There are pressure drops related with the perforation of the reservoir by the production /injection, the 'skin' factor is the parameter that is used to measure these losses. In the input screen of DoubletCalc there are two boxes in which the skin factor is considered; one must be indicated by the user (usually defined equal to zero) and the other is calculated by the software depending on the penetration angle specified by the user.

The inclination of the well has a direct impact of the flow direction within the aquifer, causing a larger flow than for a perpendicular well. A well with a certain level of inclination with respect to the horizontal will have a skin with a negative sign.

The skin computed by DoubletCalc is a function of the penetration angle, the aquifer thickness and the anisotropy of the system, and is calculated by the software using the follow equation (valid for penetration angles up to 85°) [74]:

$$S_\theta = -2.48 \frac{(sin\theta)^{5.87} \times L_{R,d}^{0.152}}{I_{ani}^{0.964}};\ for\ I_{ani} \geq 1 \qquad \text{(D.1)}$$

With:

- S_θ = Skin as a result of obliquely drilling in the reservoir [-];
- θ = Well deviation from the vertical [°];
- L_R = Aquifer thickness [m];
- $D_{w,out}$ = Outer diameter of the well [m];
- $L_{R,d}$ = Dimensionless aquifer thickness = $\frac{L_R}{D_{w,out}}$ [-];
- k_h = Horizontal permeability [m^2];
- k_v = Vertical permeability [m^2];
- I_{ani} = Anisotropy index = $\sqrt{\frac{k_h}{k_v}}$ [-];

To have a better understanding of the effect caused by implementing a reservoir drilling with a certain penetration angle is useful to consider the ratio between the productivity index of the system with and without taking into account the skin. The productivity index can be calculated using the equation proposed by Verruijt [3] and Dake [22] :

$$J = \frac{\dot{V}}{P_W - P_R} = \frac{2\pi k L_R R_{ntg}}{\mu(\ln\left(\frac{L}{D_{w,out}}\right) + S)} \quad \text{(D.2)}$$

With:

- J = Well productivity [m^3/s/Pa];
- P_w = Pressure in the well at reservoir level [Pa];
- P_R = Initial hydrostatic pressure in the reservoir [Pa];
- $\dot{V} = \dot{m} / \rho$ = Flow rate. Positive for flows from the well towards the aquifer [m^3/s];
- μ = Viscosity of the geothermal fluid [Pa·s];
- k = Aquifer permeability [m^2];
- R_{ntg} = Net-to-gross ratio;
- L = Distance between the production and injection wells [m];
- $D_{w,out}$ = Outer diameter of the well [m];
- S = skin [-];

Then, the ratio between the productivity index with an inclined well and the one with a perpendicular well is given by:

$$\frac{J_{inclined\ well}}{J_{vertical\ well}} = \frac{\ln(\frac{L}{D_{w,out}})}{\ln\left(\frac{L}{D_{w,out}}\right) + S_\theta} \quad \text{(D.3)}$$

Considering common values for the distance between the wells and the outer diameters (L around 1500 and 2000 [m] and $D_{w,out}$ about 0.1 [m]), the improvement of the productivity index due to the utilization of an inclined well is approximately 10% per unit skin (for a skin of 1) [2].

Appendix E: Parametric optimization of the simple saturated ORC plant with different working fluids.

Down-hole pump pressure difference	11.5	[bar]
$T_{geo,out}$	70	[°C]
Cooling medium	Water	[-]
Mass flow rate (cooling water)	340	[kg/s]
Temperature of the cooling water	10	[°C]
Target Net Power (approximate)	1	[MW]

Table 58: Parameters to consider for the simulations of the ORC plant.

Pressure at the primary heat exchanger	10.71	[bar]
Mass flow rate	87.14	[kg/s]
Temperature at the heat exchanger	102.62	[°C]

Table 59: Data taken from the DoubletCalc simulation (results of the percentile 50).

Time of the year	Summer	[-]
T_{amb}	20	[°C]
η_{pump}	0.75	[-]
$\eta_{pump,mec-el}$	0.95	[-]
$\eta_{turb,is}$	0.85	[-]
$\eta_{turb,mec-el}$	0.97	[-]
$\Delta T_{pp,cond}$	2	[°C]
$\Delta T_{pp,PHE}$	3	[°C]
$\Delta P_{cond,wf}$	0.1	[bar]
$\Delta P_{PHE,wf}$	1	[bar]
Fixed fraction of cooling power for the water loop	1.5	%
Fixed amount of consumption for the other auxiliaries	7	[kW]

Table 60: Assumptions for the simulations of the simple saturated ORC plant [69, 64, 65].

R245fa

Working Fluid	MM [g/mol]	T_{cr} [°C]	P_{cr} [bar]
R245fa	134	154	36.51

Table 61: Main characteristics of the R245fa.

	P_{eva} [bar]	P_{cond} [bar]	$T_{geo,out}$ [°C]	Mass flow [kg/s]	$\dot{W}_{net}$ ORC [kW]
No $T_{geo,out}$ lim.	6.40	1.30	68.63	59.89	1200.92
$T_{geo,out} = 70\ [°C]$	8.10	1.18	70.52	49.32	1132.16

Table 62: Optimized values of the simulation of the simple saturated ORC plant using R245fa as working fluid.

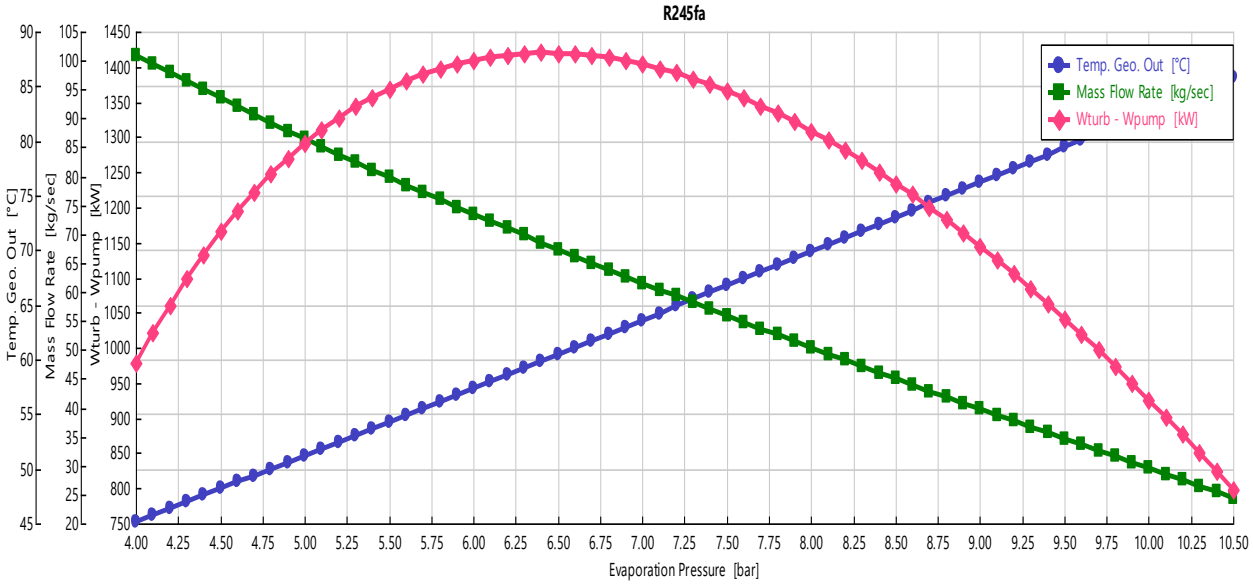

Figure 59: Graph of the optimization of the simple saturated ORC plant using R245fa as working fluid.

R236fa

Working Fluid	MM [g/mol]	T_{cr} [°C]	P_{cr} [bar]
R236fa	152.04	124.92	32

Table 63: Main characteristics of the R236fa.

	P_{eva} [bar]	P_{cond} [bar]	$T_{geo,out}$ [°C]	Mass flow [kg/s]	$\dot{W}_{net}$ ORC [kW]
No $T_{geo,out}$ lim.	10.25	2.46	56.70	94.47	1268.15
$T_{geo,out} = 70\ [°C]$	13.50	2.19	70.64	62.21	1133.37

Table 64: Optimized values of the simulation of the simple saturated ORC plant using R236fa as working fluid.

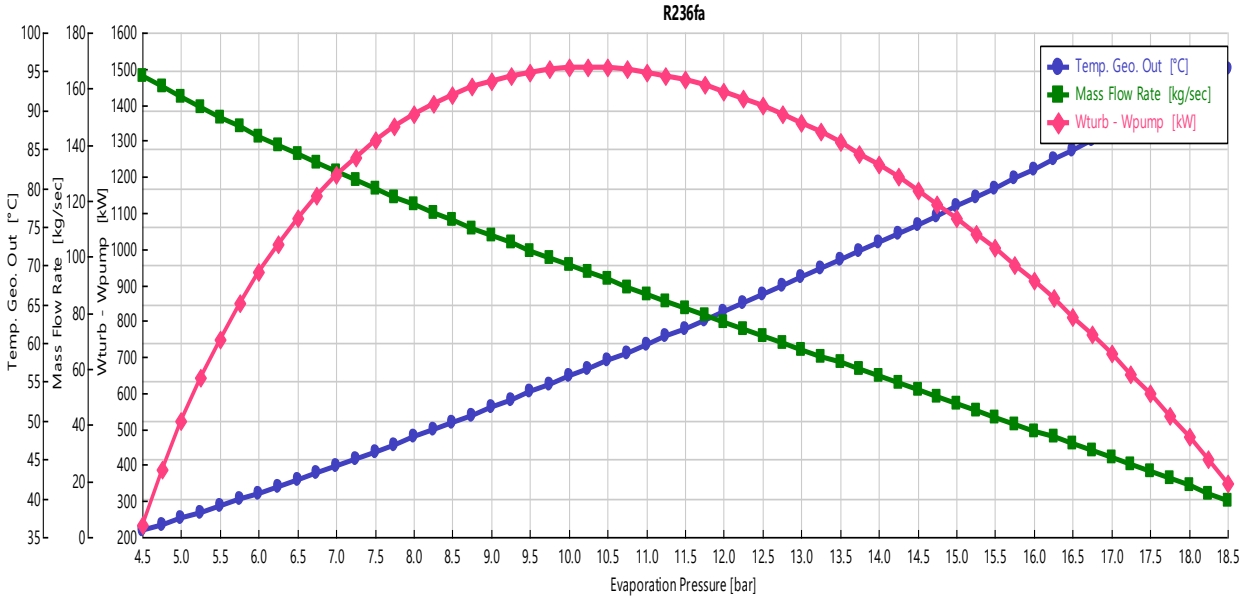

Figure 60: Graph of the optimization of the simple saturated ORC plant using R236fa as working fluid.

Iso-Butane

Working Fluid	MM [g/mol]	T_{cr} [°C]	P_{cr} [bar]
Iso-Butane	58.12	135.9	36.8

Table 65: Main characteristics of the Iso-Butane.

	P_{eva} [bar]	P_{cond} [bar]	$T_{geo,out}$ [°C]	Mass flow [kg/s]	$\dot{W}_{net}$ ORC [kW]
No $T_{geo,out}$ lim.	11.00	3.19	58.03	41.47	1237.46
$T_{geo,out} = 70$ [°C]	14.00	2.91	71.11	27.82	1131.92

Table 66: Optimized values of the simulation of the simple saturated ORC plant using Iso-Butane as working fluid.

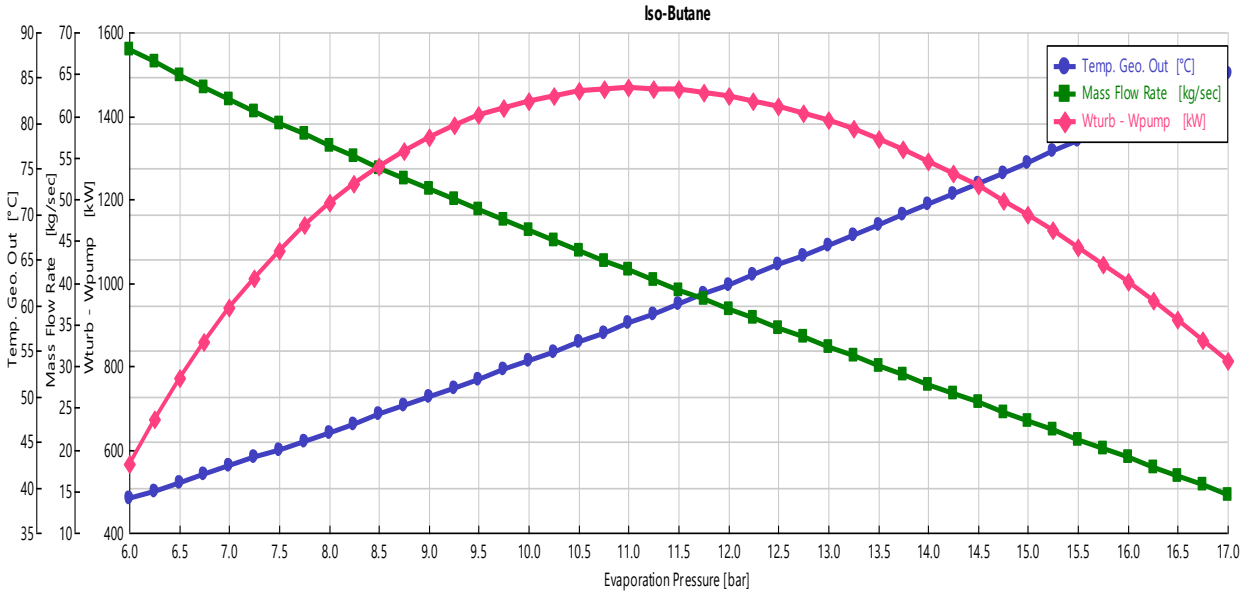

Figure 61: Graph of the optimization of the simple saturated ORC plant using Iso-Butane as working fluid.

Iso-Pentane

Working Fluid	MM [g/mol]	T_{cr} [°C]	P_{cr} [bar]
Iso-Pentane	72.15	187.25	33.8

Table 67: Main characteristics of the Iso-Pentane.

	P_{eva} [bar]	P_{cond} [bar]	$T_{geo,out}$ [°C]	Mass flow [kg/s]	$\dot{W}_{net}$ ORC [kW]
No $T_{geo,out}$ lim.	4.00	0.80	61.97	35.08	1103.80
$T_{geo,out} = 70\ [°C]$	4.80	0.74	70.86	26.23	1066.29

Table 68: Optimized values of the simulation of the simple saturated ORC plant using Iso-Pentane as working fluid.

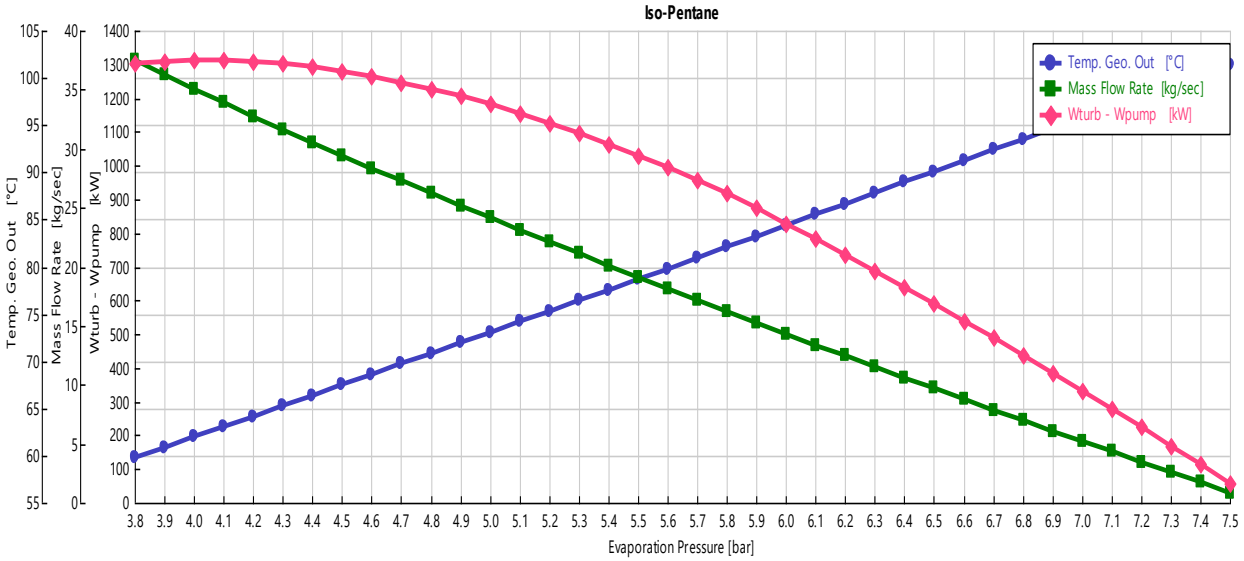

Figure 62: Graph of the optimization of the simple saturated ORC plant using Iso-Pentane as working fluid.

R236ea

Working Fluid	MM [g/mol]	T_{cr} [°C]	P_{cr} [bar]
R236ea	152.04	139.3	32.4

Table 69: Main characteristics of the R236ea.

	P_{eva} [bar]	P_{cond} [bar]	$T_{geo,out}$ [°C]	Mass flow [kg/s]	$\dot{W}_{net}$ ORC [kW]
No $T_{geo,out}$ lim.	8.25	1.83	58.14	84.77	1242.22
$T_{geo,out} = 70$ [°C]	10.75	1.64	71.21	56.59	1117.75

Table 70: Optimized values of the simulation of the simple saturated ORC plant using R236ea as working fluid.

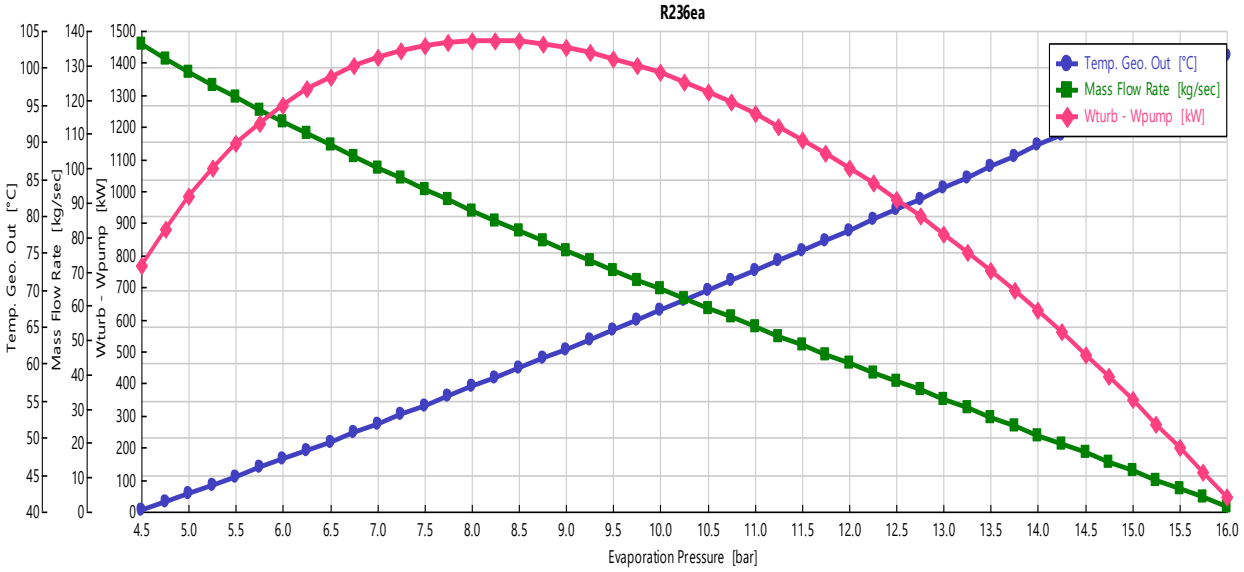

Figure 63: Graph of the optimization of the simple saturated ORC plant using R236ea as working fluid.

Butane

Working Fluid	MM [g/mol]	T_{cr} [°C]	P_{cr} [bar]
Butane	58.12	152	37.96

Table 71: Main characteristics of the Butane.

	P_{eva} [bar]	P_{cond} [bar]	$T_{geo,out}$ [°C]	Mass flow [kg/s]	$\dot{W}_{net}$ ORC [kW]
No $T_{geo,out}$ lim.	8.25	2.18	59.64	36.46	1205.94
$T_{geo,out} = 70\ [°C]$	10.25	2.00	70.67	25.89	1135.46

Table 72: Optimized values of the simulation of the simple saturated ORC plant using Butane as working fluid.

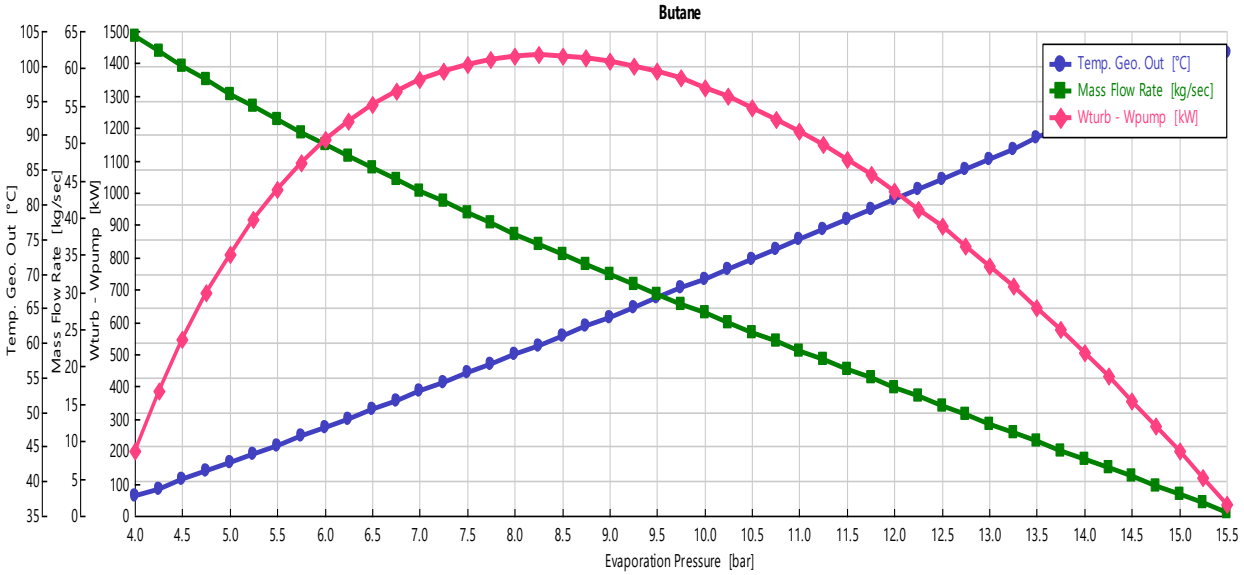

Figure 64: Graph of the optimization of the simple saturated ORC plant using Butane as working fluid.

Appendix F: Parametric optimization of the saturated recuperative ORC plant with different working fluids.

Down-hole pump pressure difference	11.5	[bar]
$T_{geo,out}$	70	[°C]
Cooling medium	Water	[-]
Mass flow rate (cooling water)	340	[kg/s]
Temperature of the cooling water	10	[°C]
Target Net Power (approximate)	1	[MW]

Table 73: Parameters to consider for the simulations of the ORC plant.

Pressure at the primary heat exchanger	10.71	[bar]
Mass flow rate	87.14	[kg/s]
Temperature at the heat exchanger	102.62	[°C]

Table 74: Data taken from the DoubletCalc simulation (results of the percentile 50).

Time of the year	Summer	[-]
T_{amb}	20	[°C]
η_{pump}	0.75	[-]
$\eta_{pump,mec-el}$	0.95	[-]
$\eta_{turb,is}$	0.85	[-]
$\eta_{turb,mec-el}$	0.97	[-]
$\Delta T_{pp,cond}$	2	[°C]
$\Delta T_{pp,PHE}$	3	[°C]
$\Delta T_{pp,rec}$	5	[°C]
$\Delta P_{cond,wf}$	0.1	[bar]
$\Delta P_{PHE,wf}$	1	[bar]
$\Delta P_{rec,cold\ side}$	0.5	[bar]
Fixed fraction of cooling power for the water loop	1.5	%
Fixed amount of consumption for the other auxiliaries	7	[kW]

Table 75: Assumptions for the simulations of the saturated recuperative ORC plant [69, 64, 65].

R245fa

Working Fluid	MM [g/mol]	T_{cr} [°C]	P_{cr} [bar]
R245fa	134	154	36.51

Table 76: Main characteristics of the R245fa.

P_{eva} [bar]	P_{cond} [bar]	Mass flow [kg/s]	$T_{geo,out}$ [°C]	$\dot{W}_{net}$ ORC [kW]
8.50	1.18	50.12	71.55	1145.56

Table 77: Optimized values of the simulation of the saturated recuperative ORC plant using R245fa as working fluid.

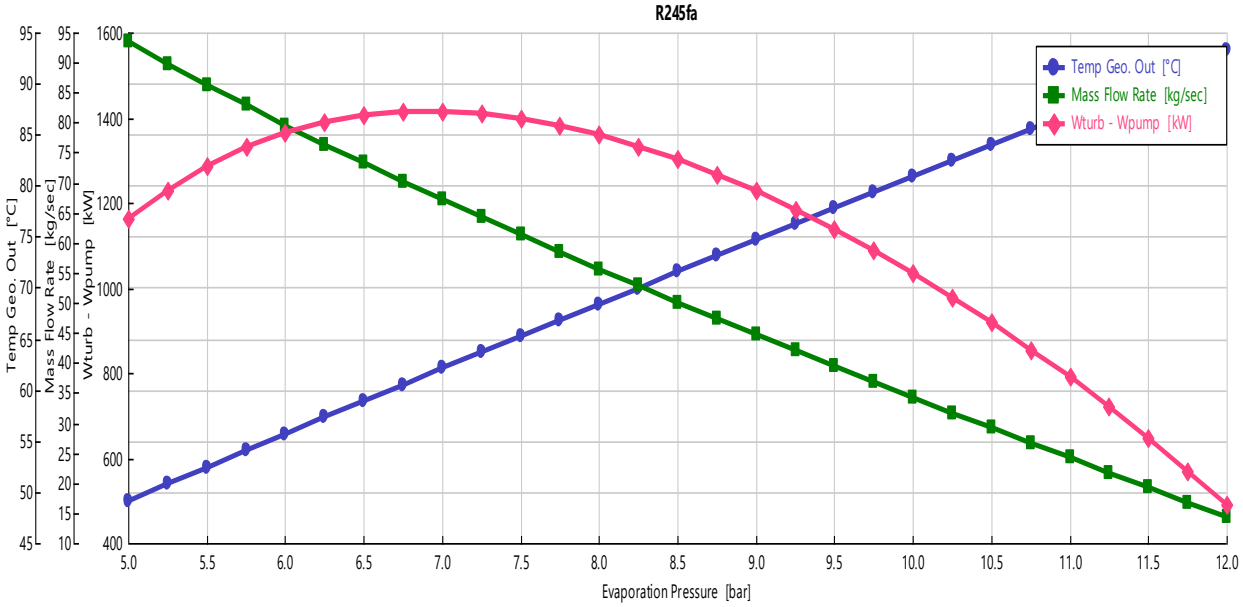

Figure 65: Graph of the optimization of the saturated recuperative ORC plant using R245fa as working fluid.

R236fa

Working Fluid	MM [g/mol]	T_{cr} [°C]	P_{cr} [bar]
R236fa	152.04	124.92	32

Table 78: Main characteristics of the R236fa.

P_{eva} [bar]	P_{cond} [bar]	Mass flow [kg/s]	$T_{geo,out}$ [°C]	$\dot{W}_{net}$ ORC [kW]
13.50	2.22	66.74	70.68	1183.59

Table 79: Optimized values of the simulation of the saturated recuperative ORC plant using R236fa as working fluid.

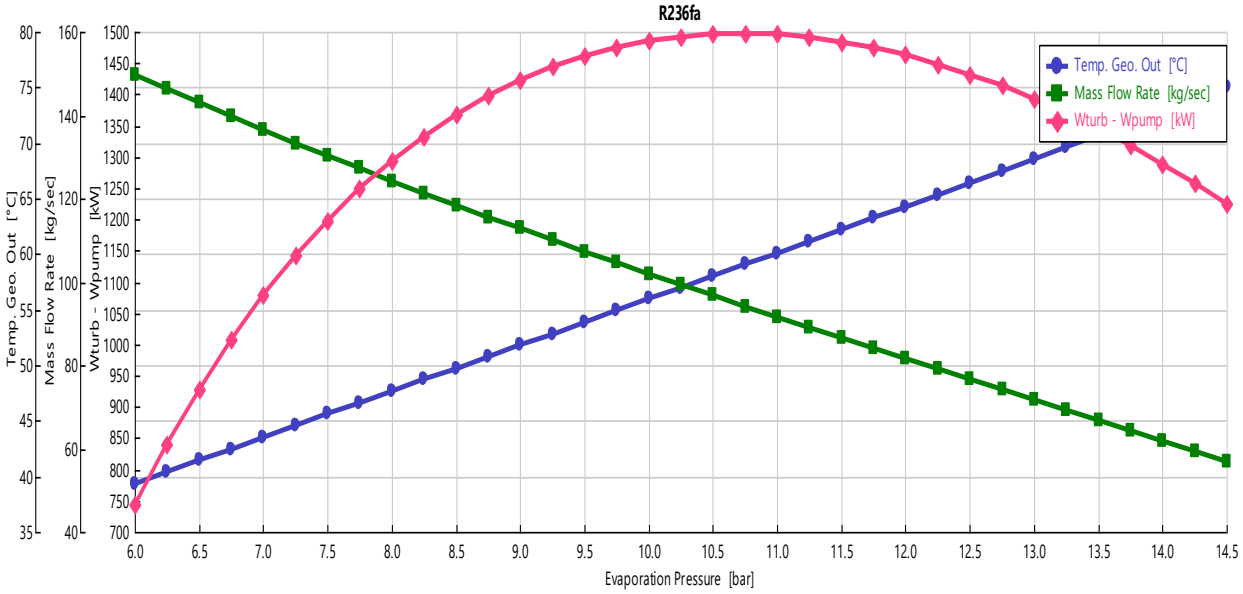

Figure 66: Graph of the optimization of the saturated recuperative ORC plant using R236fa as working fluid.

Iso-Butane

Working Fluid	MM [g/mol]	T_{cr} [°C]	P_{cr} [bar]
Iso-Butane	58.12	135.9	36.8

Table 80: Main characteristics of the Iso-Butane.

P_{eva} [bar]	P_{cond} [bar]	Mass flow [kg/s]	$T_{geo,out}$ [°C]	$\dot{W}_{net}$ ORC [kW]
14.00	2.94	29.94	70.48	1175.35

Table 81: Optimized values of the simulation of the saturated recuperative ORC plant using Iso-Butane as working fluid.

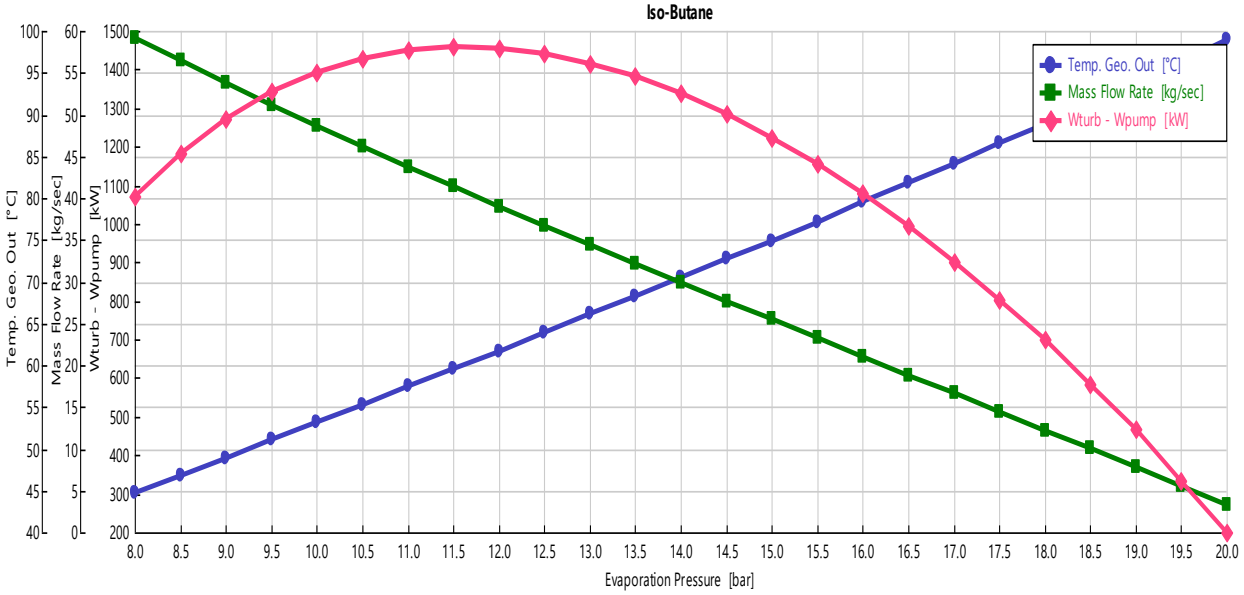

Figure 67: Graph of the optimization of the saturated recuperative ORC plant using Iso-Butane as working fluid.

Iso-Pentane

Working Fluid	MM [g/mol]	T_{cr} [°C]	P_{cr} [bar]
Iso-Pentane	72.15	187.25	33.8

Table 82: Main characteristics of the Iso-Pentane.

P_{eva} [bar]	P_{cond} [bar]	Mass flow [kg/s]	$T_{geo,out}$ [°C]	$\dot{W}_{net}$ ORC [kW]
5.00	0.75	29.00	70.41	1105.74

Table 83: Optimized values of the simulation of the saturated recuperative ORC plant using Iso-Pentane as working fluid.

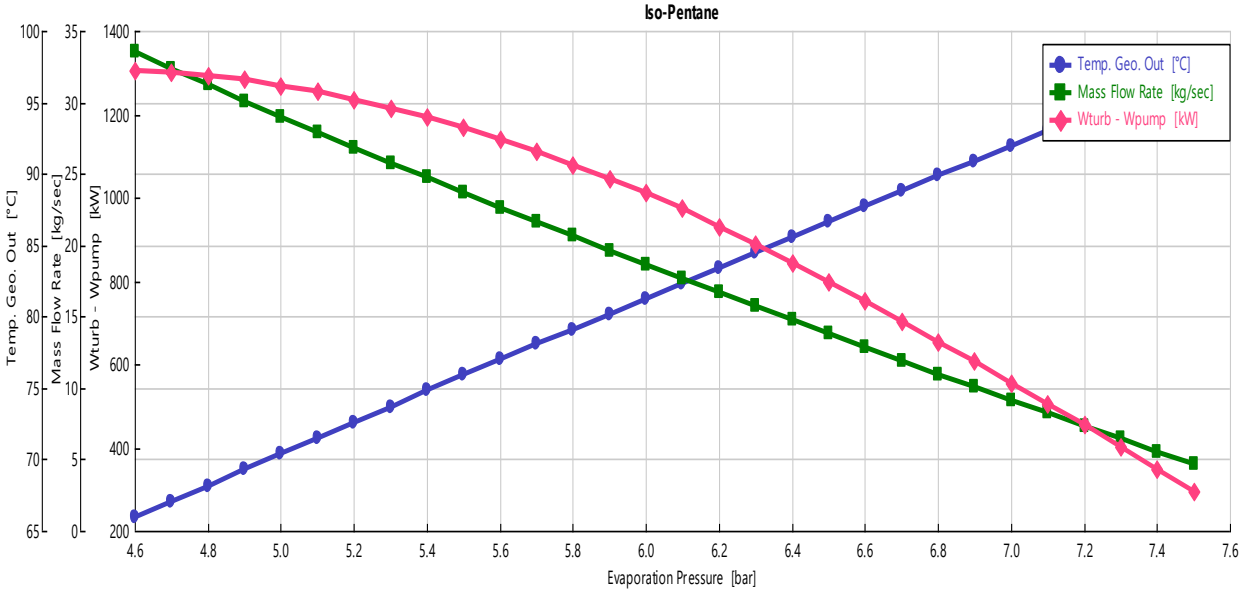

Figure 68: Graph of the optimization of the saturated recuperative ORC plant using Iso-Pentane as working fluid.

R236ea

Working Fluid	MM [g/mol]	T_{cr} [°C]	P_{cr} [bar]
R236ea	152.04	139.3	32.4

Table 84: Main characteristics of the R235ea.

P_{eva} [bar]	P_{cond} [bar]	Mass flow [kg/s]	$T_{geo,out}$ [°C]	$\dot{W}_{net}$ ORC [kW]
11.00	1.64	58.87	72.44	1150.75

Table 85: Optimized values of the simulation of the saturated recuperative ORC plant using R236ea as working fluid.

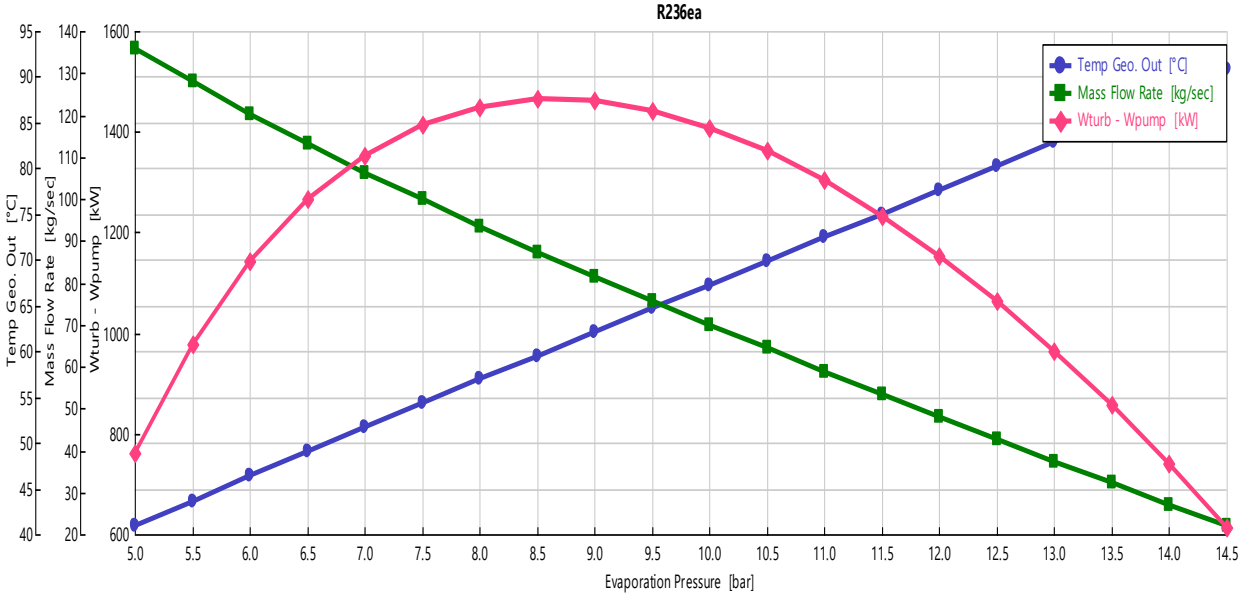

Figure 69: Graph of the optimization of the saturated recuperative ORC plant using R236ea as working fluid.

Butane

Working Fluid	MM [g/mol]	T_{cr} [°C]	P_{cr} [bar]
Butane	58.12	152	37.96

Table 86: Main characteristics of the Butane.

P_{eva} [bar]	P_{cond} [bar]	Mass flow [kg/s]	$T_{geo,out}$ [°C]	$\dot{W}_{net}$ ORC [kW]
10.50	2.02	27.03	70.91	1160.03

Table 87: Optimized values of the simulation of the saturated recuperative ORC plant using Butane as working fluid.

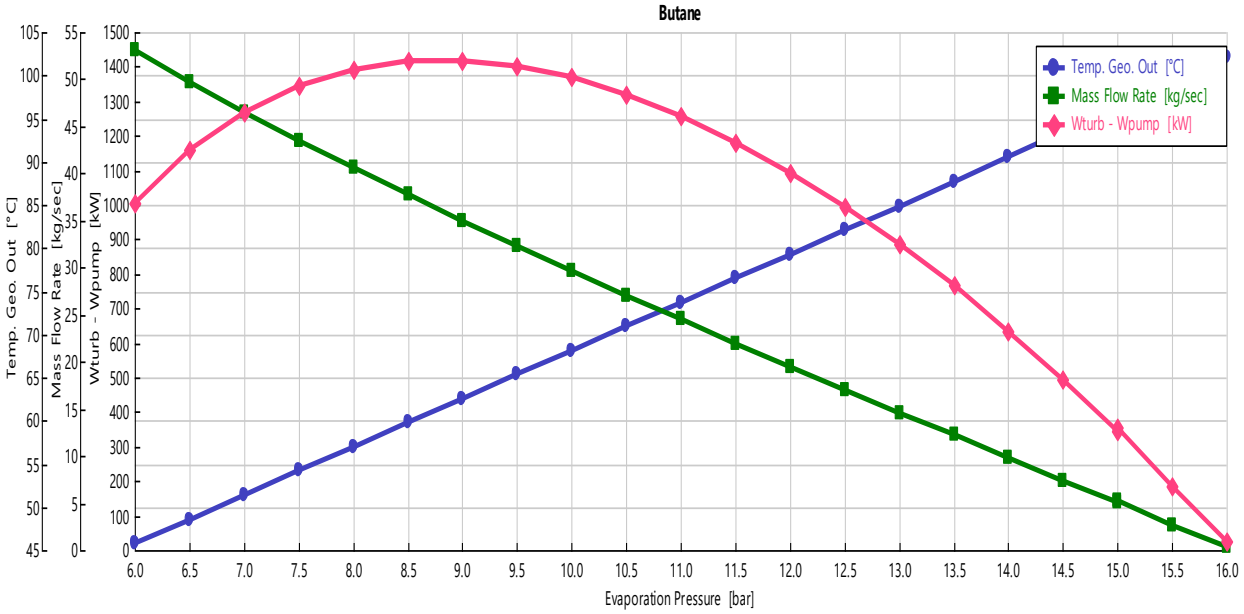

Figure 70: Graph of the optimization of the saturated recuperative ORC plant using Butane as working fluid.

Appendix G: Fingerprint graphs of the coupling of the two simulation models for the simple saturated ORC plant with temperature limit.

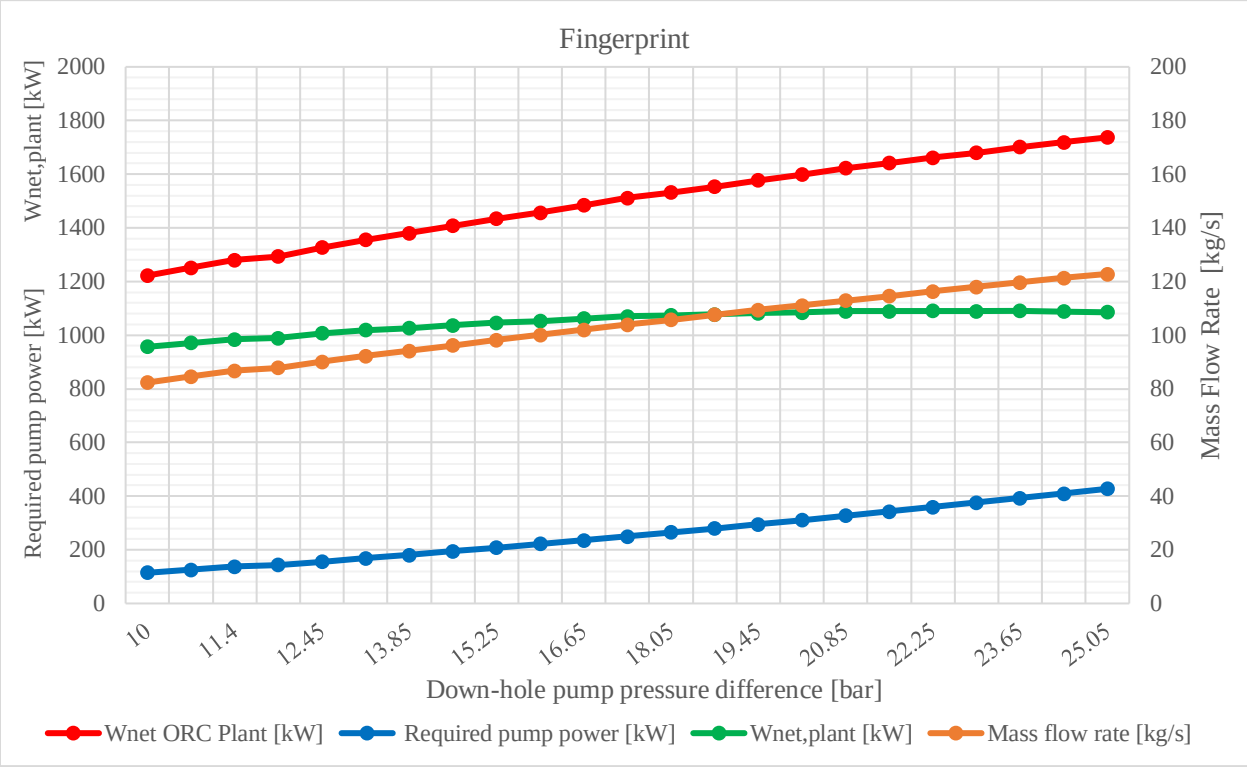

Figure 71: Fingerprint graph of the reference case scenario for the simple saturated ORC plant with temperature limit.

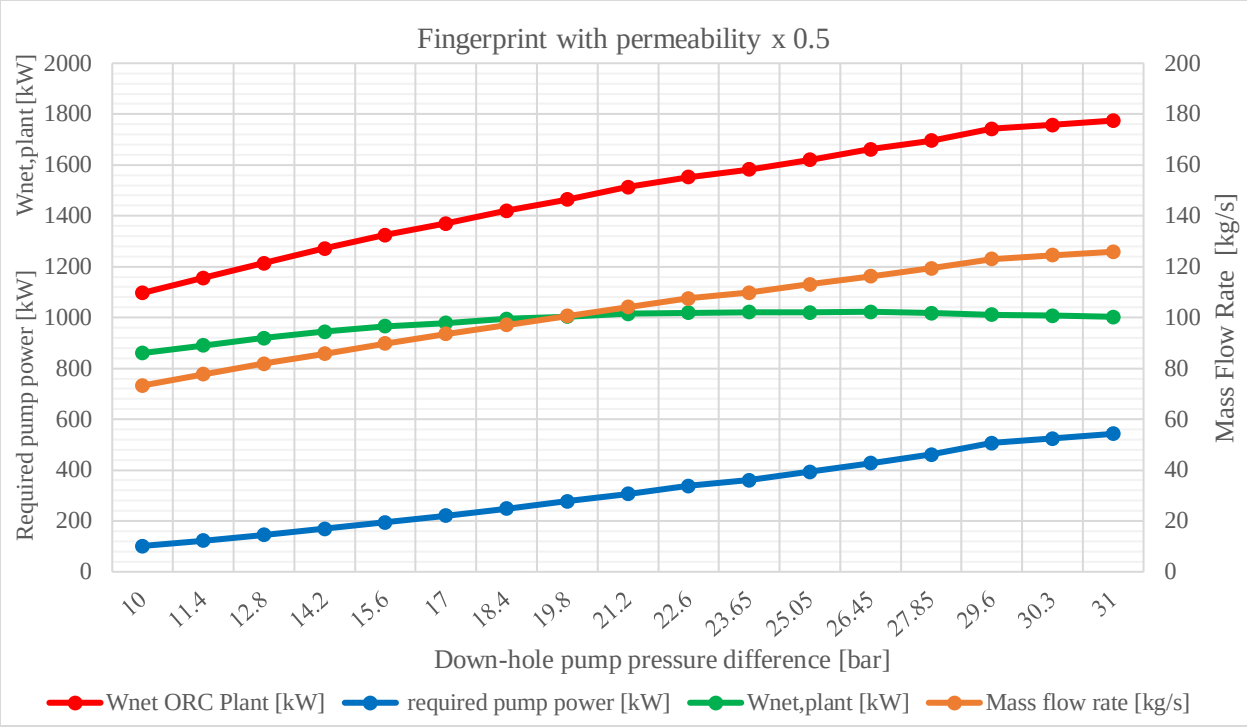

Figure 72: Fingerprint graph of the scenario with permeability x 0.5 for the simple saturated ORC plant with temperature limit.

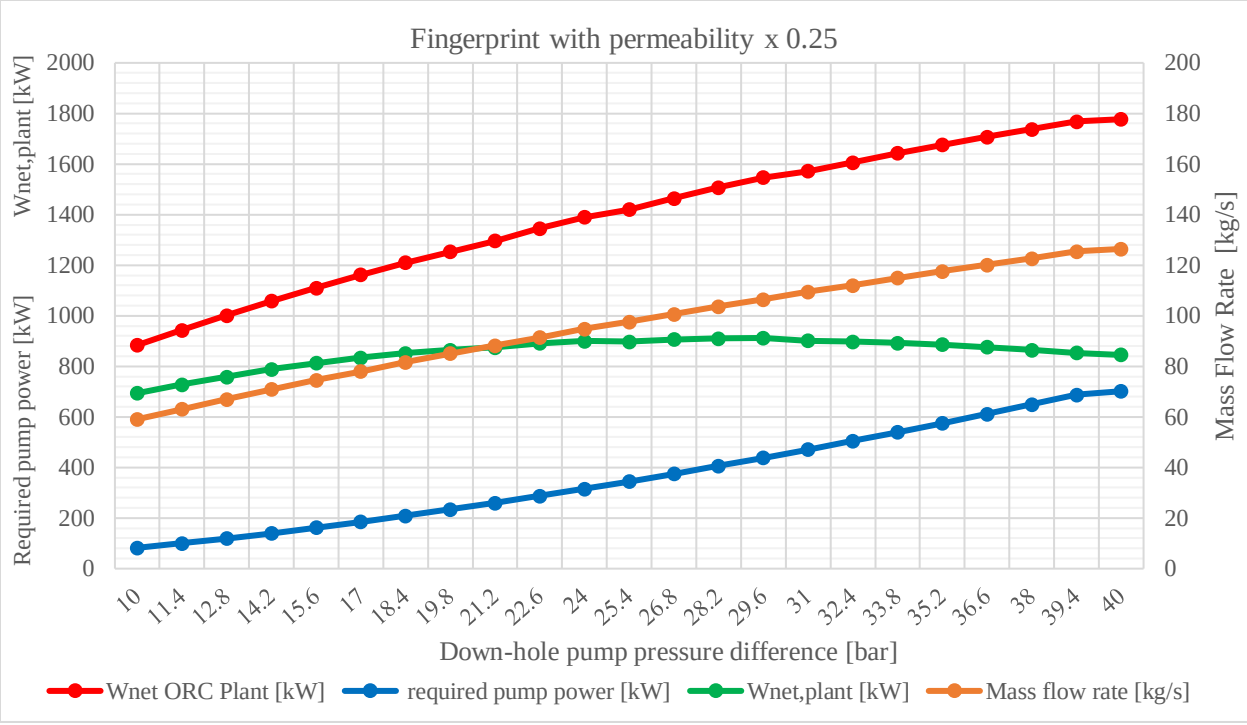

Figure 73: Fingerprint graph of the scenario with permeability x 0.25 for the simple saturated ORC plant with temperature limit.

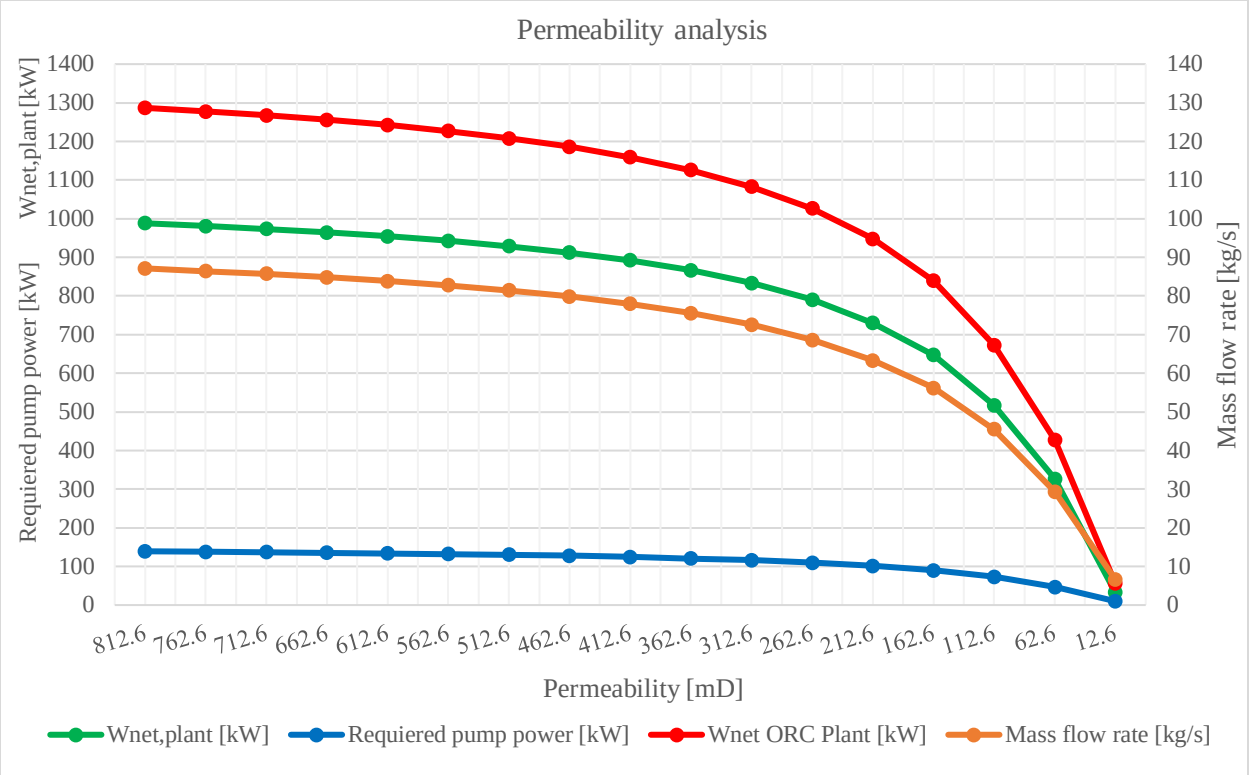

Figure 74: Permeability analysis for the simple saturated ORC plant with temperature limit.

Appendix H: Fingerprint graphs of the coupling of the two simulation models for the saturated recuperative ORC plant with temperature limit.

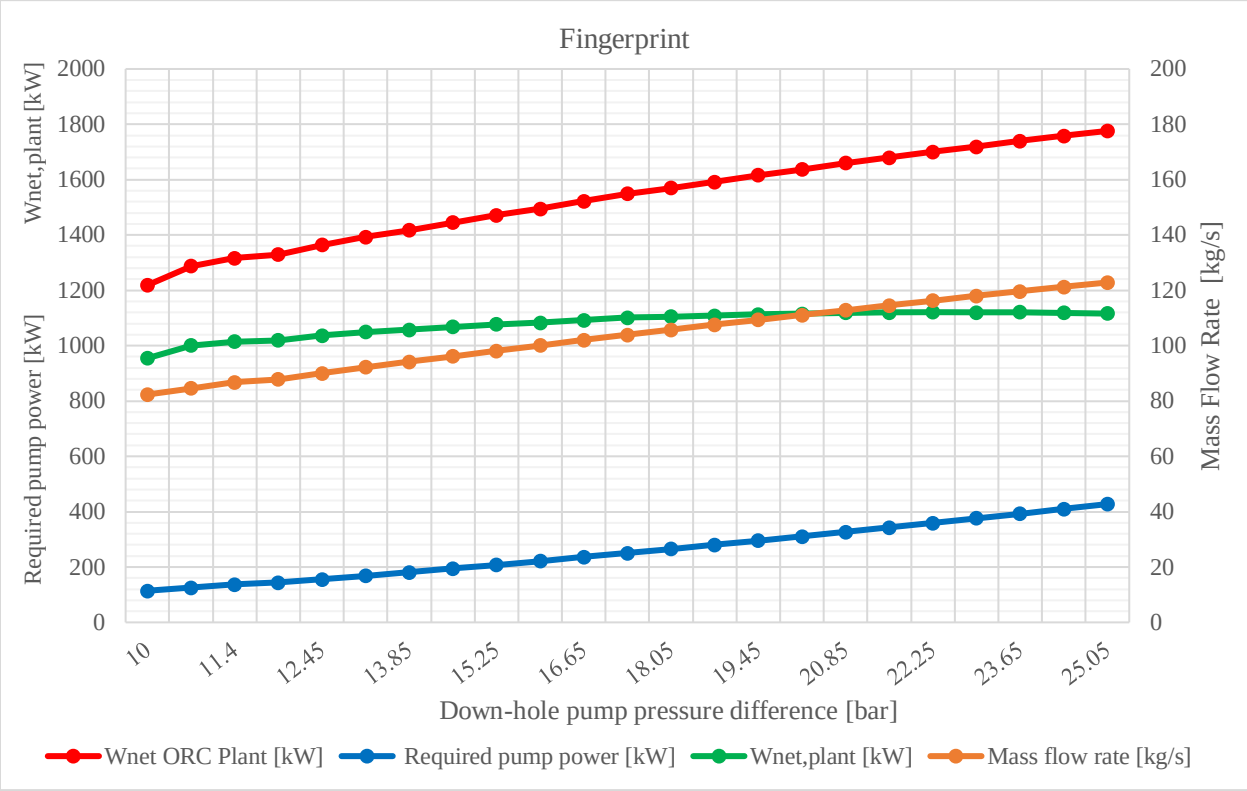

Figure 75: Fingerprint graph of the reference case scenario for the saturated recuperative ORC plant with temperature limit.

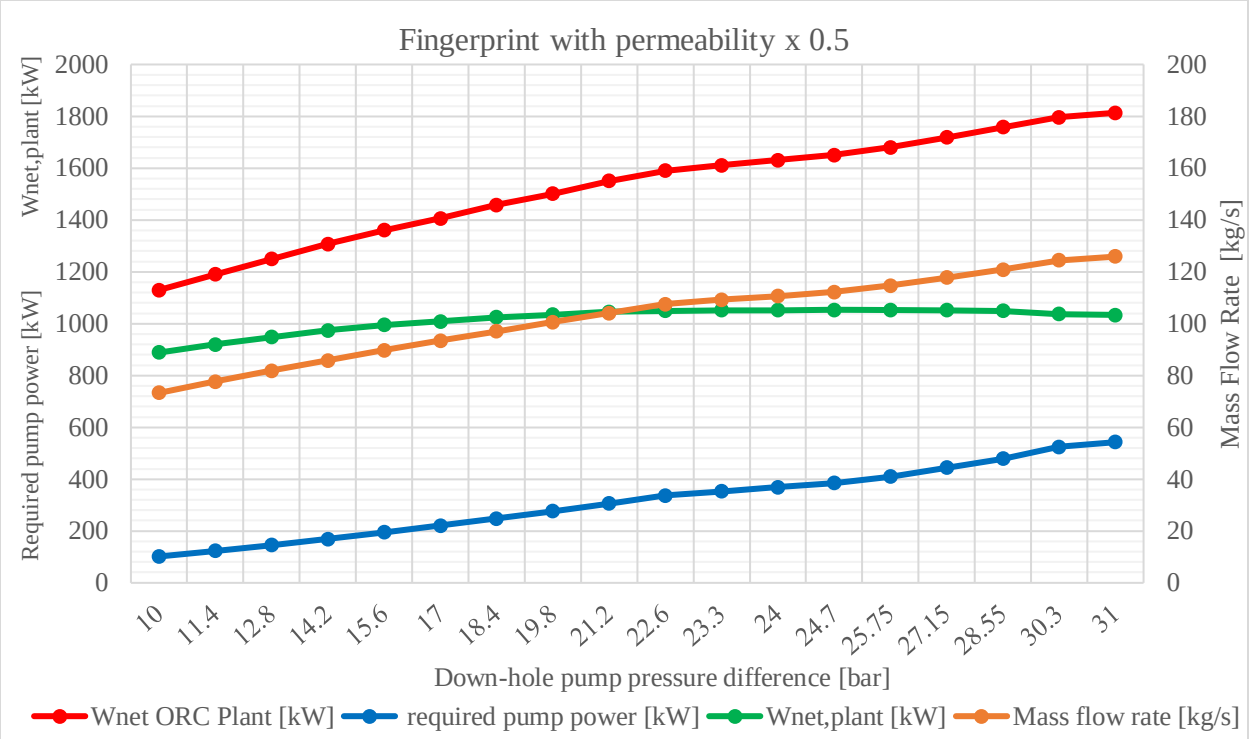

Figure 76: Fingerprint graph of the scenario with permeability x 0.5 for the saturated recuperative ORC plant with temperature limit.

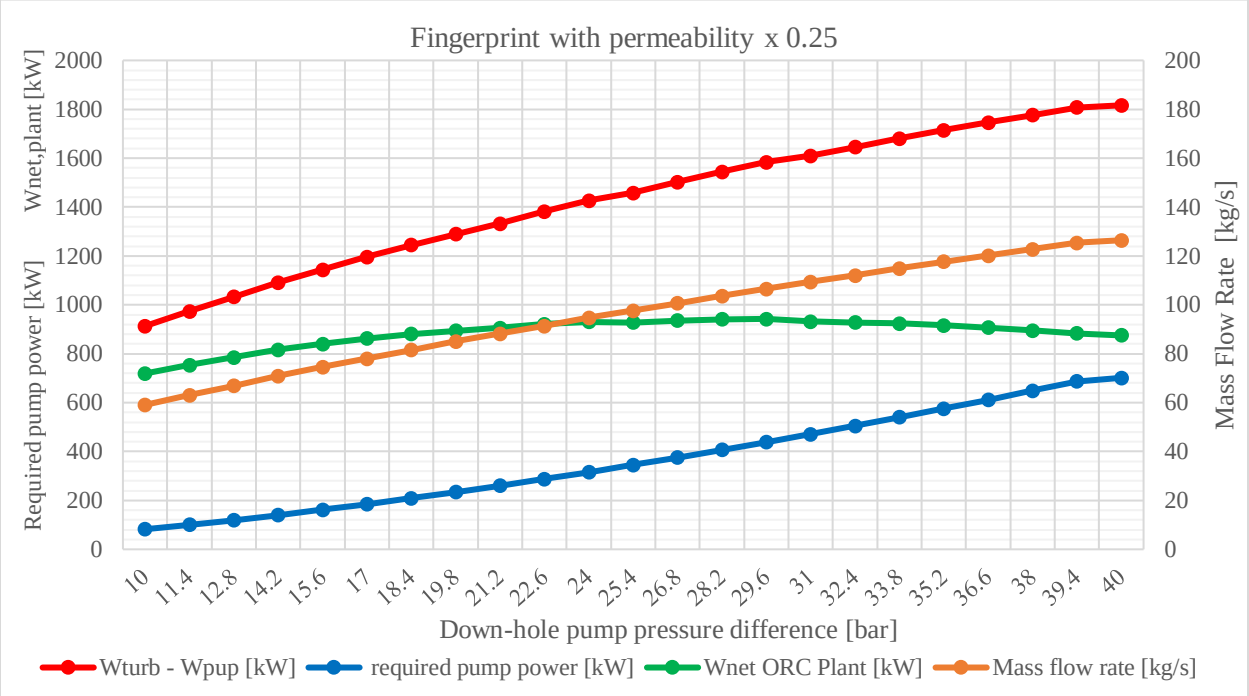

Figure 77: Fingerprint graph of the scenario with permeability x 0.25 for the saturated recuperative ORC plant with temperature limit.

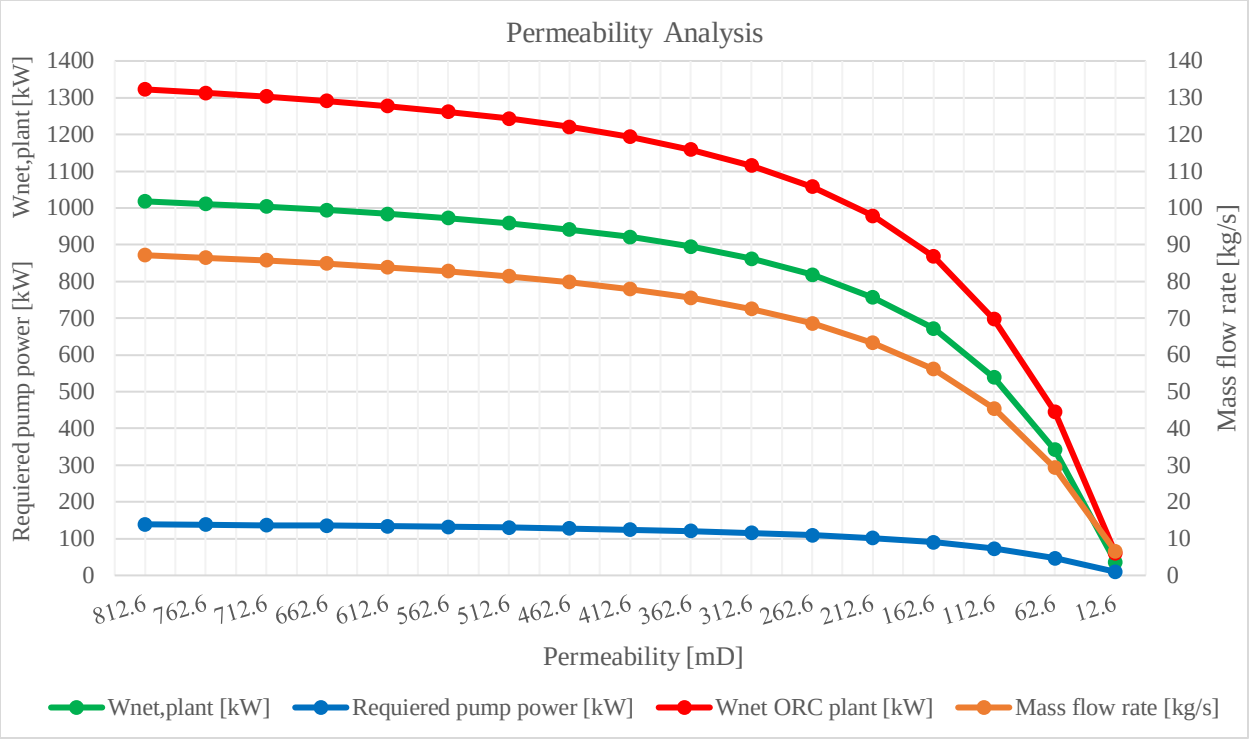

Figure 78: Permeability analysis for the saturated recuperative ORC plant with temperature limit.